Novel Function of the Retinol Saturase (RetSat) in Murine Kidneys

Inaugural-Dissertation
to obtain the academic degree
Doctor rerum naturalium (Dr. rer. nat.)

Submitted to the
Department of Biology, Chemistry, Pharmacy
of
Freie Universität Berlin

by

Sascha Wulff
2023

The present doctoral study was carried out from October 2018 to April 2023 at the Institute of Pharmacology at Charité – University Medicine Berlin under the supervision of Prof. Dr. rer. nat. Michael Schupp.

1st reviewer: Prof. Dr. rer. nat. Michael Schupp

2nd reviewer: Prof. Dr. rer. nat. Sigmar Stricker

Date of defense: 18. September 2023

Acknowledgement

During this long journey of my doctoral thesis I have interacted with many people who have directly or indirectly helped to shape me as a person and as a scientist. I would therefore like to thank all of those who have supported, motivated, challenged, and distracted me over the past few years.

First of all, Prof. Dr. Michael Schupp. Thank you very much for allowing me to do my doctoral thesis in your research group at the Charité. I still remember our first interview and the phone call in which you offered me the position as a doctoral student, which turned out to be one of the happiest days of my life. This thesis would not have been possible without your advice, encouragement, inspiration, motivation, and perfect timing to push me in the right direction. It has truly been a pleasure to work with you and the lab you have created. I appreciate your ability to share scientific knowledge and ideas with me and others.

Secondly, I would like to thank Prof. Dr. Sigmar Stricker, for the opportunity to be supervised at the Freie Universität Berlin, for his support, feedback and interest in my work.

A big thank you to all current and previous members of the AG Schupp, for making the work fun. Especially the presence of Marie, Konstantin, Moritz, Sylvia, Julia, Na, Yueming, Manuela, Roberto, Till, Catrin, Sarah,and Chen who supported me as close friends or helped in various experiments. Our sense and non-sense moments, scientific and non-scientific conversations, and actions will be among my best memories as a doctoral student.

A special thank you to everyone whom I have worked with as part of my doctoral project: Dr. Tilman Breiderhoff, for providing the transgenic mouse, Patrick Langner at the MDC phenotyping platform for analysing my samples, and all colleagues at the Max Rubner Center (former CCR) at the Charité, who supported me with their knowledge, ideas, materials and emotional support. I would also like to thank the Deutsche Forschungsgemeinschaft for funding my doctoral project.

Whenever I needed it, I could count on my dearest friends. David, Clemens, Dennis, Robert, Hansi, Simon, Annettchen, Mikey, Euan, Hubi, Jenny and Johnny. I am endlessly grateful for the support, motivation, and enthusiasm I received from you throughout this journey. I would like to thank my college friends Joaquin, Martin, Laura, Hannes, Ulrich, and Dima for the trips we have had over the years and for the ones to come. I also want to thank Andreas and Norbert for introducing me to science. To all the others I have not mentioned, you know what you have contributed to my development and my thesis, thank you all.

The last years were full of experiences, good vibes and life. I am glad that I was entitled to have this opportunity. The doctoral thesis is not only an experience of working in science, it is a challenge with one`s self. This experience improved my confidence and makes me feel proud of myself. It will be forever part of my life.

Mein größter Dank gilt meiner Familie, insbesondere meiner Mutter Kerstin und meinem Vater Karsten. Ohne eure jahrzehntelange Unterstützung, Liebe und Verständnis hätte ich das alles nicht geschafft. Ich bin unendlich glücklich, euch meine Eltern nennen zu dürfen – vielen herzlichen Dank für alles. Einen großen Teil meiner Entwicklung verdanke ich meinen Großeltern Oma Antje und Opa Horst. Eure Energie, eure Liebe und die Möglichkeit, mit Euch von klein auf die Welt zu erkunden, haben meinen Charakter wesentlich geprägt. Vielen Dank auch an Silke, Jörg, Markus und Sanjana für eure emotionale Unterstützung in dieser Zeit. Meine anderen Großeltern, Margarethe und Karl-Heinz wären heute sicher sehr stolz auf mich, wenn sie noch hier wären. Zu guter Letzt möchte ich mich bei meiner Partnerin Joschi bedanken, die immer ein offenes Ohr für meine Belange hatte, mir neue Sichtweisen aufzeigte und mich in den letzten eineinhalb Jahren auf meinem Weg begleitet hat.

Vielen herzlichen Dank für alles, ohne Euch wäre ich nicht der Mensch geworden, der ich heute bin. Diese Arbeit ist für Euch!

Declaration of Independence

Herewith I certify that I have prepared and written my thesis independently and that I have not used any sources and aids other than those indicated by me. I also declare that I have not submitted the dissertation in this or any other form to any other institution as a dissertation.

Berlin, April 20th, 2023

Table of Contents

List of Figures

List of Tables

Abbreviations

1α,25(OH)$_2$D$_3$	1*α*,25-Dihydroxycholecalciferol
9-*cis* RA	9-cis retinoic acid
ANOVA	analysis of variance
atRA	all-*trans*-retinoic acid
BAT	brown adipose tissue
BP	biological processes
BW	body weight
BUN	blood urea nitrogen
Calcr	calcitonin receptor
CC	cellular component
CD	collecting duct
cDNA	complementary DNA
Cdh16-Cre	cadherin16-Cre recombinase
ChREBP	carbohydrate response element binding protein
Cldn10	claudin 10
CRTISO	carotenoid isomerase
ddH_2O	double distilled water
DGAP	Diabetes Genome Anatomy Project
DCT	distal convoluted tubule
DROL	all-*trans*-13,14-dihydroretinol
DSC1	desmocollin 1
DSC2	desmocollin 2
DSG1	desmoglein 1
EE	energy expenditure
ER	endoplasmic reticulum
eWAT	epididymal white adipose tissue
FAD	flavin adenine dinucleotide
FC	fold change
FE	fractional excretion
FGF23	fibroblast growth factor 23
FoxO1/FOXO1	forkhead box O1
FXYD5	FXYD Domain Containing Ion Transport Regulator 5
G6p	Glucose-6-Phosphatase
GO	gene ontology
H&E	haematoxylin & eosin staining
HEK293	human embryonic kidney cell line 293
HFD	high-fat diet
HPLC	high-performance liquid chromatography

ipGTT	intraperitoneal glucose tolerance test
ipITT	intraperitoneal insulin tolerance test
Kcnj10	potassium inwardly rectifying subfamily j member 10
LFQ	label-free quantitation
LPL	lipoprotein lipase
MFG-E8	milk fat globule-EGF-factor 8
MF	molecular function
mRNA	messenger RNA
MUPs	major urinary proteins
NaCl	sodium chloride
NAD(P)	nicotinamide adenine dinucleotide (phosphate)
NC	normal chow
NCBI	National Library of Medicine
NEFAs	non-esterified fatty acids
NMR	nuclear magnetic resonance
padj	p-value adjusted
Pck1	phosphoenolpyruvate phosphatase
Pi	inorganic phosphate
PPARα	peroxisome proliferator-activated receptor α
PPARγ	peroxisome proliferator-activated receptor γ
PTH	parathyroid hormone
PT	proximal tubule
Pvalb	parvalbumin
RAR	retinoic acid receptor
RBP4/RBP4	retinol binding protein 4
RetSat/RETSAT	Retinol Saturase
RER	respiratory exchange rate
ROS	reactive oxygen species
RPKM	reads per kilobase of transcript per million mapped reads
RXR	retinoid X receptor
SDS-PAGE	sodium dodecyl sulfate-polyacrylamide gel electrophoresis
STRA6	stimulated by retinoic acid 6
TAL	thick ascending limb of the loop of Henle
TPO-Cre	thyroid peroxidase-Cre recombinase
TTR	transthyretin
UCP1	uncoupling protein 1
UCP3	uncoupling protein 3
Vdr	vitamin D receptor
WAT	white adipose tissue
Zfx	zinc finger protein X-linked

Abstract

The oxidoreductase Retinol Saturase (RetSat), known to catalyse the reaction of all-*trans*-retinol to all-*trans*-13,14-dihydroretinol, is highly expressed in metabolically active tissues and differentially regulated in metabolic disorders such as insulin resistance and type 2 diabetes. To date, RetSat has been shown to be involved in adipocyte differentiation, to act as an upstream regulator of hepatic glucose and lipid metabolism, to alter macrophage function, to affect avian vision and to be associated with the generation of reactive oxygen species (ROS). These effects appear to be independent of the originally described saturation reaction, suggesting alternative enzymatic reactions that may lead to the observed effects. RetSat is highly expressed in the metabolically active kidneys, which regulate the filtration, reabsorption and excretion of metabolites. The function of RetSat in the mouse kidney is completely unknown and its role in the development of metabolic diseases remains to be elucidated.

The aim of this study was to generate and characterize a mouse model with kidney-specific deletion of *RetSat* to investigate its function in the kidney. Loss of *RetSat* in adult male and female C57BL/6J mice resulted in profound proteinuria with additional hyperphosphaturia. Using a label-free quantification (LFQ) proteomics approach, we identified increased excretion of a number of proteins in 24 h urine, including RBP4 and FXYD5.

Middle-aged *RetSat*-deficient mice fed normal chow (NC) showed an increase in body weight that was independent of food intake, with no change in body composition or metabolic profile. Middle-aged male mice lacking *RetSat* showed hypercalciuria without the development of nephrocalcinosis and an unexpected hypophosphaturia. In addition, RNA-sequencing analysis revealed upregulation of the vitamin D receptor (*Vdr*) and differential mRNA expression of its target genes in whole kidney tissue. Subsequent Gene Ontology (GO) analysis revealed involvement in the biological process of cell junction assembly.

RetSat-deficient mice fed with a high-fat diet (HFD) showed an increase in body weight that was independent of food intake, with a relative increase in fat mass, a decrease in lean mass, and impaired glucose clearance. In *RetSat*-deficient mice, relative energy expenditure (EE) changed without changes in respiratory exchange rate (RER), locomotor activity, or drinking volume. Interestingly, there was a reduction in absolute and relative kidney weight in *RetSat*-deficient mice in the fed state and less accumulation of fat droplets in the renal cortex.

In conclusion, we have successfully generated, validated and metabolically characterized a new mouse model with kidney-specific deletion of *RetSat*. In this thesis, we have identified a previously unknown link between the renal loss of *RetSat* and the upregulation of renal *Vdr*.

Kurzzusammenfassung

Die Oxidoreduktase Retinol Saturase (RetSat), von der bekannt ist, dass sie die Reaktion von all-*trans*-Retinol zu all-*trans*-13,14-Dihydroretinol katalysiert, wird in stoffwechselaktiven Geweben stark exprimiert und bei Stoffwechselstörungen wie Insulinresistenz und Typ-2-Diabetes unterschiedlich reguliert. Bisher wurde gezeigt, dass RetSat an der Differenzierung von Adipozyten beteiligt ist, als Regulator des hepatischen Glukose- und Lipidstoffwechsels fungiert, die Funktion von Makrophagen verändert, das Sehvermögen von Vögeln beeinflusst und mit der Bildung reaktiver Sauerstoffspezies (ROS) in Verbindung gebracht wird. Diese Wirkungen scheinen unabhängig von der ursprünglich beschriebenen Sättigungsreaktion zu sein, was auf alternative enzymatische Reaktionen hindeutet. *RetSat* wird in hohem Maße in den stoffwechselaktiven Nieren exprimiert, die die Filtration, Reabsorption und Ausscheidung von Metaboliten regulieren. Die Funktion von RetSat in der Mausniere ist völlig unbekannt, sowie seine Rolle in der Entstehung von Stoffwechselkrankheiten.

Ziel dieser Studie war die Entwicklung und Charakterisierung eines Mausmodells mit nierenspezifischer Deletion von *RetSat*, um seine Funktion in der Niere zu untersuchen. Der Verlust von *RetSat* bei erwachsenen männlichen und weiblichen C57BL/6J-Mäusen führte zu einer ausgeprägten Proteinurie mit zusätzlicher Hyperphosphaturie. Mithilfe eines markierungsfreien Quantifizierungsansatzes (LFQ) für die Proteomik konnten wir eine erhöhte Ausscheidung einer Reihe von Proteinen im 24-Stunden-Urin feststellen, darunter RBP4 und FXYD5.

Adulte *RetSat*-defiziente Mäuse, die mit normalem Futter (NC) gefüttert wurden, zeigten eine Zunahme des Körpergewichts, die unabhängig von der Nahrungsaufnahme war, ohne dass sich die Körperzusammensetzung oder das Stoffwechselprofil veränderten. Männliche Mäuse mittleren Alters, denen *RetSat* fehlte, zeigten eine Hypercalciurie ohne Entwicklung einer Nephrocalcinose und eine unerwartete Hypophosphaturie. Darüber hinaus ergab die RNA-Sequenzierungsanalyse eine Hochregulierung des Vitamin-D-Rezeptors (*Vdr*) und eine unterschiedliche mRNA-Expression seiner Zielgene in Nierenlysaten. Eine anschließende Gene Ontology (GO)-Analyse ergab eine Beteiligung an dem biologischen Prozess des Aufbaus von Zellverbänden.

RetSat-defiziente Mäuse, die mit einer fettreichen Diät (HFD) gefüttert wurden, zeigten eine Zunahme des Körpergewichts, die unabhängig von der Nahrungsaufnahme war, mit einer relativen Zunahme der Fettmasse, einer Abnahme der Magermasse und einer beeinträchtigten Glukose-Clearance. In RetSat-defizienten Mäusen, änderte sich der relative Energieverbrauch (EE), ohne dass es zu Veränderungen bei der respiratorische Austauschrate (RER), der Bewegungsaktivität oder dem Trinkvolumen kam. Interessanterweise kam es zu einer Reduktion des absoluten und relativen Nierengewichts bei Mäusen mit *RetSat*-Defizienz im gefütterten Zustand und zu einer geringeren Akkumulation von Fetttröpfchen in der Nierenrinde.

Zusammenfassend lässt sich sagen, dass wir erfolgreich ein neues Mausmodell mit nierenspezifischer Deletion von *RetSat* erzeugt, validiert und metabolisch charakterisiert haben. In dieser Arbeit haben wir eine bisher unbekannte Verbindung zwischen dem renalen Verlust von *RetSat* und der Hochregulierung vom renalen *Vdr* identifizieren können.

1 Introduction

1.1 The kidneys and their function

The kidneys are paired organs located retroperitoneally on either side of the spine and have a variety of functions including ultrafiltration of plasma, reabsorption of solutes, excretion of metabolic waste products and maintenance of water and pH homeostasis. The filtration process regulates the body's fluid homeostasis by influencing electrolyte composition, osmolarity and acidity [4]. They also contribute to many other metabolic processes such as gluconeogenesis, vitamin D activation and the production of hormones such as erythropoietin and renin [6-8]. The functional subunit of the kidney is called the nephron. In adult humans, each kidney contains about 1 million nephrons [9], while mice develop about 16,000 nephrons during nephrogenesis [10]. This number is highly variable and is influenced by genetic, epigenetic and environmental factors [9, 11-13]. Each nephron consists of five major segments: glomerulus, proximal tubule, loop of Henle, distal tubule and collecting duct, which can be further subdivided according to their renal localisation and structure as shown in **Figure 1A**. Each segment of the nephron contributes to complex homeostasis by handling specific reabsorption or excretion processes.

The main function of the glomerulus is the ultrafiltration of blood plasma. The glomerulus acts as a molecular sieve with size- and charge-selective properties that allow filtration of small molecules and retention of larger molecules such as albumin [14, 15]. The ultrafiltrate undergoes a wide range of reabsorption processes in different nephron segments to reabsorb small organic and soluble molecules such as glucose, amino acids, vitamins, water and different types of ions to maintain physiological blood concentrations **Figure 1B** [16-19].

In addition to their central role in electrolyte and water balance, the kidneys regulate and contribute to glucose homeostasis through glucose reabsorption, glycolysis and gluconeogenesis [20, 21]. The latter has classically been attributed to the liver, but the kidneys make a significant contribution to gluconeogenesis in the post-absorptive state [21]. Renal gluconeogenesis has been shown to be altered in metabolic diseases such as type 2 diabetes and obesity [22-24]. Furthermore, type 2 diabetes and hypertension

are the major risk factors for the development of chronic kidney disease (CKD) in adults [25]. The underlying mechanisms remain to be elucidated.

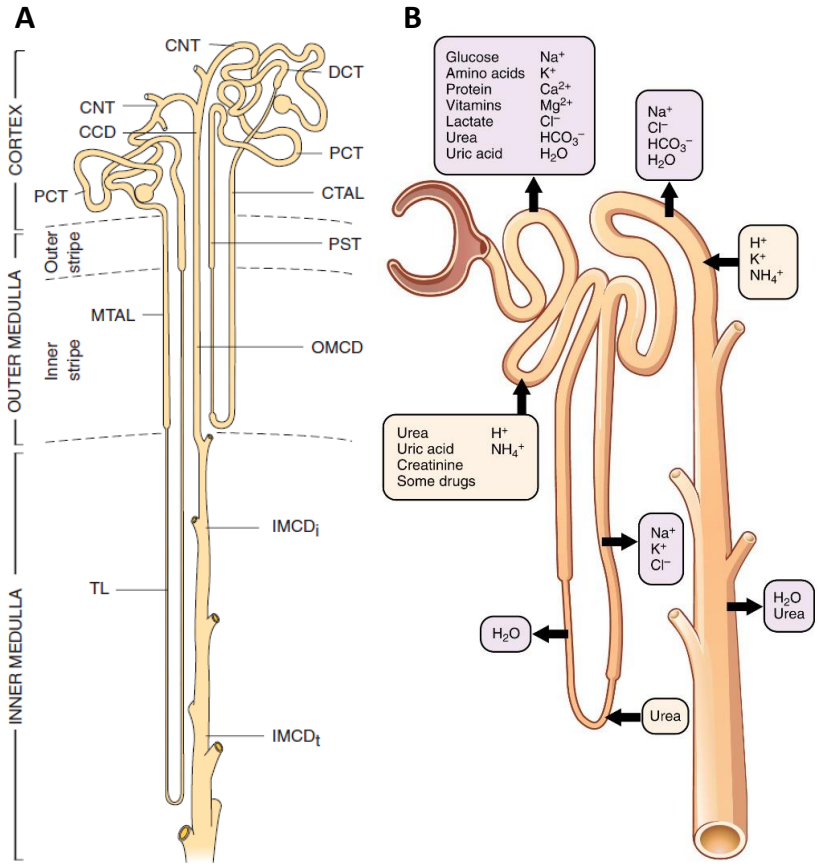

Figure 1: Illustration of a nephron and its functions. (A) Diagram illustrating cortical and juxtamedullary nephron. CCD, cortical collecting duct; CNT, connecting tubule; CTAL, cortical thick ascending limb; DCT, distal convoluted tubule; IMCDi, initial inner medullary collecting duct; IMCDt, terminal inner medullary collecting duct; MTAL, medullary thick ascending limb; OMCD, outer medullary collecting duct; PCT, proximal convoluted tubule; PST, proximal straight tubule; TL, thin limb of loop of Henle. (Modified from Madsen KM, Tisher CC: Structural-functional relationship along the distal nephron. Am J Physiol 250:F1-F15, 1986 and taken from [4]). **(B)** Locations of secretion and reabsorption in the nephron (https://openstax.org/books/anatomy-and-physiology/pages/25-6-tubular-reabsorption).

In addition, studies have shown that the kidneys are crucial for the metabolism and secretion of fat-soluble vitamins such as vitamin D and vitamin A [8, 26]. In the physiological state, the kidneys activate endogenously produced vitamin D to generate its metabolically active form [27]. Furthermore, they retain filtered and protein bound vitamin A through the megalin system [28, 29]. In contrast, in the pathophysiological state, reduced vitamin D and altered circulating vitamin A levels are associated with impaired glomerular filtration rate and renal function and increased mortality in patients with CKD [30-34]. The functional relationship between vitamin A metabolism and renal disease is still unknown and needs to be investigated.

1.2 Retinoids

Retinoids are a class of compounds chemically related to vitamin A, also known as retinol. Fat-soluble vitamin A is essential for vertebrates and must be obtained from dietary sources [35], either as carotenoids from plant sources or as retinyl esters from animal sources [36]. Vitamin A and its derivatives contribute to several biological functions, including vision, embryonic development, reproduction, immune cell function, and regulation of cell proliferation and differentiation [37-41]. In humans, vitamin A deficiency has been shown to correlate with reduced vision and subsequent symptoms such as night blindness or even complete blindness [42].

In addition, retinoids can also be considered hormones, based on their nuclear receptor signaling [43, 44]. All-*trans* retinoic acid (atRA) has been shown to be the biologically active metabolite of vitamin A and acts as a ligand for the retinoic acid receptors (RAR) α, β and γ [44]. It is known that RAR can bind to another nuclear receptor, the retinoid X receptor (RXR), and form a heterodimer [45, 46]. 9-*cis* retinoic acid (9-*cis* RA) is a known ligand for RXR, but its biological relevance is still unclear [47]. Other RXR-activating retinoids have been identified, such as 9-*cis*-13,14-dihydroretinoic acid in mice [48, 49].

1.2.1 Retinol uptake, storage, transport, and metabolism

Intestinal absorption of dietary retinoids involves hydrolysis of retinyl esters to retinol, followed by re-esterification of retinol after absorption into enterocytes [50]. Retinyl esters are then packaged with other dietary lipids into chylomicrons. A quarter of the released chylomicrons containing retinyl esters deliver retinoids directly to their target tissues, where they are hydrolysed by the membrane-bound enzyme lipoprotein lipase (LPL) and prepared for their designated purpose [51]. The remaining retinoids are transported to the liver, where ~80% of all retinoids are stored [52].

The liver plays a major role in the uptake, storage and mobilisation of retinoids. Hepatocytes contain 10-20% of hepatic retinoids and are the site of synthesis and secretion of the serum transport protein for retinol, retinol binding protein 4 (RBP4) [53, 54]. RBP4 is a plasma protein required to transport lipophilic retinol through the

bloodstream to the periphery where it can perform its physiological function [55]. Retinol-bound RBP4 forms a complex with the tetrameric protein transthyretin (TTR) within the hepatocyte to stabilise the complex during transport and prevent renal filtration [56, 57]. Transport of retinol across cell membranes in extrahepatic tissues is facilitated by the membrane protein stimulated by retinoic acid 6 (STRA6) [58]. To regulate intracellular retinoid homeostasis, STRA6 is capable of bidirectional transport of retinol [59]. Once the cell has taken up retinol-bound RBP4 via STR6, retinol binds to cellular retinol-binding protein 1 [60] and can be converted to atRA by a two-step oxidation process [61] which can then regulate gene expression in the target cell. Retinoic acid has a short half-life of approximately 1 h and its tissue levels are highly regulated by metabolic degradation with retinoic acid feedback loops [62, 63]. Retinoic acid-inducible cytochrome P450 enzymes such as CYP26A1, B1 and C1 have been shown to catabolize retinoic acid predominantly [64].

1.2.2 Retinoids in Kidney

Retinoids are critical for kidney development in humans and mice [65]. atRA is essential for branching morphogenesis and contributes to the final number of nephrons [66]. In addition, atRA signalling appears to be beneficial in several renal diseases by inducing protective genes or attenuating injury factors. In the physiological state, atRA is repressed in the adult kidney, but is reactivated in acute kidney injury to reduce renal tubular cell death and interstitial inflammation [67-69]. In contrast, atRA signalling is impaired in CKD with manifestations of renal fibrosis, inflammation and glomerulosclerosis [70-72]. Preservation of renal function in CKD has been achieved by treatment with atRA [71-74].

Other studies have shown an association between alterations in atRA metabolism and diabetic kidney in rodents [66, 75]. Furthermore, the renoprotective effects of atRA in diabetic kidney disease were mediated by an anti-inflammatory mechanism [76]. The low intracellular levels of retinoids and their labile nature in biological systems, as well as their incompletely understood underlying mechanism of biotransformation, suggest that a variety of enzymes involved in retinoid metabolism remain to be discovered.

1.3 Retinol Saturase (RetSat)

In 2004, Moise *et al.* performed a screen for enzymes involved in carotenoid and retinoid metabolism in vertebrates [77]. The group performed a species-wide homology search for the protein sequence of tomato and *Arabidopsis* carotenoid isomerase (CRTISO), which has been shown to catalyse the conversion of tetra-cis-lycopene to all-*trans*-lycopene in plants and cyanobacteria [78, 79]. Identification of a conserved family of proteins in many chordates and subsequent phylogenetic analysis revealed a homology of ~40% between plant CRTISO and vertebrate proteins. Surprisingly, rodent and human homologs shared 90% of their protein sequence and a highly conserved genomic organisation with 11 exons and the same exon-intron boundaries [77].

Figure 2: Secondary structure prediction of murine RETSAT. Mathematical prediction and illustration of the murine RETSAT secondary protein structure (609 aa), generated with the Phyre2 algorithm (http://www.sbg.bio.ic.ac.uk/phyre2).

This CRTISO-like murine protein is encoded by 609 amino acids and has a predicted size of ~67 kDa, based on the theoretical mass calculation of the translated sequence (https://web.expasy.org/compute_pi/). The secondary structure prediction was generated using Phyre2 (http://www.sbg.bio.ic.ac.uk/phyre2/) and is shown in **Figure 2**. It consists of a N-terminal signal peptide (amino acids 1 – 18) that targets the protein to endoplasmic reticulum (ER). It also has a dinucleotide-binding domain (amino acids 73 – 118) that is common to a variety of oxidoreductases including monoamine oxidases, protoporphyrinogen oxidases and phytoene desaturases [3, 80]. This dinucleotide-binding domain serves as a potential binding site for the cofactors FAD or NAD/NADP.

The mouse ortholog was cloned from reverse transcribed RNA of the retina and retinal pigment endothelium to analyze its enzymatic activity. In the human embryonic kidney (HEK293) cell line, ectopic expression of CRTISO-like protein was inactive towards lycopene, but instead catalyzed the saturation of all-*trans*-retinol at the 13 – 14 bond to produce all-*trans*-13,14-dihydroretinol (DROL) [77] (**Figure 3**). Based on its function in catalyzing the described reaction, Moise *et al.* named the murine CRTISO-like protein Retinol Saturase (RetSat) [77]. In an independent study by Schupp *et al*., the retinol-reducing activity was reproduced [81]. In a follow-up study using chiral high-performance liquid chromatography (HPLC), Moise *et al.* demonstrated that murine RETSAT selectively produces the (*R*)-all-*trans*-13,14-dihydroretinol enantiomer [82]. In lecithin:retinol acyltransferase-deficient mice, DROL was shown to be further oxidized to all-*trans*-13,14-dihydroretinoic acid (DRA) [83] (**Figure 3**). In the same study, DRA was shown to be a ~10-fold less potent activator of the RAR compared to retinoic acid. Authors proposed that RETSAT inherently protects RAR activity by reducing the retinol available for retinoic acid synthesis and increasing the formation of less potent dihydroretinol metabolites [83]. In addition, DRA showed no activity in the RXR-reporter assay in HEK293 cells [83], but the proposed isomerization to (R)-9-cis-9-13,14-dihydroretinoic acid activated RXR reporter activity in cells and target gene expression in mice [49].

Two putative RetSat homologs have been identified in zebrafish, of which only one showed retinol saturating activity. In addition to saturating the 13 – 14 double bond, it was able to saturate the 7 – 8 double bond of retinol side chain [84]. Another putative RetSat substrate was discovered in the avian retina in 2016. The researchers were interested in an enzymatic function that could reduce a double bond in the side chain of an apocarotenoid in zebra finch. They transfected HEK293 cells with zebra finch RetSat and showed that it catalyses the reaction of 10'-apo-β-carotene-3,10'-diol (galloxanthin) to 11',12'-dihydro-10'-apo-β-carotene-3,10'-diol (dihydrogalloxanthin) [85].

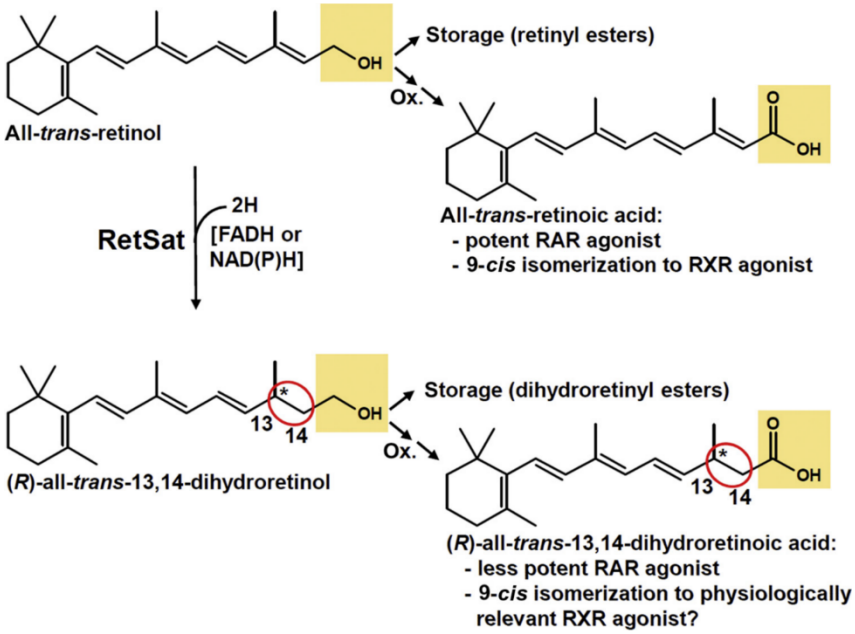

Figure 3: Enzymatic reaction of RetSat involving retinol. Mammalian RetSat transforms all-trans-retinol to (R)-alltrans-13,14-dihydroretinol, which can be stored as dihydroretinyl esters or oxidized to (R)-all-trans-13,14-dihydroretinoic acid. The latter metabolite activates RAR less potently than all-trans-retinoic acid. Its isomerization may generate (R)-9-cis-13,14-dihydroretinoic acid, that was suggested to be a physiologically relevant RXR agonist. Note that zebrafish but not murine RetSat also generates all-trans-7,8-dihydroretinol. Taken from [3].

To date, the only known substrates of RetSat are all-*trans* retinol and galloxanthin, which have been shown to be saturated at the double bond of the polyene chain. The discovery of the function of avian RetSat shows that the enzymatic specificity may have a wider range of possible substrates from non-carotenoid and carotenoid species [3].

1.3.1 RetSat's expression profile, transcriptional regulation and subcellular localization

To understand the genetics of type 2 diabetes and insulin resistance, the Diabetes Genome Anatomy Project (DGAP) was launched in the early 2000s. Using a bioinformatics approach, gene expression profiles of datasets from related animal models, human data, and *in vitro* studies were analyzed to provide biological insights into the biology of insulin resistance. This integrative analysis of different datasets revealed that RetSat was the gene (*RetSat/RETSAT*) with differential expression in 8 out of 16 datasets [86].

RetSat mRNA can be detected in a wide range of human and mouse tissues with varying expression patterns. In humans, the highest expression is in adipose tissue and intestine [1]. In mice, tissue with the highest expression is liver and kidney, followed by brown and white adipose tissue (BAT, WAT) [77, 81, 87].

In mice, *RetSat* has been shown to be transcriptionally regulated by the nuclear peroxisome proliferator-activated receptor α (PPARα) in liver [88] and PPARγ in adipose tissue [81]. This transcriptional regulation is mediated by a PPAR-response element in intron 1 of the murine [81, 88] and human [89] *RetSat* gene. In addition, the induction of murine *RetSat* during fasting in various organs has been shown by Sun *et al*. [88]. Forkhead box 1 (FoxO1), a transcription factor that is under the control of insulin and important to induce gluconeogenesis [90] binds close to the *RetSat* gene in the liver and transactivates its expression in primary hepatocytes [91]. Furthermore, the deletion of Zinc Finger Protein X-Linked (Zfx) resulted in a reduction of *RetSat* mRNA levels in embryonic and haematopoietic stem cells [92].

Moise *et al.* showed that murine RETSAT protein was predominantly found in the ER [77], while Schupp *et al*. showed that it colocalized with the ER marker protein disulfide isomerase [81]. Localization to the ER and protein stability were reduced when the N-terminal signal peptide was deleted [81].

1.3.2 RetSat's involvement in oxidative stress sensitivity, reactive oxygen species (ROS) formation and macrophage function

Nagaoka-Yasuda and colleagues performed a RNA interference screen in murine fibroblast cells (NIH3T3) and identified *RetSat* as a major mediator of oxidative stress sensitivity. When *RetSat* was depleted by shRNA, an increase in cell viability was observed upon the exposure to tert-butylhydroperoxide or H_2O_2 which correlated strongly with knockdown efficiency [93]. *RetSat* depleted fibroblasts were not protected when exposed to other sources of oxidative stress, such as ultraviolet light or paraquat. The authors suggested that loss of *RetSat* selectively increased resistance to hydroperoxide-specific damage [93].

In line with these findings, Pang and colleagues confirmed the protective nature against peroxide-specific reactive oxygen stress in *RetSat* depleted cells [94]. The addition of DROL did not rescue the increased viability in *RetSat*-depleted fibroblasts. The authors concluded that the response to oxidative stress is independent of retinol saturation. In the same study, overexpression of RetSat in HEK293 cells consistently increased ROS generation in an assay measuring the redox-sensitive dye 2',7'-dichlorodihydrofluorsecein diacetate (H_2DCFDA) [94]. In addition, malondialdehyde levels were lower in the livers of *RetSat* knockout mice compared to their respective wild-type littermates [94]. Taken together, RetSat depletion resulted in a protection against peroxide-induced stress while its overexpression increased peroxide sensitivity and ROS generation in mouse cells and liver.

In the thymus, induction of *RetSat* mRNA expression was achieved by triggering the thymic apopto-phagocytosis programme by an injection of dexamethasone [95]. In *RetSat*-null mice, bone marrow-derived macrophages showed an impaired long-term phagocytosis of apoptotic cells that could be rescued by providing the recombinant bridging molecule milk fat globule EGF-factor 8 (MFG-E8) [96]. In female *RetSat*-null mice, the development of a mild systemic lupus erythematosus-like autoimmunity was observed upon aging, with an increase in spleen weight, delayed clearance of apoptotic cells, and the deposition of immune complexes in the kidney [3, 96]. The authors analyzed the effect of DRO on macrophage gene expression and phagocytosis

and concluded that these effects were most likely independent of dihydroretinoid production [96].

1.3.3 RetSat's involvement in adipocyte differentiation and liver metabolism

During adipocyte differentiation of mouse and human preadipocytes, RetSat mRNA levels and protein expression were upregulated [81, 97]. Induction or knockdown of the master regulator of adipogenesis in adipocytes, PPARγ [98], resulted in an increased or decreased expression of *RetSat* mRNA in mature adipocytes [81]. In the same study, *RetSat* depletion resulted in an impairment of adipocyte differentiation of 3T3-L1 cells that was independent of DROL, as its addition failed to rescue impaired differentiation [81]. Addition of a synthetic PPARγ agonist and overexpression of *RetSat* were able to rescue differentiation [81]. Weber *et al*. have suggested a recently identified link to *de novo* lipogenesis, which is known to control PPARγ activity that may account for the observed effect [3, 87, 99].

In contrast to *in vitro* results, an *in vivo* model of *RetSat*-null mice showed an increase in adiposity, but no effect on global levels of retinoids [97]. Authors suggested that low abundance, but highly potent vitamin A metabolites could regulate pathways in neutral lipid accumulation [97]. From previous experiments, it is known that DROL can activate RAR and antagonize PPARα, but not PPARγ [61]. Based on observed intracellular DROL levels *in vivo*, authors concluded it is unlikely that DROL achieves sufficient cellular concentrations to antagonize PPARα. On the other hand, downstream DROL metabolites could act as potential PPARγ antagonists *in vivo* [61]. A more detailed characterization confirmed the increase in weight gain in mice fed either a normal chow or a 45 kcal % fat diet [94]. Metabolic profiling of these mice showed that energy expenditure and food intake were unaffected by the knockout, whereas the locomotor activity was increased [94].

In livers of *RetSat*-null mice on a mixed 129Sv/C57BL/6 background, no differences in hepatic triglycerides, cholesterol, phospholipids, or non-esterified fatty acids (NEFAs) could be observed [97]. Backcrossing to C57BL/6N resulted in increased hepatic triglyceride levels but a decrease in the abundance of many polar unsaturated lipid species [94].

Acute liver-specific knockout of *RetSat* did not induce any major abnormalities in mice normal chow-fed mice [87], which is in contrast to the findings of Pang *et al*., where mice fed an HFD accumulated less triglycerides in liver tissue and had lower levels of circulating triglycerides and NEFA's, a reduction in blood glucose and insulin levels [3, 87]. Acute liver-specific depletion of *RetSat* resulted in decreased mRNA and protein levels and reduced target gene expression of carbohydrate response element binding protein (ChREBP), a transcriptional regulator of *de novo* lipogenesis and glycolysis [100]. Heidenreich *et al*. demonstrated that *RetSat* is required for glucose-induced *ChREBP* activity and its nuclear accumulation in primary mouse hepatocytes. They concluded that *RetSat* is an upstream regulator of *ChREBP*. Furthermore, reduced expression of *ChREBP* de novo target genes could not be rescued by the addition of DROL [87]. These results add another layer of *RetSat* involvement in hepatic glucose and lipid metabolism that remains to be linked to a yet unknown enzymatic reaction catalyzed by *RetSat*.

1.4 Aims of this research

RetSat is an oxidoreductase that catalyzes the reaction of all-*trans*-retinol to (*R*)-all-*trans*-13,14-dihydroretinol [77, 82]. The enzyme is expressed in a variety of metabolically active tissues and is highly regulated in conditions associated with insulin resistance and type 2 diabetes [86, 87]. In addition, RetSat is involved in adipocyte differentiation, hepatic glucose and lipid metabolism, avian vision, macrophage function and ROS generation [81, 85, 87, 94, 96]. The underlying mechanism of the observed effects of RetSat are still unknown and may be due to alternative enzymatic functions of the enzyme.

The high expression of RetSat in mouse kidney tissue and its function as a major contributor to glucose homeostasis by glucose reabsorption and gluconeogenesis suggested a central role of the enzyme in renal metabolism [2, 6, 20]. To date, the function of RetSat in the mouse kidney is unknown. Therefore, the aim of this work was to investigate the function of RetSat in the mouse kidney. To achieve this aim, we have set three objectives:

1. Generate and validate a novel mouse model with kidney-specific knockout of RetSat
2. Metabolic characterization of this novel mouse model on NC
3. Metabolic characterization of this novel mouse model on HFD

The obtained data will provide insights into the underlying molecular mechanisms of the murine RetSat and its possible association with metabolic diseases.

2 Materials

2.1 Chemicals and Reagents

The used chemicals and reagents are listed in **Table 1**.

Table 1: Chemicals and Reagents

Substance	Supplier
0.9% Saline solution	B. Braun Melsungen AG (Melsungen, DE)
2-mercaptoethanol	Sigma Aldrich (St. Louis, MO, USA)
5x PCR master mix „ready-to-load”	Bio & Sell (Feucht, DE)
Acetic acid	Carl Roth GmbH & Co. KG (Karlsruhe, DE)
Acetone	Sigma Aldrich (St. Louis, MO, USA)
Acrylamide solution 30%	AppliChem GmbH (Darmstadt, DE)
Alizarin Red S	Sigma Aldrich (St. Louis, MO, USA)
Ammonium persulfate (APS)	Sigma Aldrich (St. Louis, MO, USA)
Bovine serum albumin fatty acid free (BSA)	Sigma Aldrich (St. Louis, MO, USA)
Chloroform	Merck KGaA (Darmstadt, DE)
D-(+)-Glucose	Sigma Aldrich (St. Louis, MO, USA)
dNTP Mix	Invitrogen, Thermo Fisher Scientific Inc.(Waltham, MA, USA)
Eosin Y	Merck KGaA (Darmstadt, DE)
Ethanol	Merck KGaA (Darmstadt, DE)
Ethylenediaminetetraacetic acid (EDTA)	Sigma Aldrich (St. Louis, MO, USA)
Formaldehyde solution 4%, buffered	Merck KGaA (Darmstadt, DE)
Insulin solution human	Sigma Aldrich (St. Louis, MO, USA)
Image-iT™ fixative solution	Thermo Fisher Scientific Inc. (Waltham, MA,USA)
Isoflurane (Forene)	AbbVie Inc. (North Chicago, IL, USA)
Isopropanol	Merck KGaA (Darmstadt, DE)
Mayer`s hemalaun solution acidic	Merck KGaA (Darmstadt, DE)
M-MLV reaction buffer (5x)	Promega Corporation (Fitchburg, WI, USA)
M-MLV reverse transcriptase	Promega Corporation (Fitchburg, WI, USA)
Methanol	Sigma Aldrich (St. Louis, MO, USA)
Milk powder	Carl Roth GmbH & Co. KG (Karlsruhe, DE)

Molecular weight marker ProSleve color protein marker	Lonza (Basel, CH)
NeoClear	Merck KGaA (Darmstadt, DE)
NeoMount	Merck KGaA (Darmstadt, DE)
No ROX SYBR MasterMix blue dTTP	Eurogentec (Seraing, BE)
Paraffin Type 6 & 9	Thermo Fisher Scientific Inc. (Waltham, MA,USA)
Paraffinum perliquidum	Thermo Fisher Scientific Inc. (Waltham, MA,USA)
Pierce ECL western blotting substrate	Thermo Fisher Scientific Inc. (Waltham, MA,USA)
Ponceau S	Cayman Chemical Company (Ann Arbor, MI, USA)
Protease inhibitor cocktail tablets complete, EDTA-free	F. Hoffmann-La Roche AG (Basel, CH)
QIAzol lysis reagent	Qiagen GmbH (Hilden, DE)
Random hexamer primer	Invitrogen, Thermo Fisher Scientific Inc. (Waltham, MA, USA)
RNase-free water	Gibco, Thermo Fisher Scientific Inc. (Waltham, MA, USA)
Sodium chloride	Merck KGaA (Darmstadt, DE)
Sodium dodecyl sulfate (SDS)	Carl Roth GmbH & Co. KG (Karlsruhe, DE)
Sodium hydroxide solution	Sigma Aldrich (St. Louis, MO, USA)
Tetramethylethylenediamine (TEMED)	Sigma Aldrich (St. Louis, MO, USA)
Tris hydrochloride (tris HCl)	Carl Roth GmbH & Co. KG (Karlsruhe, DE)
Tris(hydroxymethyl)-aminomethane (tris base)	Merck KGaA (Darmstadt, DE)
Tween 20	Merck KgaA (Darmstadt, DE)
Ultrapure distilled water DNase/RNase free	Invitrogen, Thermo Fisher Scientific Inc. (Waltham, MA, USA)
VectaMount AQ aqueous mounting medium	Vector Laboratories (Burlingame, CA, USA)

2.2 Kits

The used kits are listed in **Table 2**.

Table 2: Kits

Kit	Supplier
Calcium stain kit (modified von Kossa)	ScyTek Laboratories (Logan, UT, USA)
PeqGOLD total RNA kit	VWR (Radnor, PA, USA)
Pierce BCA protein assay kit	Thermo Fisher Scientific Inc. (Waltham, MA,USA)
Rneasy mini kit	Qiagen GmbH (Hilden, DE)
RNA clean & concentrator-5	Zymo Research (Irvine, CA, USA)

2.3 Buffers and Solutions

All buffers and solutions were prepared in double distilled water (ddH_2O) if not declared otherwise and are listed in **Table 3**.

Table 3: Buffers and Solutions

Buffer/Solution	Purpose	Composition
Alizarin Red S solution	Calcium staining histology	2% [m/v] Alizarin Red S
APS solution	Preparation of gels for SDS-PAGE	10% [m/v] APS
Blocking solution	Blocking of membrane after western blot	4% [m/v] milk powder in 1:1 TBS/TBST buffer
EDTA buffer	Immunohistochemistry	10 mM TRIS 1mM EDTA 0.05% Tween-20
Electrophoresis buffer (pH 8.3 - 8.8)	Buffer for SDS-PAGE	16.7 mM tris base 8.3 mM tris HCl 192 mM Glycine 0.1% [m/v] SDS
Eosin Y solution	H&E staining histology	0.5% Eosin Y
Loading buffer	Buffer for samples to load on gel for SDS-PAGE	87.5% [m/v] 5x pierce lane marker nonreducing sample buffer 12.5% [m/v] 2 - mercaptoethanol

Ponceau S solution	Protein staining on PVDF membrane	0.1% [m/v] Ponceau S in 1% [v/v] acedic acid
Protein lysis buffer (RIPA)	Lysis buffer for protein extraction	2 mM EDTA (pH 8.0) 150 mM NaCl 50 mM NaF 50 mM tris HCl (pH 7.2) 0.5% [m/v] sodium deoxycholate 1% [v/v] IGEPAL CA-630 0.1% [v/v] SDS 1 tablet protease inhibitor cocktail tablets complete, EDTA-free per 50 mL buffer
SDS solution	Compound of gel for SDS-PAGE	10% SDS
Tris-buffered saline (TBS)-buffer	Washing buffer for PVDF membranes; antibody dilution	40.1 mM tris base 159.9 mM tris HCl 137 mM NaCl
Tris-buffered saline buffer with tween (TBST)	Washing buffer for PVDF membranes; antibody dilution	40.1 mM tris base 159.9 mM tris HCl 137 mM NaCl 0.1% [v/v] Tween 20
Transfer buffer (pH 8.1 - 8.5)	Buffer for western blot transfer	25 mM tris base 192 mM Glycine 20% [v/v] methanol 0.05% [v/v] SDS
Tris HCl buffer 0.5 M (pH 6.8)	Buffer for stacking gel for SDS-PAGE	15.3 mM tris base 485 mM tris HCl
Tris HCl buffer 1.5 M (pH 8.8)	Buffer for separation gel for SDS-PAGE	0.3 M tris base 1.2 M tris HCl
Wash buffer	Immunohistochemistry	20 mM TRIS 150 mM NaCl 0.05% Tween-20

2.4 Antibodies

Primary antibodies used for western blot analysis were listed in **Table 4.** The antibodies were diluted as indicated in a solution of TBS/TBST (1:1) containing 4% milk powder.

Table 4: Primary Antibodies for Western Blot Analysis

Antibody	Species	Product ID	Supplier	Dilution
GAPDH	rabbit	14C10 (#2118)	Cell Signaling Technology, Inc. (Danvers, MA, USA)	1:2000
TUBA	rabbit	#2144	Cell Signaling Technology, Inc. (Danvers, MA, USA)	1:2000
RETSAT	rabbit	HPA046513	Sigma-Aldrich, (St. Louis, USA)	1:2500

In the second step of western blot analysis, a horseradish peroxidase (HRP) conjugated secondary antibody was used in accordance to the rabbit species of the primary antibody (**Table 5**). The secondary antibody was diluted as indicated in a solution of TBS/TBST (1:1) containing 4% milk powder.

Table 5: Secondary Antibody for Western Blot Analysis

Antibody	Species	Product ID	Supplier	Dilution
Anti-rabbit; HRP-conjugated	goat	31460	Thermo Fisher Scientific Inc. (Waltham, MA, USA)	1:2000

2.5 Oligonucleotides

The primer pairs that were used for quantitative real-time polymerase chain reaction (qRT-PCR) were either designed with the primer-blast online tool from the National Library of Medicine (NCBI) [101] using the primer3 algorithm or looked up from already published data. Primer pairs were ordered from and produced by Thermo Fisher Scientific. The used primer and their sequence from (5’ to 3’) are listed in **Table 6**.

Table 6: Oligonucleotides for qRT-PCR

Gene	Primer direction	Primer sequence
36b4	Forward	TCATCCAGCAGGTGTTTGACA
	Reverse	GGCACCGAGGCAACAGTT
Aldh1a1	Forward	CTGGCTGACTTAATGGAGAGAGATC
	Reverse	AGTATGCATTGGCAAAGACTTTCC
Aqp2	Forward	CTGGCTGTCAATGCTCTCCAC
	Reverse	TTGTCACTGCGGCGCTCATC
Aqp8	Forward	TGTGTAGTATGGACCTACCTGAG
	Reverse	ACCGATAGACATCCGATGAAGAT
Atp2b4	Forward	GGATTGGAGAACTTTTGTGGG
	Reverse	ATCTCGGCAAGGTCAATCTC
Calcr	Forward	TTCCCGGACTTTGACACAGC
	Reverse	GTGAAAGCGTTGCACAGAGT
cre	Forward	GCTTGCATGATCTCCGGTAT
	Reverse	ATACCTGGCCTGGTCTGGA
Dsp	Forward	CTGGCAAACGAGACAAATCA
	Reverse	GATGCCAGCTGCAGTTCATA
Ephb2	Forward	ACGCCACGGCCATAAAAAGCCC
	Reverse	TTGCCACTGTAGCGCCCATAGC
Hk1	Forward	GAAAGGAGACCAACAGCAGAGC
	Reverse	TTCGTTCCTCCGAGATCCAAGG
Id1	Forward	ACCCTGAACGGCGAGATCA
	Reverse	TCGTCGGCTGGAACACATG
Jup	Forward	GCCCATCAAGGTGACAGAGTGG
	Reverse	GCAGGCATCATCCTCATCCATG
Kcnj10	Forward	CACCTTCGAGCCAAGATGAC
	Reverse	GGCCACAGCTACCAGATACC
Kim1	Forward	TGGTTGCCTTCCGTGTCTCT
	Reverse	TCTTCAGCTCGGGAATGCA
Ngal	Forward	GGCCTCAAGGACGACAACA
	Reverse	TCACCACCCATTCAGTTGTCA
Pvalb	Forward	GCTTCATTGAGGAGGATGAG
	Reverse	CCAGAGTGGAGAATTCTTCAAC
RetSat	Forward	GCGGCTGTTGTCATACCTTT
	Reverse	CCAAGATAAAACGGCCAATG
Scnn1a	Forward	CATGCCTGGAGTCAACAATG
	Reverse	CCATAAAAGCAGGCTCATCC
Sgk2	Forward	CCAATGGGAACATCAACC
	Reverse	CAGTAGGACCTTCCCGTAGT
Slc26a4	Forward	TCATTGCCTTTGGGATAAGC
	Reverse	GGCAACCATCACAATCACAG
Sphk2	Forward	CCCCGAGATGGTCTAGTCT
	Reverse	GTGGGTAGGTGTAGATGCAGA
Stk39	Forward	TGCCAGACCAGTATGGATGAA
	Reverse	GGTGTAATAGGTCACTACGTTGG
Trpv5	Forward	TCCTTTGTCCAGGACTACATCCCT
	Reverse	TCAAATGTCCCAGGGTGTTTCG

2.6 Experimental Animals and Husbandry

All experimental procedures in mice were approved by the Landesamt für Gesundheit und Soziales Berlin (State Office for Health and Social Affairs Berlin) under the number G 0130/17 and conducted in accordance with national and European guidelines for the proper conduct of animal experiments. Male and female C57BL/6J mice, aged between 12 and 42 weeks, were used in all experiments described. The mice were bred at the Forschungseinrichtung für Experimentelle Medizin (Research Facility for Experimental Medicine) of the Charité. Housing and experimental procedures were performed in their facility in the Center for Cardiovascular Research (CCR) of the Charité. At the CCR, mice were housed under standardized conditions, with room temperature of 22 ± 2 °C, humidity set to 60 ± 15%, and a 12 h day-and-night rhythm.

The mice were housed in cages of different sizes: type I with a maximum of three mice, type II with a maximum of five mice, and type III with a maximum of eight mice. Twice a week, trained personnel placed the animals into new cages, which contained the dry litter FS14/Fichte (Altromin Spezialfutter GmbH & Co. KG, Lage, DE) and to which objects were added for environmental enrichment. The animals were fed *ad libitum* with the standard diet V1124-300 (ssniff-Spezialdiaten GmbH, Soest, DE) and had free access to water.

2.7 Consumables

The employed consumables are listed in **Table 7**.

Table 7: Consumables

Consumable	Supplier
0.5 mL insulin syringe U-100 0.3 mm (30G) x 12 mm	B. Braun Melsungen AG (Melsungen, DE)
15 mL and 50 mL PP conical tubes	Corning Inc. (Corning, NY, USA)
Cannula Sterican (different sizes)	B. Braun Melsungen AG (Melsungen, DE)
Contour next glucose test strips	Ascensia Diabetes Care Holdings AG (Basel, CH)
Disposable scalpel	Feather Safety Razor Co., Ltd (Osaka, JP)

Filter paper	Bio-Rad Laboratories (Hercules, CA, USA)
FreeStyle precision pro β-ketone test strips	Abbott Laboratories (Chicago, IL, USA)
Hard-shell PCR plates 364 wells and 96 wells	Bio-Rad Laboratories (Hercules, CA, USA)
Microseal PCR plate sealing film, adhesive	Bio-Rad Laboratories (Hercules, CA, USA)
Microplate, 96-well, flat-bottom	Greiner Bio-One GmbH (Kremsmunster, AT)
PCR-tubes	neoLab Migge GmbH (Heidelberg, DE)
Pipette tips (10 µL, 200 µL, 1000 µL)	Sarstedt AG & Co. KG (Numbrecht, DE)
Polyvinylidene fluoride (PVDF) membrane	Bio-Rad Laboratories (Hercules, CA, USA)
Safe seal tube 1.5 mL	Sarstedt AG & Co. KG (Numbrecht, DE)
Safe seal tube 2 mL PP	Sarstedt AG & Co. KG (Numbrecht, DE)
Syringes without cannula (0.5 mL, 1 mL)	B. Braun Melsungen AG (Melsungen, DE)

2.8 Equipment

Table 8 contains a list of all equipment used.

Table 8: Equipment

Article/Device	Supplier
Analytical balance	Sartorius AG (Gottingen, DE)
AU480 chemistry analyzer	Beckman Coulter (Krefeld, DE)
Biofuge 13-R centrifuge	Heraeus (Berlin, DE)
Biofuge universal 32-R centrifuge	Heraeus (Berlin, DE)
Bruker minispec liver mice analyzer (LF50)	Bruker Optics, Inc. (Billerica, MA, USA)
CFX connect real-time PCR detection system	Bio-Rad Laboratories (Hercules, CA, USA)
Chemidoc imaging system	Bio-Rad Laboratories (Hercules, CA, USA)
ContourXT glucose meter	Ascensia Diabetes Care Holdings AG (Basel, CH)
Equipment for polyacrylamide gels	Bio-Rad Laboratories (Hercules, CA, USA)
Equipment for western blot	Bio-Rad Laboratories (Hercules, CA, USA)
Fiske single-sample micro osmometer, model 210	VWR (Radnor, PA, USA)

FreeStyle precision neo	Abbott Laboratories (Chicago, IL, US)
Heating plate MR 2002	Heidolph Instruments GmbH & Co.KG (Kelheim, DE)
Incubator	Heraeus (Berlin, DE)
TSE LabMaster Indirect Calorimetry System	TSE Systems (Chesterfield, MO, USA)
Microscope Keyence BZ-9000	Keyence (Neu-Isenburg,DE)
MiniSpin plus benchtop centrifuge	Eppendorf AG (Hamburg, DE)
Mortar and pestle	Self-made, stainless steel
NanoDrop ND-1000 spectrophotometer	PEQLAB Biotechnologie GmbH (Erlangen, DE)
PTC-200 peltier thermal cycler	Bio-Rad Laboratories (Hercules, CA, USA)
Restrainer rotating tail injector RTI	Braintree Scientific, Inc. (Braintree, MA, USA)
Rotamax 120 shaker	Heidolph Instruments GmbH & Co.KG (Kelheim, DE)
Thermomixer comfort	Eppendorf AG (Hamburg, DE)
Vortex genie 2	Scientific Industries, Inc. (Bohemia, NY, USA)
xMark microplate spectrophotometer	Bio-Rad Laboratories (Hercules, CA, USA)

2.9 Software

All the software used to obtain, analyze, process, and present data is listed in **Table 9**.

Table 9: Software

Software	Purpose	Supplier
CFX Manager, Software Version 3.1	qRT-PCR signal detection	Bio-Rad Laboratories (Hercules, CA, USA)
EndNote X9, software version 9.3.3	References management	Clarivate Analytics (Philadelphia, PA, USA)
GraphPad PRISM 9, software version 9.3.0	Scientific graphing and statistical analysis	GraphPad Software Inc. (San Diego, CA, USA)
Image J, software version 1.53k	Protein signal quantification	National Institutes of Health(Bethesda, MD, USA)

Image Lab, software version 6.1.0	Protein signal detection for western blot	Bio-Rad Laboratories (Hercules, CA, USA)
Keyence BZ-X analyzer software	Modification of microscope images	Keyence (Neu-Isenburg, DE)
Microplate Manager 6, software version 6.2	Measurement of colorimetric signals	Bio-Rad Laboratories (Hercules, CA, USA)
MS Office 2019	Data processing and presentation	Microsoft Corporation (Redmond, WA, USA)
ND-1000, software version 3.8.1	RNA quantification	Thermo Fisher Scientific Inc. (Waltham, MA, USA)
Primer blast	Design tool for primer	https://www.ncbi.nlm.nih.gov/tools/primer-blast/
R-Studio	Statistical computing and graphics	open source: https://www.r-studio.com
R-Project	Statistical computing and graphics	open source: www.r-project.org

3 Methods

3.1 Molecular Biological Methods

3.1.1 RNA Extraction from Kidney Tissue

RNA from kidney tissue was extracted and isolated using QIAzol and the QIAgen RNeasy kit. Approximately 50 mg of shock-frozen kidney tissue was homogenized in a homemade stainless-steel mortar that could be cooled down in liquid nitrogen. The powdered tissue was added into a safe-lock 2 mL Eppendorf tube containing 500 µL of QIAzol. Another 500 µL QIAzol was added, and the tube was inverted and incubated for 5 min at room temperature. Then, 200 µL of chloroform per 1 mL was added and vortexed thoroughly for approximately 20 sec, followed by centrifugation at 12,000 rpm for 15 min at 4 °C. 400 µL of the upper, aqueous phase containing nucleic acids was transferred into a fresh 1.5 mL tube. An equal volume of 70% ethanol was added and incubated for 10 min at room temperature to precipitate the RNA. 700 µL of the sample was applied to a QIAgen RNeasy spin column and the following isolation of RNA was performed according to the specifications provided in the manual. RNA was eluted with 40 µL RNase- and DNase-free water, the concentration was measured using a Nanodrop ND-1000 spectrometer and the samples were stored at -80 °C.

3.1.2 Complementary DNA (cDNA) synthesis

Each sample of 1 µg RNA, which had been calculated from the results of the NanoDrop ND-1000 measurement was mixed with 0.25 µg of random hexamer primer and ultrapure water to a volume of 15 µL. This mixture was heated to 70 °C for 5 min, and then cooled to 4 °C. A mixture consisting of 5.0 µL M-MLV reaction buffer (5x), 1.25 µL dNTP mix, 1.0 µL M-MLV reverse transcriptase, and 2.75 µL of ultrapure water to a total volume of 10 µL per sample was prepared and added to the samples as indicated in **Table 10**. This mixture was then incubated for 1 h at 37 °C and the synthesized cDNA samples were stored at -20 °C.

Table 10: Composition of Reverse Transcriptase Mixture for cDNA Synthesis

Reagent	Volume [µL]	Concentration
5x M-MLV reaction buffer	5.0	1x
dNTP mix [10 mM]	1.25	0.5 mM per dNTP
M-MLV reverse transcriptase [200 u/µL]	1.0	200 u
Ultrapure water	2.75	
Total volume	10	

3.1.3 Quantitative Real-Time Polymerase chain reaction (qRT-PCR)

The principle of this method is to amplify DNA by PCR and quantify it by adding a fluorescent dye that intercalates with the DNA. The fluorescence signal is then related to the PCR product. A standard curve has been generated for qRT-PCR. To obtain a 1:5 dilution in 220 µL ultrapure water, 5 µL of each cDNA sample was taken, mixed and used as the most concentrated sample for the standard curve. Three further 1:10 dilutions were made, resulting in four samples for the standard curve (100%, 10%, 1%, 0.1%). The remaining sample volume was diluted 1:10 with ultrapure water. For one sample, a mixture containing 0.1 µL forward primer for the target gene, 0.1 µL reverse primer for the target gene, 2.5 µL 2x Fast Start Universal SYBR Green Master (ROX) and 0.3 µL ultrapure water was prepared to a total volume of 3 µL as described in **Table 11**. This mixture and 2 µL of the diluted samples or standards were pipetted together onto a 384-well plate and measured with the CXF Connect Real-Time System using the appropriate program as described in **Table 12**. The standard curve allowed quantification of the relative levels of expressed mRNA in relation to the housekeeper genes, which are robustly expressed genes that are not normally regulated.

Table 11: Mixture for qRT-PCR

Reagent	Volume [µL]	Concentration
Forward primer [5 µM]	0.1	200 nM
Reverse primer [5 µM]	0.1	200 nM
2x fast start universal SYBR green master (ROX)	2.5	1x
Ultrapure water	0.3	
Total volume	3.0	

Table 12: Program for qRT-PCR

qRT-PCR	Temperature [°C]	Time	Cycles
Initial denaturation	95	10 min	1
Denaturation of DNA primer hybridization/ amplification	95	15 seconds	40
Annealing	60	1 min	40
Melting curve	95 60 → 95	30 seconds 30 seconds	1

3.1.4 Genomic DNA isolation and polymerase chain reaction (PCR)

Ear biopsies were collected and incubated overnight at 55 °C in tailcut-buffer containing Proteinase K (0.6 mg/mL). The samples were heated to 95°C for 10 min and then cooled to -20°C for a further 10 min. 400 µL TE buffer containing RNase A (1.3 µg/mL) was added to denature residual RNA. 1 µL of DNA solution was used as template for the PCR reaction. The volumes of the solutions used for the PCR process are listed in **Table 13**.

Table 13: Program for qRT-PCR

Reagent	Volume [µL]
5 x PCR master mix “ready-to-load”	4
Forward primer [10 µM]	0.8
Reverse primer [10 µM]	0.8
Ultrapure water	13.4
Total volume	19

The initial denaturation step of the PCR was 94°C for 2 min, followed by 35 cycles of 94°C for 15 seconds, 59.5°C for 1 min and 72°C for 1 min. Upon completion of the amplification cycles, a final step of 72°C for 5 min was performed. PCR samples were then stored at -20°C.

The following primer pair was used to identify the *RetSat* wild-type and floxed alleles: 5'-CTCCTTTTCTGAGGCTGGTG and 5'-AAGGCAGACCTTTCTTTTAAGG (wild-type allele 416 bp amplicon and floxed allele 539 bp amplicon) (**Figure 5A**). Primer sequences used to detect the Cdh16-promoter segment-driven Cre expression cassette were 5'-GCAGATCTGGCTCTCCAAAG and 5'-CCTCATCACTCGTTGCATCG (482 bp amplicon). The murine *myog* gene was used as an internal control for correct PCR amplification: 5'-TTACGTCCATCGTGGACAGC and 5'-TGGGCTGGGTGTTAGCCTTA (250 bp amplicon). To discriminate between C57BL/6N and C57BL/6J backgrounds, the murine *Nnt* gene was analyzed for exon 6: 5'-GGGTTTCGATTGCTGTCATT and 5'-AGTCAGCAGCACTCCTCCAT (170 bp amplicon) and exon 9: 5'-CCAGCATGCACTCTCTTCTG and 5'-TGGTCTCCAAGTGCACAGAG (418 bp amplicon). PCR products were separated on a 1% agarose gel and visualized using ROTI®GelStain (Carl Roth).

3.2 Protein Biochemical Methods

3.2.1 Isolation of Protein Extracts from Kidney Tissue

Approximately 50 mg of kidney were placed in 750 µL of ice-cold protein lysis buffer (RIPA) and were homogenized with a micro pestle, sonicated five times at the lowest intensity, and centrifuged for 30 min at 13,000 rpm and 4 °C. The supernatant was transferred into a new tube and stored at -80 °C.

3.2.2 Protein Concentration Measurement

Protein concentration was measured using the Pierce BCA protein assay kit. In this assay the protein reduces Cu^{2+} to Cu^{+}. In a second reaction, bicinchoninic acid forms a complex with Cu^{+} that can be detected photometrically. The manufacturer's instructions have been adapted. For the assay, the working reagent was prepared with the supplied reagents A and B in a 50:1 ratio. 5 µL of each standard and sample were pipetted into a flat-bottomed 96-well plate. Then 95 µL of the prepared working reagent was added and incubated at 37 °C for 30 min. The samples and the standard curve were measured in duplicate using a photometer at a wavelength of 562 nm. Using a standard curve, a relationship between the photometric signal and the protein concentration was determined and used to calculate the protein concentration of the samples.

3.2.3 Sodium Dodecyl Sulfate-Polyacrylamide Gel Electrophoresis (SDS-PAGE)

Table 14: Gel Preparation for SDS-PAGE

Reagent	10% separation gel	Stacking gel
ddH_2O	4.1 mL	3.05 mL
1.5 M TRIS HCL buffer pH 8.8	2.5 mL	-
0.5 M TRIS HCL buffer pH 6.8	-	1.25 mL
10% SDS solution	100 µL	50 µL
Acrylamide solution 30%	3.3 mL	0.65 mL
10% APS solution	75 µL	50 µL

TEMED	7.5 µL	6 µL

Separation of proteins according to their molecular weight by SDS-PAGE 1.5 mm thick polyacrylamide gels were prepared as shown in **Table 14** using the equipment provided. The gels were then placed in an electrophoresis chamber filled with electrophoresis buffer. 30 µg of protein was diluted in protein loading buffer containing β-mercaptoethanol to denature disulfide bonds in proteins, heated to 95 °C for five min, centrifuged at 13,000 rpm for three min at room temperature, and then loaded onto the gel along with a molecular weight size marker. SDS-PAGE was started at 80 V through the stacking gel and then increased to 120 mV.

3.2.4 Western Blot Analysis

After separating the proteins by SDS-PAGE, the proteins were transferred to a PVDF membrane for detection and analysis. The separation gel was placed on the PVDF membrane, which was activated in methanol for 1 min and sandwiched between filters and sponges. The cassette and a cooling unit were placed in the tank exactly as described in the manufacturer's manual. The tank was filled with transfer buffer and a voltage of 80 V was applied for 2 h while the tank was kept on ice, or 29 V overnight at 4 °C. After transfer, the membrane was washed three times for 5 min in ddH2O, air dried for at least 20 min, reactivated in methanol for 1 min, stained with 0.1% Ponceau S solution for 10 min and imaged using the BioRad ChemiDoc imaging system. The membrane was then destained by immersion in 0.1 M NaOH solution three times for 5 min, washed three times for 5 min in TBST buffer and blocked in 4% milk solution for 1 h. The membrane was incubated overnight at 4°C in a primary antibody solution containing the antibody to the protein of interest. After three 10 min washes in TBST, the membrane was incubated for 1 h at room temperature in a secondary antibody solution containing an HRP-conjugated antibody to the species of the primary antibody. The membrane was then washed three times for 10 min in TBST and the signal of the protein of interest was detected with enhanced chemiluminescence (ECL) Western blotting substrate solution according to the manufacturer's instructions. The signal was also detected using the Biorad ChemiDoc imaging system.

3.3 Histological Methods

3.3.1 Paraffin Embedding of Kidneys

Kidneys were rapidly excised, the renal capsule removed, sagittally sectioned and fixed in 4% formaldehyde solution in phosphate buffer at 4°C overnight. The next morning, the sections were dehydrated through a graded series of ethanol to acetone, embedded in paraffin and cut into 5 µm sections. Sections were deparaffinised in NeoClear and rehydrated in descending ethanol to ddH_2O before further staining.

3.3.2 Hematoxylin and Eosin Staining (H&E):

Sections were placed in Mayer's haemalaun solution, acidic, for 5 min, then rinsed in tap water for 5 to 10 min and cleared with ddH2O before adding a 0.5% Eosin Y solution for 30 seconds. Sections were placed in Mayer's haemalaun solution, acidic, for 5 min, then rinsed in tap water for 5 to 10 min and cleared with ddH_2O before adding a 0.5% Eosin Y solution. Sections were then rinsed in tap water, dehydrated in ascending ethanol to NeoClear and mounted in NeoMount media. Sections were allowed to dry for 24 h at room temperature in Y solution for 30 seconds. Sections were then rinsed in tap water, dehydrated in ascending ethanol to NeoClear and mounted in NeoMount media. Sections were left to dry for 24 h at room temperature.

3.3.3 Von Kossa Staining (modified):

Sections were incubated with silver nitrate solution (5%) for 30 min under UV light, rinsed with tap water and then incubated with sodium thiosulphate solution (5%) for 2 min. This was followed by rinsing and counterstaining with nuclear fast red solution for 2.5 min. Sections were rapidly dehydrated in two changes of absolute alcohol and a dip in NeoClear before mounting with NeoMount. Sections were left to dry for 24 h. Positive controls were a generous gift of Claudin 10 (Cldn10) knockout mice from Dr. Tilman Breiderhoff (Max Delbrück Center for Molecular Medicine). Images were taken on a Keyence BZ-9000 microscope.

3.3.4 Alizarin Red S stain

Sections were stained with alizarin red solution (2%) for 2 min, shaken off excess dye and dehydrated in acetone 20 times before addition to NeoClear and mounting in NeoMount. Sections were allowed to dry for 24 h. Positive controls were a generous gift from Dr. Felix Knauf and mice fed a high oxalate diet. Images were taken on a Keyence BZ-9000 microscope.

3.3.5 Immunhistochemistry

Antigen retrieval was performed using EDTA buffer. Sections were immersed in EDTA buffer for 30 min in a water bath heated to 94°C. Sections were rinsed with ddH2O, wash buffer and PBS before exposure to Image-iT at room temperature for 30 min. Sections were rinsed with PBS and blocked with PBS + 2% normal goat serum for 1 h. Diluted anti-RETSAT primary antibody 1/200 in PBS + 1% BSA and incubated overnight at 4°C. The next day, sections were rinsed with PBS and incubated with anti-rabbit Alexa 555 secondary antibody diluted 1/500 in PBS + 1% for 1 h. Sections were rinsed with PBS and incubated with DAPI diluted 1/1000 in PBS for five mi at room temperature. Sections were then rinsed with PBS and mounted using VectaMount AQ aqueous mounting medium. Images were captured using a Keyence BZ-9000 microscope. Images were taken at either 2x, 4x or 20x magnification.

3.4 Animal Experiments

3.4.1 Generation of C57BL/6J mice with kidney-specific knockout of *RetSat*

Mice with floxed *RetSat* alleles have been generated in our laboratory by Steffi Heidenreich. This was described in her Ph.D. thesis [102]. Briefly, loxP sites flanking exons 2 and 3 of *RetSat*, the gene encoding retinol saturase (RetSat), were introduced into the mouse genome by homologous recombination in embryonic stem cells. These exons encode for FAD or NAD/NADP binding domain and their deletion results in a premature stop codon (**Figure 4B).** In addition, it has been shown that mutations in this region of the binding domain result in a lack of activity of the enzyme [81]. Mice carrying the floxed allele were crossed with mice expressing Cre recombinase under the mouse Cdh16 promoter [B6.Cg-Tg(Cdh16-Cre)91Igr/J] [103, 104].

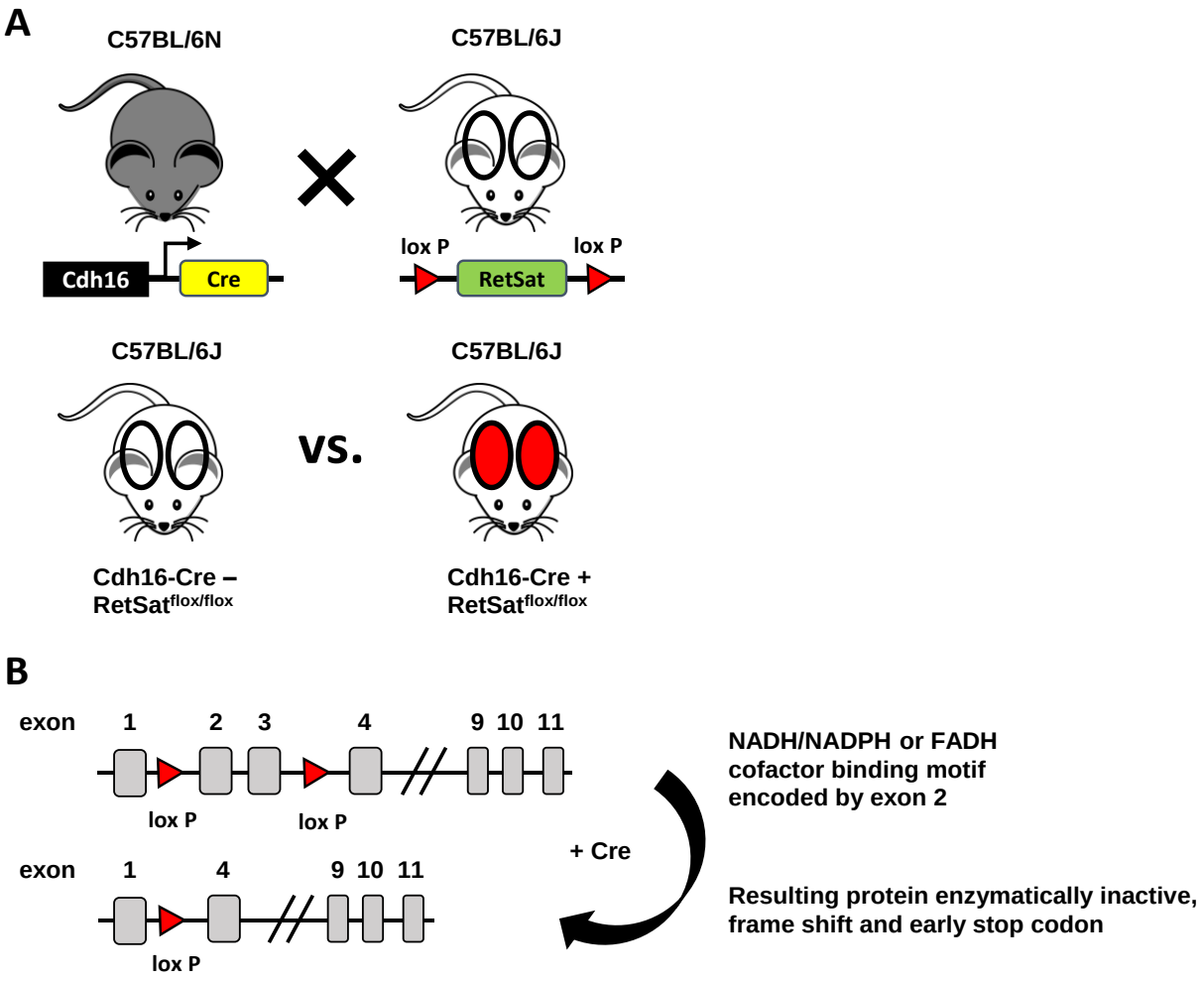

Figure 4: Experimental scheme for generating Cdh16-Cre RetSat$^{flox/flox}$ mice. (A) Breeding strategy and genetic background**. (B)** Cre-induced recombination of the floxed allele.

Dr. Tilman Breiderhoff generously provided the Cdh16-Cre animal on a C57BL/6N background (**Figure 4A**). C57BL/6J *RetSat*$^{flox/flox}$ mice were crossed with C57BL/6N Cdh16-Cre mice. This resulted in a mixed genetic background. To obtain mice with a C57BL/6J background, which are highly susceptible to develop insulin resistance and obesity when fed a high-fat diet [105, 106], backcrossing was performed over at least 4 generations. To ensure the correct background, exon 9 of *Nnt* gene was analyzed by PCR, which has been shown to be deleted exclusively in C57BL/6J mice [107]. Two founder animals with a deletion of exon 9 in the *Nnt* gene were selected for breeding (**Figure 5B**). After breeding to homozygosity for the floxed allele (*RetSat*$^{flox/flox}$), mice carrying Cdh16-Cre transgene (Cre (+)) were used for experiments. Littermates without the transgene (Cre (-)) were used as controls.

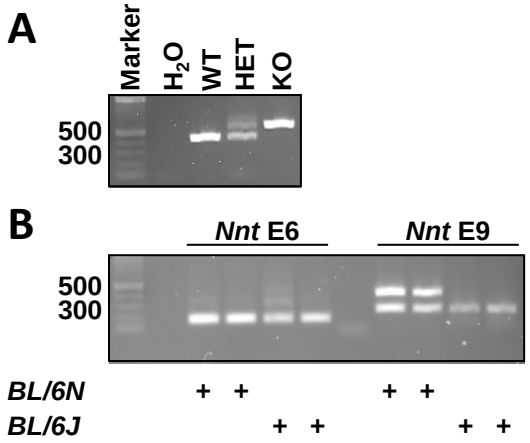

Figure 5: Verification of genetic background. (A) Cdh16-Cre background, WT = wild type, HET = heterozygous, KO = homozygous **(B)** C57BL/6J background, *Nnt* E6 = *Nnt* exon 6, *Nnt* E9 = *Nnt* exon 9.

3.4.2 Body Weight Measurement

Mice on NC and HFD were weighted weekly within the same daytime and day to have consistent measurements. On the day of euthanization mice were weighted.

3.4.3 24 h Food Intake

Mice were single housed for 24 h. Measurement of food intake for mice on NC were conducted at the age of 38 weeks. Food intake measurement for mice on HFD was performed between the age of 22 - 23 weeks. The amounts of food at the beginning and at the end were measured by weighting them on a scale. Then, the differences between both timepoints were calculated.

3.4.4 Organ and Tissue Weight

Organs and tissues were weighed immediately after sacrifice on the day of euthanasia on pre-calibrated aluminium foil. Organs and tissues were then snap frozen in liquid nitrogen and stored at -80° C. Weights were determined using an analytical balance with an accuracy of 0.1 mg.

3.4.5 Blood Glucose Measurement

Blood glucose was measured before and after the 16 h fasting experiment and on the day of euthanasia. Blood was collected by gently scratching the tail with a scalpel, discarding the first drop of blood and immediately applying the blood to a blood glucose test strip to measure concentrations in duplicate. If there was a deviation of more than 10%, another measurement was performed. Blood glucose was always measured at the same time of day.

3.4.6 Ketone Bodies Determination

Ketone bodies were measured before and after the 16 h fast. Blood was collected by gently scratching the tail with a scalpel, discarding the first drop of blood and immediately applying the blood to a ketone body test strip to measure concentrations in duplicate. If there was a deviation of more than 10%, another measurement was performed. The ketone body concentration was always measured at the same time of day.

3.4.7 Analysis of Serum and Urinary Parameter

Analysis of serum and urinary parameter was conducted at the Mouse Phenotyping Platform at the Max-Delbrück-Center in Berlin-Buch. Measurement of Ca^{2+}, Mg^{2+}, inorganic phosphate (Pi), urea, creatinine, urinary protein, urinary albumin and glucose in serum and urine was performed with an AU480 Chemistry Analyzer. Additionally, Na^{+}, K^{+} and Cl^{-} were measured with ion-selective electrodes. First, mass

concentrations for urinary Na^+, K^+ and Cl^- molar concentrations were calculated with following formula:

$$mass\ concentration\ \left[\frac{g}{L}\right] = \left(\frac{molar\ concentration\ (analyte)\left[\frac{mM}{L}\right]}{1000}\right) \times molecular\ weight\ (analyte)\left[\frac{g}{M}\right]$$

Afterwards, mass concentrations of all urinary analytes were used to calculate the excreted amount considering the urinary output over a period of 24 h:

$$amount\ excreted\ in\ 24h\ [mg] = \left(\frac{mass\ concentration\ (analyte)\left[\frac{g}{L}\right]\ \times\ urinary\ volume\ [\mu L]}{1000000}\right) \times 1000$$

For some specific analytes, the fractional excretion (FE) that represents the percentage of analyte filtered by the kidney and excreted in the urine, could be calculated with following formula:

$$FE(analyte)[\%] = 100\ \times \left(\frac{urinary\ concentration\ (analyte) \times serum\ concentration\ (creatinine)}{urinary\ concentration\ (creatinine) \times serum\ concentration\ (analyte)}\right)$$

3.4.8 24 h urine Collection and Sample Preparation

To collect urine and measure urine volume and water intake, mice were placed individually in metabolic cages (Tecniplast, Italy) for 24 h. Metabolic cages for 24 h urine collection consist of a circular upper part that accommodates the mouse, a wire mesh floor and a collection chamber with a special funnel that separates faeces and urine drops that fall into a 15 mL Falcon collection tube filled with paraffinum perliquidum to reduce evaporation. Mice were given *ad libitum* access to water and food unless otherwise stated. In addition, mice were provided with a red plastic house for environmental enrichment and retreat. To ensure equal experimental conditions and to minimise variation between cohorts, mice were placed in metabolic cages at 9:00 am and removed at 9:00 am the following day. Metabolic cages were cleaned with tap water and rinsed three times with ddH_2O before being used for the next experiment to wash out any residues.

After 24 h, urine was immediately placed on ice and the aqueous urine phase was transferred to 2 mL Eppendorf tubes for centrifugation at 13.000 rpm for 5 min at 4 °C. Urine volume was determined and samples were aliquoted for long-term storage at -80°C or for osmolality analysis at 4°C. 200 µL were used for urinary parameter analysis at the Animal Phenotyping Platform at the Max-Delbrück-Center Berlin-Buch, 120 µL for pH determination and 60 µL for osmolality measurement.

3.4.9 Determination of Osmolality

For osmolality measurement, thawed 24 h urine samples stored at 4 °C were placed in a Fiske 210 single-sample micro-osmometer using freezing point depression. Measurements were expressed as mOsm/kg H_2O.

3.4.10 Serum Collection

On the day of euthanasia, mice were deeply anaesthetised with isoflurane before being sacrificed by a final cardiac puncture in which approximately 500 to 900 µL of whole blood was collected from the heart using a 1 mL syringe and a 26 G needle. Whole blood was incubated for 1 h at room temperature before centrifugation at 3.000 rpm for 15 min at 4°C. 120 µL of serum was transferred to tubes for the mouse phenotyping platform, while the remaining serum was aliquoted. All samples were immediately stored at -80° C.

3.4.11 Nuclear Magnetic Resonance (NMR) Analysis

For NMR analysis, mice were scanned using the Bruker Minispec Live Mice Analyzer LF50 (Bruker Optics, Inc.). This time domain nuclear magnetic resonance (TD-NMR) system detects signals generated by hydrogen spins from soft tissues such as muscle and fat. It uses the contrast in hydrogen spin relaxation times, duration or amplitude and spatial distribution of these NMR signals from different tissues to estimate body composition [108]. On each experimental day, NMR measurements were performed on adult mice (aged 8-36 weeks) on either NC or HFD at approximately 10 am. Prior to measurement, a quality control was performed using a standard provided by the manufacturer. Animals were placed in an orange plastic cylinder and immobilised by

inserting a tight-fitting plunger into the cylinder. The cylinder was then lowered into the sample chamber of the instrument for approximately 1 to 2 min. The values obtained were analyzed using internal software and exported to Excel.

3.4.12 Activity and Calorimetric Analysis

Several phenotypic parameters were assessed in metabolic cages of a TSE LabMaster system (TSE Systems, Bad Homburg, Germany). Mice were acclimated to special water bottles for 24 h prior to measurement. Mice were fed either NC or HFD during the 72 h measurement period. After a 24 h acclimation period, data on gas exchange, activity and food/water intake were collected from individually housed mice for 48 h. Calorimetric measurements were performed using a computer-controlled open-circuit calorimetry system consisting of 10 metabolic/respiratory cages. Each cage was equipped with a special water bottle and food dish connected to a balance and an activity monitor. Oxygen consumption and carbon dioxide production were measured in each cage at 3 min intervals. The RER was calculated as the ratio of CO_2 production to O_2 consumption. Energy expenditure (EE) was adjusted either to lean body mass for animals on NC [109] or to body weight$^{0.75}$ for mice on HFD. Data collected after 48 h were analyzed as a daily average and presented as light and dark phases.

3.4.13 Intraperitoneal Glucose Tolerance Test (ipGTT)

Basal glucose and ketone body concentrations were measured by tail scratch with a scalpel before the HFD mice were fasted overnight for 16 h. After 16 h, glucose and ketone body concentrations were measured again and used as t = 0 for glucose concentration. After determination of t = 0, mice were injected intraperitoneally with a glucose bolus of 0.5 mg/kg body weight in sterile 0.9% NaCl. Blood glucose was then measured at 15, 30, 60 and 120 min.

3.4.14 Intraperitoneal Insulin Tolerance Test (ipITT)

Basal glucose concentration was measured by tail scratch with a scalpel before mice on HFD were fasted for 4 h from 10 am. After 4 h of fasting, blood glucose was measured and used as t = 0. After determination of t = 0, mice were injected intraperitoneally with 0.75 U/kg body weight of insulin in sterile 0.9% NaCl. Blood glucose was then measured at 15, 30, 60 and 120 min.

3.4.15 Fasting Experiment with Mice on NC

Basal glucose and ketone body concentrations were measured by tail scratch with a scalpel before mice on NC (40 weeks of age) were fasted overnight for 16 h. After 16 h, glucose and ketone body concentrations were measured again.

3.5 Proteomics

To understand the phenotype of increased protein excretion in adult *RetSat* knockout mice and to identify specific proteins responsible for this effect, we performed a label-free proteomics approach. Eight samples of each genotype were selected for analysis using the proteomics platform at the Max-Delbrück-Center in Berlin-Buch. Protein concentrations were determined using the BCA assay.

3.5.1 Sample Preparation Protocol

Acetone precipitates were resolved in 8 M urea digestion buffer. Reduction (10 mM DTT) and alkylation (40 mM CAA) were performed before trypsin/LysC digestion (ratio 1:50) overnight. The desalting step was performed using StageTips. 2 µg of peptides per sample were used for MS analysis (label free). A 1.9 µM C18 column with a 44 min gradient was used together with a data-independent acquisition method on a Q Exactive HF-X Hybrid Quadrupole-Orbitrap Mass Spectrometer (Thermo Fisher Scientific, USA).

3.5.2 Proteomics Data Analysis

The analysis of the proteomics data was performed by the Proteomics Core Facility at the Max-Delbrück-Centre. R-Project (v4.2.1) was used for the analysis of the obtained proteomics data. Impurities were excluded, proteins with more than 50% valid values were selected and a down-shift imputation for missing values was performed. For comparison between the two genotypes, a moderate t-test from the limma package, a Fisher exact test for enrichment and Benjamini-Hochberg correction for multiple testing were used. Quantification was performed by label-free quantification using the MaxLFQ algorithm.

3.6 RNA-Sequencing library preparation and sequencing

RNA sequencing library preparation and sequencing was performed at the BIH Core Facility Genomics, Charité Berlin. 5 whole kidney tissue samples of each genotype, Cre (-) & Cre (+), were used for bulk RNA sequencing, which was obtained as described in section 3.4.4. To digest residual DNA, kidney samples were treated with the RNA Clean & Concentrator Kit (Zymo Research, USA). RNA integrity was assessed using the RNA ScreenTape System (Agilent, USA). The poly(A) selection method was used to capture only mRNA for further processing. Library preparation was performed using the NEBNext Ultra II RNA Library Prep Kit and Module (New England Biolabs, USA). Sequencing was performed on a NovaSeq 6000 system using a paired-end approach (2x51 cycles).

3.6.1 Data Processing and evaluation

Sequencing data processing was performed by the BIH Core Facility Genomics, Charité Berlin. Data were trimmed using the trimmomatic tool, mapped to the mouse genome (mm39) and annotated with ensemble annotation (GRCm39) using the STAR method (v. 2.7.6). The FeatureCounts method was used to count the reads. R-Studio (v2022.02.3+492) together with R-Project (v.4.2.1) and the publicly available DESeq2 package with default parameters were used to process the mapped counts from FeatureCounts. Lists of differentially expressed genes with Ensembl annotation, gene

symbol, log2 FC, p-value and p-value adjusted (padj.) were generated using the DESeq2 package and correction for multiple testing using the Benjamini-Hochberg procedure with default parameters. Volcano plots were generated using the EnhancedVolcano package (v1.14) and heatmaps using the heatmap function of the ggplot2 package in R-Studio.

3.7 Statistical analysis

Statistical tests are described in the figure legends. Results of animal experiments were expressed as means and the standard error of the mean (SEM) was calculated. Animal experiments were not randomised or blinded to conditions. After testing for normal distribution, statistical analysis was performed using either Student's t-test or two-way analysis of variance (ANOVA) to test for significance between the two genotypes. In the case of proteomics and RNA sequencing analysis, the Bonferroni correction was applied to reduce the false discovery rate. Grubb's test was used to test for outliers. Statistical analyses were performed using either GraphPad Prism or R-project/R-Studio.

4. Results

4.1 RetSat is highly expressed in the murine kidney

In humans, *RETSAT* mRNA expression is highest in fat tissue (181.366 RPKM) followed by the duodenum (77.197 RPKM) and the small intestine (67.462 RPKM), whereas expression in the liver (37.132 RPKM) and kidney (31.965 RPKM) is lower but comparable (**Figure 6A**) [1]. In contrast to human *RETSAT* expression, murine *RetSat* is highly expressed in liver (119.069 RPKM) and kidney tissue (90.037 RPKM) with lower expression patterns in the genital fat pad (22.564 RPKM) (**Figure 6B**) [2].

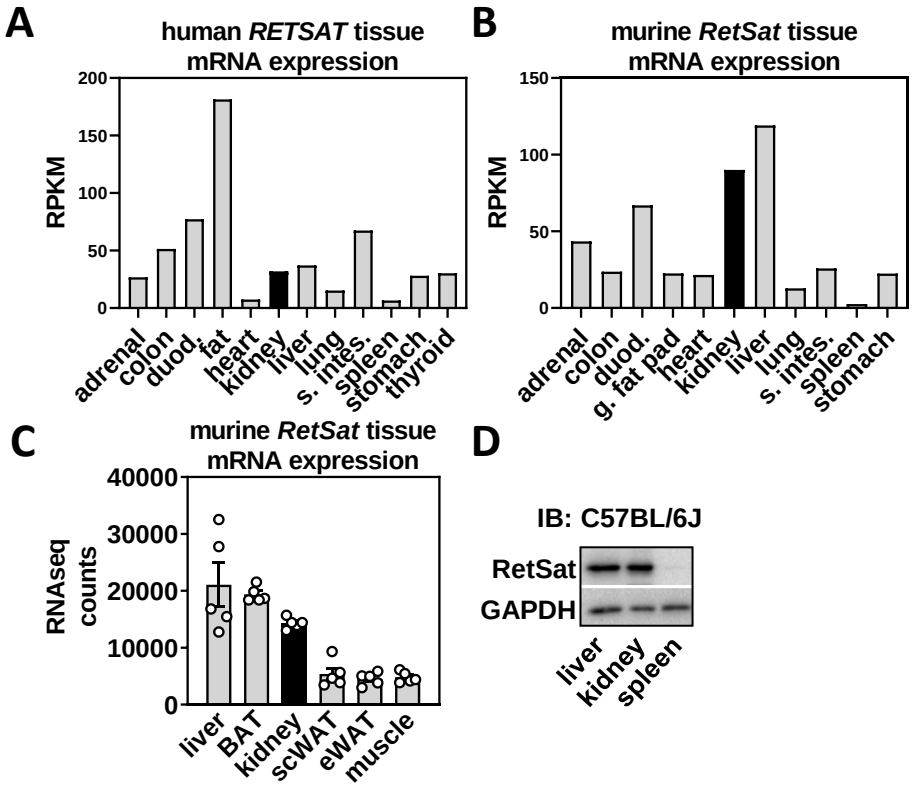

Figure 6: RetSat is highly expressed in the murine kidney. (A) RPKM of human *RETSAT* in different tissues modified by [1]. **(B)** RPKM of murine *RetSat* in different tissues modified by [2]. **(C)** RetSat mRNA expression in different tissues represented as RNAseq counts, 5 adult mice on NC, data are shown as mean ± sem (n = 5). **(D)** Liver, kidney, and spleen protein lysates were analyzed by immunoblotting for the protein expression of RETSATand GAPDH in a C57BL/6J mouse. RPKM = reads per kilobase of transcript per million, duod. = duodenum, s. intes. = small intestines, g. fat pad = genital fat pad, BAT = brown adipose tissue, scWAT = subcutaneous white adipose tissue, eWAT = epididymal white adipose tissue.

Previously generated RNA-Seq data from our working group in male C57BL/6J mice showed similar levels of *RetSat* mRNA expression in liver and brown adipose tissue (BAT) with a slightly lower expression in kidney (**Figure 6C**). Consistent with these data, we could demonstrate a comparably high expression of RETSAT in kidney and liver tissue at the protein level, whereas only a low expression was detected in spleen tissue (**Figure 6D**).

In the physiological state, RetSat appears to be highly expressed in metabolically active tissues such as liver, adipose tissue, and kidney.

4.2 *RetSat* is differentially expressed in distinct parts of the nephron and upregulated in the kidney in the fasting state in mice on NC

Histological images of the kidney from the International Mouse Phenotyping Consortium (www.mousephenotype.org) using the lacZ reporter gene from male and female mice at 38 weeks of age showed the expression of *RetSat* in renal tubular epithelial cells (**Figure 7A, right panel**) [110]. Furthermore, β-galactosidase staining revealed an accumulation of *RetSat* in the transition zone between the renal cortex and the outer stripe of the outer medulla and a lower expression profile in other parts of the mouse kidney (**Figure 7A, left panel**). Several studies using single-cell sequencing in mice [111, 112] and RNA-seq analysis of microdissected renal tubule segments from rats and mice have shown a differential expression pattern of *RetSat* along the nephron [5, 113]. *RetSat* transcripts showed a consistently high expression in the proximal tubules, with a slightly lower expression in the thick ascending limb of the loop of Henle (TAL), the distal convoluted tubules (DCT), and the connecting tubule (CNT) in the rodent datasets (**Figure 7B**).

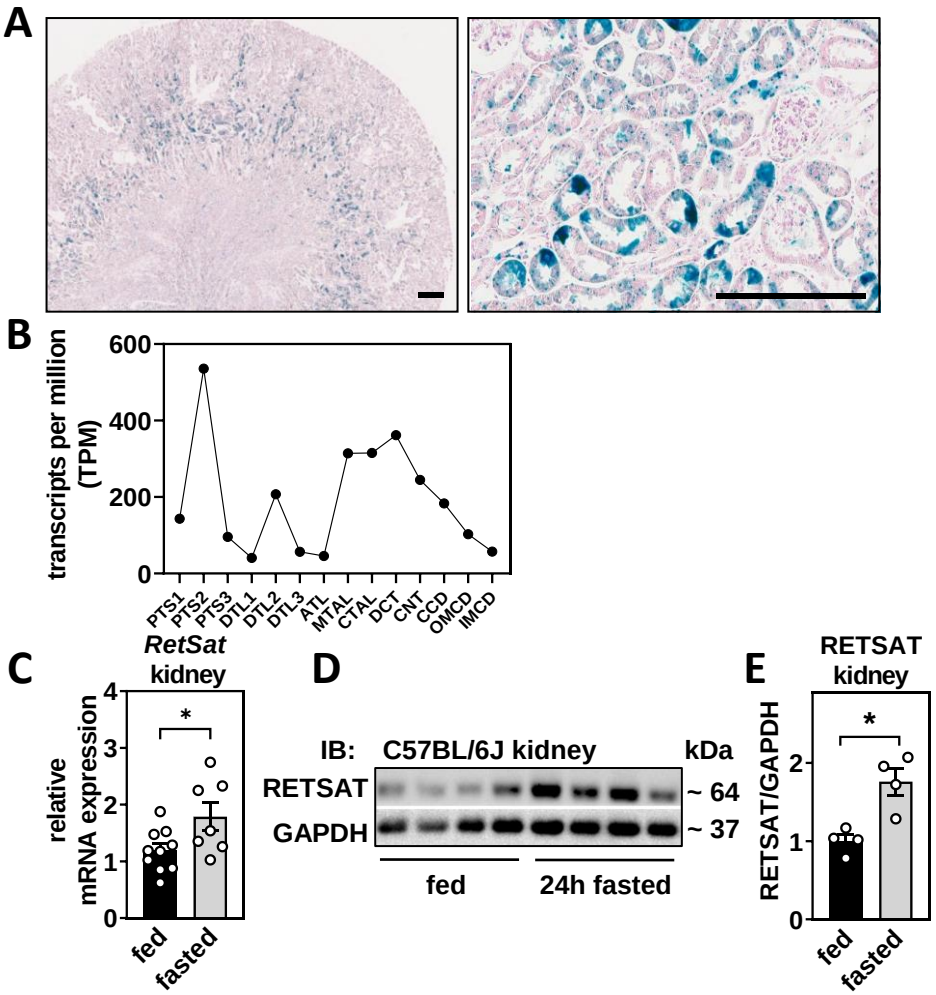

Figure 7: *RetSat* is differentially expressed in distinct parts of the murine nephron and upregulated in the kidney in the fasting state under normal chow. (A) Kidney sections of 38-week-old female (left panel) and male (right panel) mice were stained with X-gal to identify lacZ-positive *RetSat* expressing renal tubular epithelial cells, scale bars = 200 µm (left & right panel), adapted from international mouse phenotyping consortium. **(B)** *RetSat* expression of all renal tubule segments from microdissected mouse kidney expressed as transcripts per million (TPM) and adapted from [5]. **(C)** Relative mRNA expression of *RetSat* determined by qPCR in whole kidney lysates in the fed state vs. 24 h fasting in 38 – 42 week-old male mice (n = 10,7). **(D)** Immunoblot analysis of *RetSat* protein levels in whole kidney lysates of C57BL/6J mice in the fed or 24 h-fasted state with GAPDH as a loading control (n = 4,4). **(E)** Densitometric analysis of RETSAT protein levels in the fed or 24 h-fasted state (n = 4,4). Data are represented as individual data points and mean ± sem. *P-value < 0.05 by two-tailed t-test. PTS1 – 3 = proximal tubules segments 1 – 3, DTL1 = thin limbs of Henle's loop (the short descending limb of the loop of Henle, DTL2 = long descending limb of the loop of Henle in the outer medulla, DTL3 = long descending limb of the loop of Henle in the inner medulla, ATL = thin ascending limb of the loop of Henle, MTAL = thick limbs (medullary thick ascending limb of the loop of Henle, CTAL = cortical thick ascending limb of the loop of Henle, DCT = distal convoluted tubule, CNT = connecting tubule, CCD = cortical collecting duct, OMCD = cortical collecting duct, IMCD = inner medullary collecting duct.

The high expression of *RetSat* transcripts in the proximal tubules, the previously reported PPAR α-dependent upregulation of mRNA levels in mouse liver under 72 h food deprivation [88], and its differential expression in insulin resistance datasets [86] suggest a possible role in renal gluconeogenesis. The presence of a specific enzyme,

glucose-6-phosphatase (G6p), is known to be critical for gluconeogenesis in the liver, intestine and kidney of rodents [114-116] and humans [117, 118]. The exclusive expression of G6p in renal proximal tubules [119], the same subcellular localization in the ER [120] as *RetSat* [77, 81], and the transcriptional upregulation of RetSat in gluconeogenic tissues under prolonged starvation [88] suggest a functional link between RetSat and gluconeogenesis. To test whether the regulation of *RetSat* occurs only after prolonged fasting (72 h), we performed food deprivation experiments for a shorter period of 24 h. Therefore, male C57BL/6J mice on NC, 12-14 weeks old, were fasted for a period of 24 h. After sacrifice, whole kidney tissue samples were prepared as described in **section 3.4.4** for subsequent RNA and protein analysis. Consistent with previous findings, the relative mRNA expression of *RetSat* was upregulated by approximately 50% in the fasted state (**Figure 7C**). Furthermore, Western blot analysis confirmed the induction of RETSAT expression at the protein level by 75%, calculated by a densitometric approach using ImageJ (**Figure 7D & E**).

The increased expression of RetSat in metabolically active organs and the studies conducted to date in mouse liver, adipose tissue and differential expression in response to metabolic challenges may suggest a role for RetSat in the development of metabolic diseases. The specific function of RetSat in the kidney is completely unknown. To investigate this specific function, we generated a conditional knockout model with kidney-specific deletion of *RetSat* in C57BL/6J mice.

4.3 Generation and validation of kidney-specific Knockout of *RetSat* in C57BL/6J mice

Male C57BL/6J mice with two loxP sites flanking exons 2 and 3 of the *RetSat* gene were generated by homologous recombination of embryonic stem cells (ESC) as described in Steffi Heidenreich's thesis [102]. These exons encode the NADP(H) or FADH binding motif and their deletion is predicted to result in a premature stop codon, thereby inactivating the enzymatic activity. The expression of Cre recombinase is required to induce conditional excision of DNA segments [121]. Mice carrying the floxed allele were bred to mice expressing Cre recombinase under the control of the murine cadherin-16 promoter (Cdh16-Cre). The Cdh16-Cre transgene has been shown to be expressed exclusively in renal tubular epithelial cells in the adult kidney,

with highest expression in the loop of Henle and distal segments of the nephron, but with weak expression in Bowman's capsule and the proximal tubule [103, 104]. Female mice homozygous for the floxed *RetSat* allele were bred with male Cdh16-Cre positive mice to produce *RetSat*$^{flox/flox}$/Cdh16-Cre + mice (referred to as Cre (+) mice). The littermates with *RetSat*$_{flox/flox}$/Cdh16-Cre - genotype were used as control and referred to as Cre (-) mice. For basic phenotyping and characterization, adult male and female animals aged between 12 and 16 weeks, were used.

.

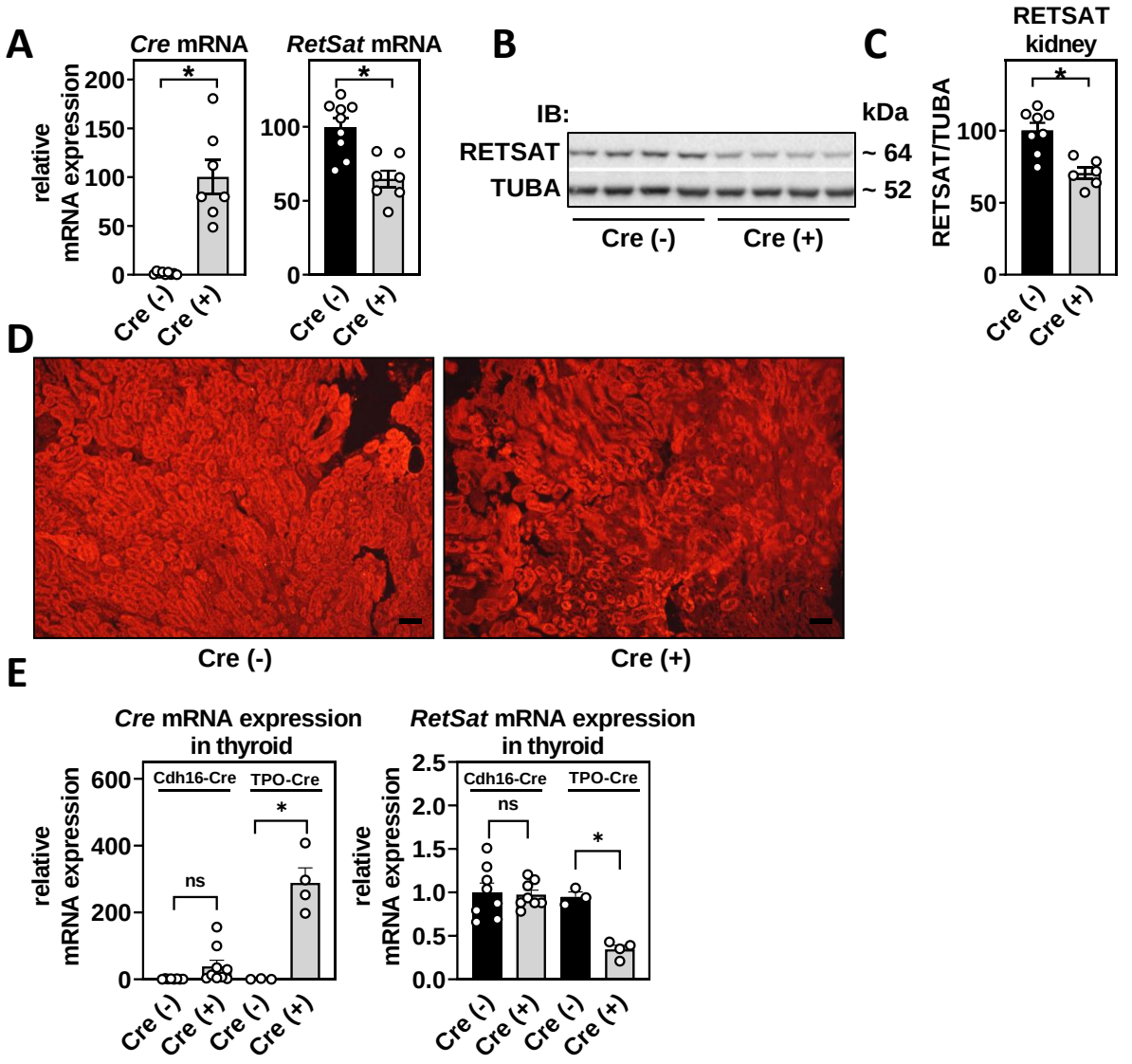

Figure 8: Generation and validation of kidney-specific knockout of *RetSat* in C57BL/6J mice. (A) Relative mRNA expression of Cre recombinase (left panel) and *RetSat* (right panel) determined by qPCR in whole kidney tissue 12 – 14 week-old male mice (n = 9,7). **(B)** Immunoblot analysis of RETSAT protein levels in whole kidney tissue of Cre (-) and Cre (+) male mice (n = 4,4). **(C)** Densitometric analysis of RETSAT protein levels in kidneys of male mice (n = 8,6). **(D)** RETSAT immunohistochemical staining in murine kidney slides with a partial deletion in renal tubular epithelial cells of Cre (+) male animals, scale bars = 200 µm. **(E)** Relative mRNA expression of Cre recombinase (left panel) and *RetSat* (right panel) determined by qPCR in thyroid tissue of 12 – 14 weeks old in Cdh16-Cre and TPO-Cre male mice, Cdh16-Cre (n = 8,9), TPO-Cre (n = 3,4). Data are represented as individual data points and mean ± sem. **P*-value < 0.05 by two-tailed t-test, ns = not significant.

Cre (+) mice were born at normal Mendelian ratios, were viable, fertile, showed no obvious growth defects and were phenotypically indistinguishable from Cre (-) littermates. An expected and strong increase in the relative mRNA expression of Cre recombinase was observed in Cre (+) animals compared to their Cre (-) littermates (**Figure 8A**). In Cre (+) mice, the relative expression of *RetSat* mRNA was reduced by approximately 35% (**Figure 8A**), while Western blot analysis confirmed the reduction of RETSAT protein by ~35% (**Figure 8B/C**).

To identify the expression of *RetSat* along the nephron in the mouse kidney, immunohistochemical staining was performed using an antibody directed against RETSAT in adult male Cre (-) and Cre (+) mice. As shown in **Figure 8D**, RETSAT was highly expressed in renal tubular epithelial cells in the mouse kidney, with differences in fluorescence intensity in Cre (-) mice. Compared to their Cre (-) littermates, sections from Cre (+) mice showed a mosaic-like reduction in the fluorescence intensity of RETSAT protein (**Figure 8D, right panel**). Thus, Cdh16-driven Cre expression resulted in the deletion of RetSat in some, but not all tubular epithelial cells.

Cdh16 was thought to be exclusively expressed in the kidney and the developing urogenital tract [122, 123]. Based on this assumption, Shao *et al*. generated the transgene construct of the Cdh16 promoter coupled to Cre recombinase in 2002 [103, 104]. Since then, published data have shown that RETSAT is expressed in the human thyroid (**Figure 6A**). Furthermore, Calí *et al*. demonstrated that Cdh16 is expressed in the basolateral membrane of developing thyroid follicular cells [124, 125]. Expression of Cdh16-Cre recombinase could have a significant impact on *RetSat* expression in thyroid cells and lead to unexpected thyroid-related phenotypes in our mouse model. To ensure that the phenotypes observed in our mouse model were related to the kidney-specific knockout of *RetSat*, we examined the relative mRNA expression of *RetSat* and Cre recombinase in the thyroid of mice with the Cdh16-Cre genotype. To compare expression levels, we used thyroids from age-matched transgenic mice carrying a thyroid-specific Cre recombinase fused to the thyroid peroxidase promoter (TPO-Cre) [126]. To compare gene expression levels in both mouse lines, equal amounts of cDNA were prepared and analyzed by qPCR.

As shown in **Figure 8E**, left panel, Cdh16-Cre expression in thyroids of Cre (+) animals is at background levels, while there was no statistical significance when compared to their Cre (-) littermates. Thyroids of TPO-Cre mice show strong mRNA expression of Cre recombinase, which was significantly different in Cre (+) animals compared to their Cre (-) littermates. In addition, the expression level of Cre recombinase was almost 100 times higher in the thyroids of TPO-Cre (+) mice compared to Cdh16-Cre (+) mice. Accordingly, *RetSat* expression levels in Cdh16-Cre mice did not differ between the two genotypes, whereas expression in TPO-Cre mice showed a significant reduction of ~ 60% at the mRNA level (**Figure 8E, right panel**).

We have generated and validated a novel transgenic mouse model with kidney-specific knockout of *RetSat*. The reduction of *RetSat* at the mRNA level by ~35% is consistent with the reduction at the protein level and could be further verified by immunohistochemistry. The shown knockout efficiency of *RetSat* in the whole kidney is consistent with the fact that RetSat expression is not only restricted to tubular epithelial cells but RetSat is present in other cell types and that the Cdh16-Cre recombinase has been shown to be inefficient for certain tubular cells within the kidney [104]. Furthermore, we were able to show that Cre (+) mice have a partial *RetSat* deletion in tubular cells of the kidney but not in thyroids.

4.4 Adult *RetSat*-deficient mice on normal chow show comparable body and organ weights

In a transgenic mouse model with germline deletion of *RetSat*, adult male mice lacking *RetSat* have been shown to have increased adiposity and higher body weight on NC [94, 97]. Therefore, we were interested in the body and organ weights of animals on NC with a kidney-specific deletion of *RetSat.* Adult male and female mice aged 12-14 weeks were sacrificed and organ weights and body weights were determined.

The body weights of Cre (+) adult male mice showed no difference compared to their Cre (-) littermates. Further evaluation of organs and epididymal white adipose tissue showed no significance in either genotype, either in absolute weights or relative to body weight (**Table 15**). In adult female mice, Cre (+) animals had a comparable body

weight compared to their Cre (-) littermates. The other absolute and relative organ weights showed no significant difference in both genotypes (**Table 16**).

Table 15: Body and organ weights of male adult animals on NC

	Cre (-)	**Cre (+)**	***n***	**sex**
body weight (BW), g	29.5 ± 0.3	29.3 ± 0.4	12/14	m
organ weight (OW), mg				
kidneys	182.9 ± 4.4	178.1 ± 4.5	12/14	m
liver	1571.2 ± 53	1596.6 ± 40	12/14	m
spleen	91.1 ± 6.4	79.3 ± 2.4	12/14	m
heart	157.4 ± 6.0	146.9 ± 3.2	12/14	m
eWAT	325.3 ± 19.0	365.6 ± 19.8	12/14	m
relative organ weight (OW/BW)				
kidneys, %	0.6 ± 0.0	0.6 ± 0.0	12/14	m
liver, %	5.3 ± 0.2	5.5 ± 0.1	12/14	m
spleen, %	0.3 ± 0.0	0.3 ± 0.0	12/14	m
heart, %	0.5 ± 0.0	0.5 ± 0.0	12/14	m
eWAT, %	1.1 ± 0.0	1.3 ± 0.0	12/14	m

Table 16: Body and organ weights of female adult animals on NC

	Cre (-)	**Cre (+)**	***n***	**sex**
body weight (BW), g	21.5 ± 0.3	22.2 ± 0.5	9/8	f
organ weight (OW), mg				
kidneys	123.0 ± 2.3	120.8 ± 3.8	9/8	f
liver	1149 ± 31	1158 ± 33	9/8	f
spleen	71.0 ± 2.5	74.4 ± 4.5	9/8	f
heart	108.8 ± 2.9	110.2 ± 4.5	9/8	f
eWAT	201.2 ± 20.5	167.9 ± 27.6	9/8	f
relative organ weight (OW/BW)				
kidneys, %	0.6 ± 0.0	0.5 ± 0.0	9/8	f
liver, %	5.3 ± 0.1	5.2 ± 0.1	9/8	f
spleen, %	0.3 ± 0.0	0.3 ± 0.0	9/8	f
heart, %	0.5 ± 0.0	0.5 ± 0.0	9/8	f
eWAT, %	0.9 ± 0.1	0.7 ± 0.1	9/8	f

4.5 Adult *RetSat*-deficient mice on NC exhibit no detectable impairment in renal morphology or function.

To assess renal morphology in adult male mice aged 12-14 weeks, hematoxylin and eosin (E&H) sections of kidneys were examined by light microscopy. The H&E-stained images shown in **Figure 9A** are representative of kidney sections examined from at least three different animals per genotype. Cortical and medullary structures and the collecting duct were intact, and we observed no evidence of morphological changes or alterations in Cre (+) mice compared to their Cre (-) littermates.

Blood urea nitrogen (BUN), serum creatinine and creatinine clearance are widely used to assess renal function in humans and mice [127-130]**.** These parameters were measured in five 12-14 week-old male mice per genotype. As shown in **Figure 9B**. BUN concentration was slightly but not significantly reduced in Cre (+) mice. Serum creatinine and creatinine clearance did not differ between genotypes.

To check for kidney injury, gene expression of *Ngal* and *Kim-1* can be analyzed as upregulation has been demonstrated in mice with acute kidney injury [131, 132]. There was no detectable significant difference in relative *Ngal* mRNA expression in the kidney of 12-week-old mice (**Figure 9C**). The relative mRNA levels of *Kim-1* were slightly increased in Cre (+), but the effect was not significant.

In summary, we have shown that kidney-specific knockout of *RetSat* does not result in morphological changes, altered parameters of renal function or increased markers of acute kidney injury in adult male mice.

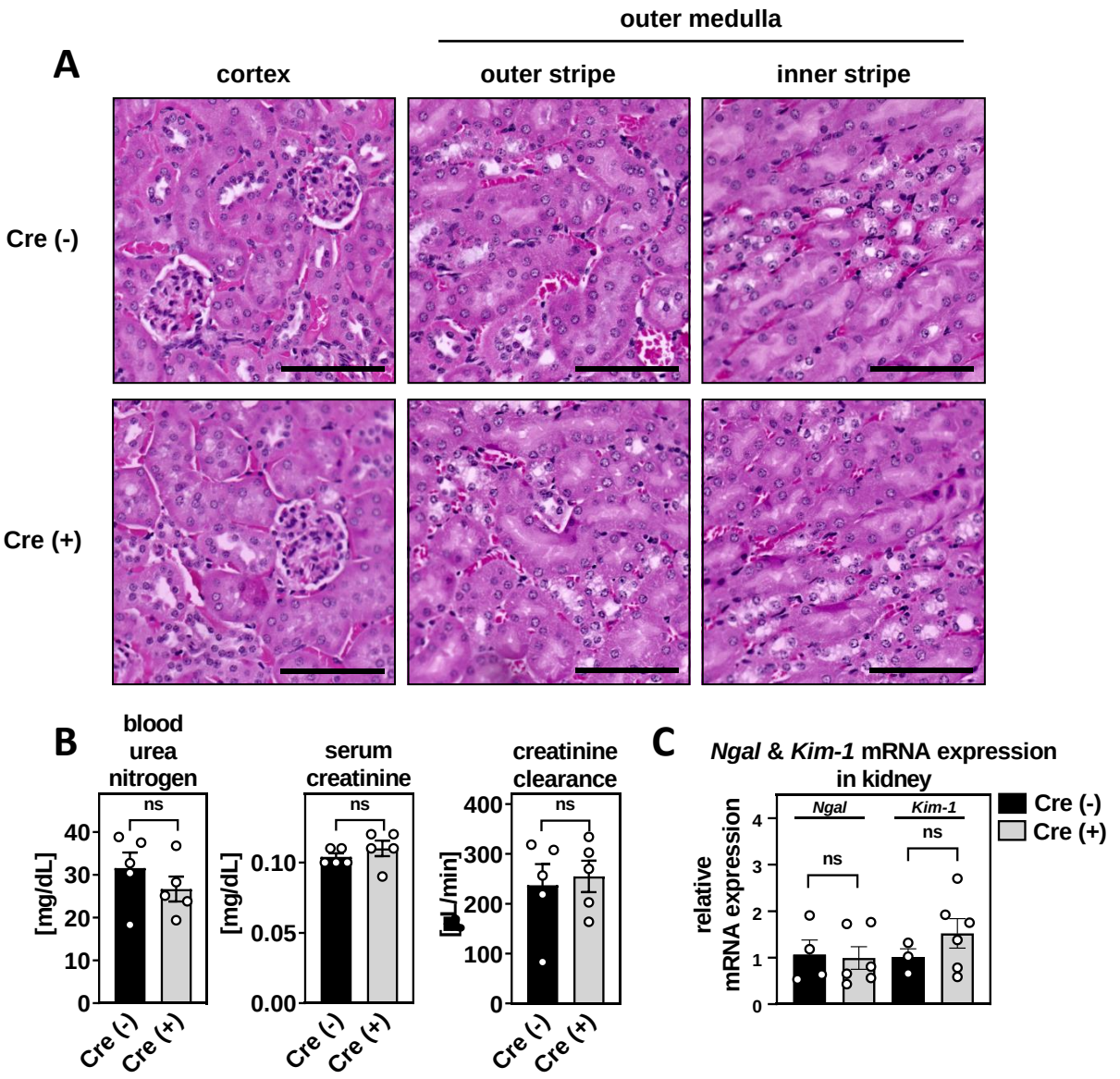

Figure 9: **Adult *RetSat* knockout mice on NC exhibit no detectable impairment in renal morphology or function. (A)** Representative images of kidney sections stained with haematoxylin and eosin (H&E) of male mice showing renal cortex, the outer and inner stripe of the outer medulla, scale bar = 200 µM. **(B)** Blood urea nitrogen (BUN) levels, serum creatinine, and creatinine clearance of Cre (-) and Cre (+) male mice, (n = 5,5). **(C)** Relative mRNA expression of *Ngal* & *Kim-1* in whole kidney mRNA of Cre (-) and Cre (+) male mice, (n = 4,6). All male mice were 12 – 14 weeks old. Data are represented as individual data points and mean ± sem. *P-value < 0.05 by two-tailed t-test, ns = not significant.

4.6 Adult *RetSat*-deficient mice on NC show proteinuria and hyperphosphaturia

To test the hypothesis that a kidney-specific knockout of *RetSat* could induce alterations in renal excretion and reabsorption of specific analytes, we collected serum and 24 h urine samples as for baseline analysis. In a pilot study, we collected serum samples from 12-week-old male (n = 5/5) and female (n = 4/7) mice. In another cohort, 24 h urine samples were collected from age-matched male and female mice (n = 12/12). Adult male Cre (+) mice showed no changes in the measured serum parameters (**Table 17**). Surprisingly, male Cre (+) mice showed a significant increase in total urinary protein of ~31% compared to Cre (-) animals. In addition, urinary albumin was significantly increased in 24 h urine samples from Cre (+) mice. Inorganic phosphate (Pi) concentrations were elevated in male Cre (+) mice, but did not show statistical significance between the two genotypes.

In the serum of female mice, we did not observe any changes in the urinary concentration of the analyzed parameter. Interestingly, adult female Cre (+) mice show a significant increase in urinary protein of ~41% compared to their Cre (-) littermates (**Table 18**). Elevated but not significant levels of Pi concentrations were also observed in female mice.

To check whether there were changes in specific analytes when male and female animals were pooled, the basal levels of Cre (-) animals were compared. In the serum of both sexes, basal levels of K^+ and Pi were significantly different. In addition, urinary parameters such as Ca^{2+}, Mg^{2+} and urinary protein showed different basal levels. Therefore, we excluded these parameters and pooled only the other parameter from male and female mice. All pooled analytes were then compared between both genotypes and are presented in **Table 19**. The serum parameters of the pooled mice did not change. Interestingly, urinary Pi concentrations, which showed a tendency to increase in male and female mice, showed a significant increase of ~23% in the pooled mice.

Basal measurement of specific analytes revealed increased proteinuria in male and female mice with kidney-specific *RetSat* knockout. Furthermore, when male and female mice were pooled, hyperphosphaturia was observed Cre (+) animals. Additionally, drinking volume, urine volume, and osmolality did not change in male and female mice

Table 17: Serum and urinary parameter of adult male animals

	Cre (-)	**Cre (+)**	***n***	**sex**
Serum parameter				
Na^+, mM/L	153.0 ± 1.0	154.4 ± 1.8	5/5	m
K^+, mM/L	10.5 ± 0.6	8.8 ± 0.6	5/5	m
Cl^-, mM/L	109.2 ± 0.7	108.5 ± 1.5	5/5	m
Ca^{2+}, mg/dL	10.5 ± 0.1	10.7 ± 0.1	5/5	m
Mg^{2+}, mg/dL	4.3 ± 0.2	4.3 ± 0.1	5/5	m
Pi, mg/dL	10.0 ± 0.4	9.6 ± 0.7	5/5	m
urea, mg/dL	67.6 ± 7.8	57.1 ± 6.2	5/5	m
creatinine, mg/dL	0.10 ± 0.0	0.11 ± 0.0	5/5	m
albumin, g/L	29.5 ± 0.7	30.9 ± 0.7	5/5	m
Urinary parameter				
Na^+, mM/L	81.1 ± 4.8	83.9 ± 3.2	12/12	m
K^+, mM/L	139.2 ± 10.8	139.2 ± 10.8	12/12	m
Cl^-, mM/L	89.4 ± 10.1	86.5 ± 4.6	12/12	m
Ca^{2+}, mg/dL	5.4 ± 0.4	5.5 ± 0.3	12/12	m
Mg^{2+}, mg/dL	36.0 ± 2.2	37.1 ± 1.2	12/12	m
Pi, mg/dL	151.8 ± 14.0	176.5 ± 11.0	12/12	m
urea, mg/dL	3255 ± 226	3527 ± 156	12/12	m
creatinine, mg/dL	22.8 ± 1.4	25.1 ± 0.8	12/12	m
urinary protein, mg/dL	762 ± 82	**996 ± 78 ***	12/12	m
urinary albumin, mg/dL	0.50 ± 0.1	**0.62 ± 0.1 ***	12/12	m
glucose, mg/dL	15.4 ± 0.9	16.8 ± 0.6	12/12	m
pH	6.1 ± 0.1	6.0 ± 0.1	12/12	m
osmolality, mOsm/kg H_2O	1229 ± 61	1271 ± 56	12/12	m
urinary volume, mL	1.6 ± 0.2	1.7 ± 0.2	12/12	m
drinking volume, mL	2.7 ± 0.3	2.5 ± 0.3	12/12	m

Table 18: Serum and urinary parameter of adult female mice

	Cre (-)	Cre (+)	*n*	sex
Serum parameter				
Na^+, mM/L	151.2 ± 0.9	152.4 ± 1.8	4/7	f
K^+, mM/L	8.6 ± 0.4	8.8 ± 0.4	4/7	f
Cl^-, mM/L	108.9 ± 0.9	109.7 ± 1.0	4/7	f
Ca^{2+}, mg/dL	10.4 ± 0.2	10.6 ± 0.3	4/7	f
Mg^{2+}, mg/dL	4.3 ± 0.1	4.3 ± 0.2	4/7	f
Pi, mg/dL	7.6 ± 0.4	8.2 ± 0.5	4/7	f
urea, mg/dL	78.9 ± 5.5	65.3 ± 4.8	4/7	f
creatinine, mg/dL	0.11 ± 0.0	0.11 ± 0.0	4/7	f
albumin, g/L	31.7 ± 0.6	32.0 ± 1.1	4/7	f
Urinary parameter				
Na^+, mM/L	78.6 ± 5.0	81.0 ± 5.3	12/12	f
K^+, mM/L	127.3 ± 9.8	132.9 ± 6.9	12/12	f
Cl^-, mM/L	88.5 ± 9.9	91.1 ± 7.5	12/12	f
Ca^{2+}, mg/dL	8.3 ± 0.7	8.2 ± 1.0	12/12	f
Mg^{2+}, mg/dL	48.1 ± 3.2	51.1 ± 3.3	12/12	f
Pi, mg/dL	135.8 ± 16.1	174.9 ± 21.6	12/12	f
urea, mg/dL	3778 ± 336	3843 ± 251	12/12	f
creatinine, mg/dL	24.5 ± 1.2	25.7 ± 1.5	12/12	f
urinary protein, mg/dL	135.6 ± 12.9	**193.6 ± 23.5 ***	12/12	f
urinary albumin, mg/dL	0.49 ± 0.0	0.57 ± 0.1	12/12	f
glucose, mg/dL	17.4 ± 1.5	18.1 ± 1.1	12/12	f
pH	6.1 ± 0.1	6.1 ± 0.1	12/12	f
osmolality, mOsm/kg H_2O	1237 ± 80	1421 ± 96	12/12	f
urinary volume, mL	1.0 ± 0.1	0.9 ± 0.1	12/12	f
drinking volume, mL	2.6 ± 0.3	2.7 ± 0.3	12/12	f

Table 19: Combined serum and urinary parameter of adult male & female mice

	Cre (-)	Cre (+)	*n*	sex
Serum parameter				
Na^+, mM/L	152.1 ± 0.7	153.2 0.8	9/12	m & f
Cl^-, mM/L	109.1 ± 0.5	109.2 ± 0.8	9/12	m & f
Ca^{2+}, mg/dL	10.4 ± 0.1	10.7 ± 0.2	9/12	m & f
Mg^{2+}, mg/dL	4.3 ± 0.1	4.3 ± 0.1	9/12	m & f
urea, mg/dL	72.6 ± 5.1	61.9 ± 3.8	9/12	m & f
creatinine, mg/dL	0.11 ± 0.0	0.11 ± 0.0	9/12	m & f
albumin, g/L	30.5 ± 0.6	31.5 ± 0.7	9/12	m & f
Urinary parameter				
Na^+, mM/L	79.9 ± 3.4	82.6 ± 2.9	24/24	m & f
K^+, mM/L	133.8 ± 7.3	142.0 ± 4.9	24/24	m & f
Cl^-, mM/L	88.9 ± 6.9	88.6 ± 4.1	24/24	m & f
Pi, mg/dL	143.3 ± 10.6	**175.7 ±11.4 ***	24/24	m & f
urea, mg/dL	3517 ± 206	3671 ± 143	24/24	m & f
creatinine, mg/dL	23.6 ± 0.9	25.4 ± 0.8	24/24	m & f
urinary albumin, mg/dL	0.49 ± 0.0	0.59 ± 0.1	24/24	m & f
glucose, mg/dL	16.3 ± 0.8	17.4 ± 0.6	24/24	m & f
pH	6.1 ± 0.1	6.0 ± 0.1	24/24	m & f
osmolality, mOsm/kg H_2O	1233 ± 50	1344 ± 55	24/24	m & f
urinary volume, mL	1.3 ± 0.1	1.3 ± 0.1	24/24	m & f
drinking volume, mL	2.7 ± 0.2	2.6 ± 0.2	24/24	m & f

4.7 *RetSat* knockout induces alterations in the composition of 24 h urine

To further investigate the nature of proteinuria in adult male mice, we performed a proteomic approach. The identification and quantification of proteins that were excreted at a higher rate could provide information on the underlying mechanism leading to proteinuria in Cre (+) animals. 24 h urine from Cre (-) and Cre (+) animals (n = 8.8) was sent to the proteomics facility of the Max-Delbrück-Centre. Equal amounts of protein (2 µg) were loaded into a Thermo Q Exactive HF-X system and quantified by label-free quantification (LFQ).

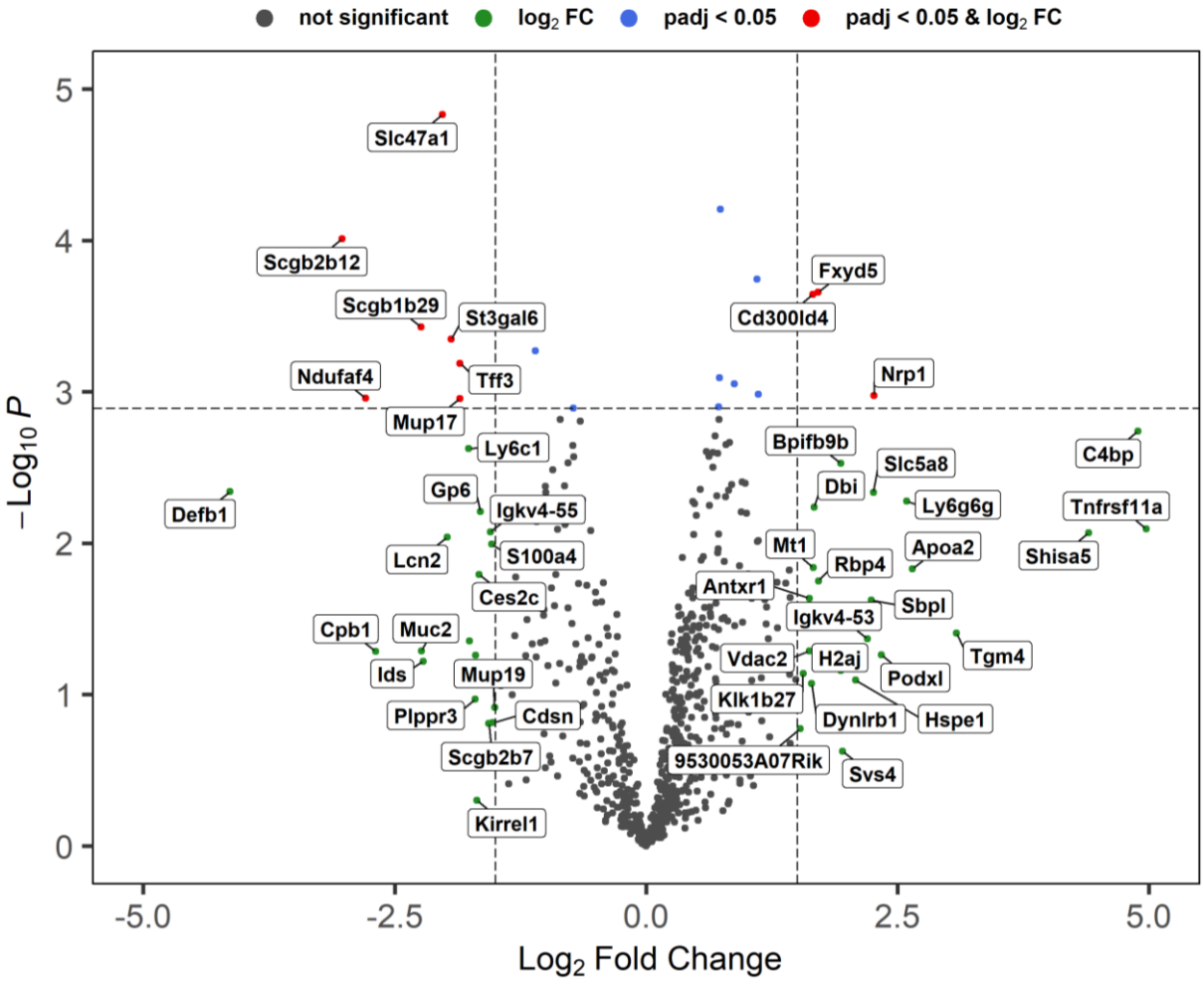

Figure 10: *RetSat* knockout changes protein composition in 24 h urine of adult male mice. A volcano plot is illustrated with differentially expressed proteins depicted as their encoding genes in 24 h urine of adult male mice (n = 7,8). Proteins are ranked according to their -$\log_{10}$ P-value and their relative abundance ratio (Log_2 Fold Change) between Cre (+) and Cre (-) mice. A total of 700 proteins were identified in both genotypes. 25 protein species were upregulated and 23 protein species were downregulated in 24 h-urine of Cre (+) mice ($\log_2$ fold change > 1.5).

A total of 700 proteins were found in the 24 h urine of adult male mice in both genotypes and are shown as their encoding genes in **Figure 10**. In Cre (+) mice, 25 proteins were upregulated (log_2 FC > 1.5), whereas 23 protein species were less abundant (log_2 FC > -1.5) when the same amount of protein was analyzed. Gene Ontology (GO) analysis of the 25 upregulated proteins suggested a possible association with lipid transport (GO:0006869) and lipid localisation (GO:0010876) (data not shown).

Normalization to total protein concentration could potentially lead to under- or overestimation of protein abundance in the 24 h urine samples. Based on the previously measured BCA concentrations, a factor was calculated for each sample and multiplied by the measured LFQ intensities. A rank-mean LFQ intensity plot with recalculated intensities for each genotype is shown in **Figure 11A**. Consistent with the previously observed proteinuria, the mean LFQ intensities of Cre (+) mice were increased compared to their Cre (-) littermates (**Figure 11A**). GO analysis of upregulated proteins (533 out of 700 identified), filtered for missing values in LFQ intensities, showed an association with wound healing (GO:0042060) and response to metal ions (GO:0010038) (**Figure 11B**).

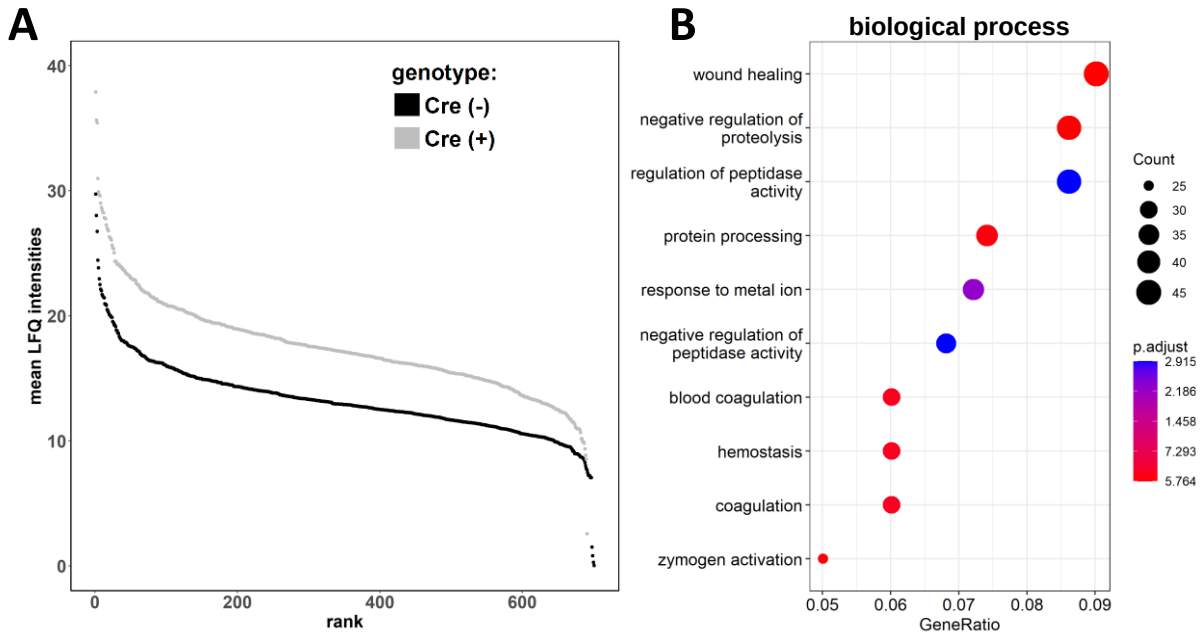

Figure 11: *RetSat* knockout increases abundance of specific proteins in 24 h urine of adult male mice. (A) mean LFQ intensity rank plot of Cre (-) and Cre (+) mice (n = 8,7). **(B)** GO analysis of recalculated and upregulated protein species (533 in total).

4.8 Adult *RetSat*-deficient mice on NC exhibited an increase in body weight without a change in compartment mass

Male mice with a whole-body knockout of *RetSat* showed an increase in total body weight when fed normal chow [94]. We were interested to see if we could observe similar effects in our mouse model with kidney-specific deletion of *RetSat*. We therefore monitored the change in body weight of male and female mice fed NC up to 42 weeks of age. Male Cre (+) animals showed a significant increase in total body weight over time, which was confirmed by analysis of variance (ANOVA) with P = 0.015 (**Figure 12D**). The onset of the increase in body weight was around 20/21 weeks of age. Female Cre (+) mice did not differ in absolute body weight from their Cre (-) littermates (data not shown).

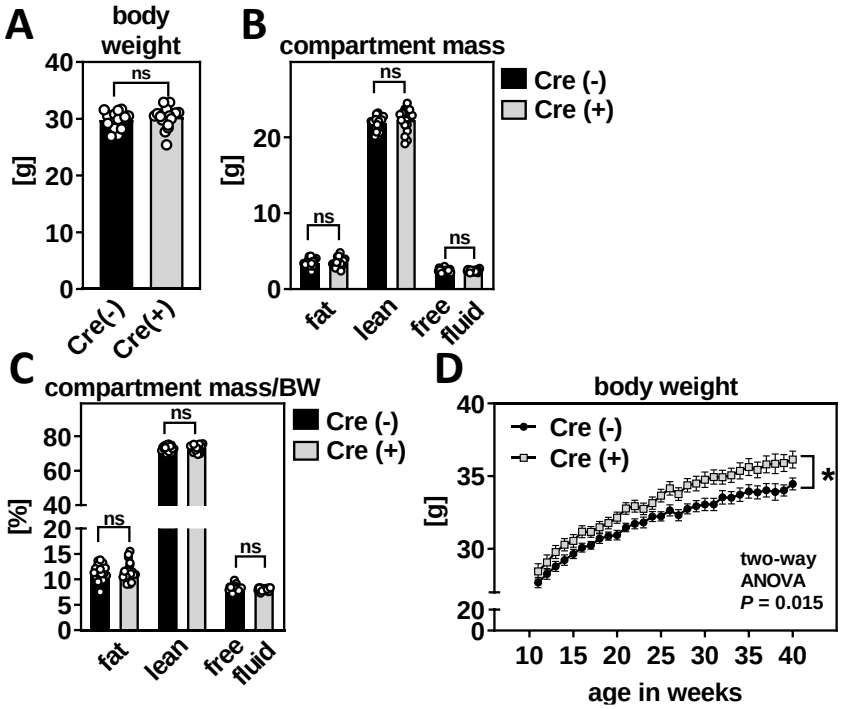

Figure 12: *RetSat* knockout adult mice on NC did not show alterations in body weight or body composition, but middle-aged knockout mice showed an increase in body weight. **(A)** Body weights, **(B)** Absolute compartment mass, **(C)** Compartment mass relative to body weight (BW) measured with NMR of 12 – 14 weeks old mice on NC, (n = 18,19). Data are represented as individual data points and mean ± sem. *P-value < 0.05 by two-tailed t-test, ns = not significant. **(D)** Weekly body weight measurement. Data are represented as means ± sem. The effect of genotype was analyzed by a two-way ANOVA, *P-value < 0.05.

To assess the body composition of adult 13-week-old male and female mice, we performed NMR measurements. Body weight was measured prior to NMR measurements to normalise body composition. Absolute body weights of male mice did not differ between genotypes (**Figure 12A**). The absolute and relative

compartmental mass of 13-week-old male mice did not change (**Figure 12B & C**). Body weights and compartmental masses of female mice did not differ between genotypes (data not shown).

4.9 Kidney-specific *RetSat* deletion did not affect the metabolic profile in adult male mice

It is generally accepted that perturbations in energy balance can lead to changes in body weight and/or body composition [133, 134]. Therefore, we examined the energy homeostasis and drinking volume in adult male mice in another cohort that had the same body weight gain with a similar onset at approximately 20 weeks of age (data not shown).

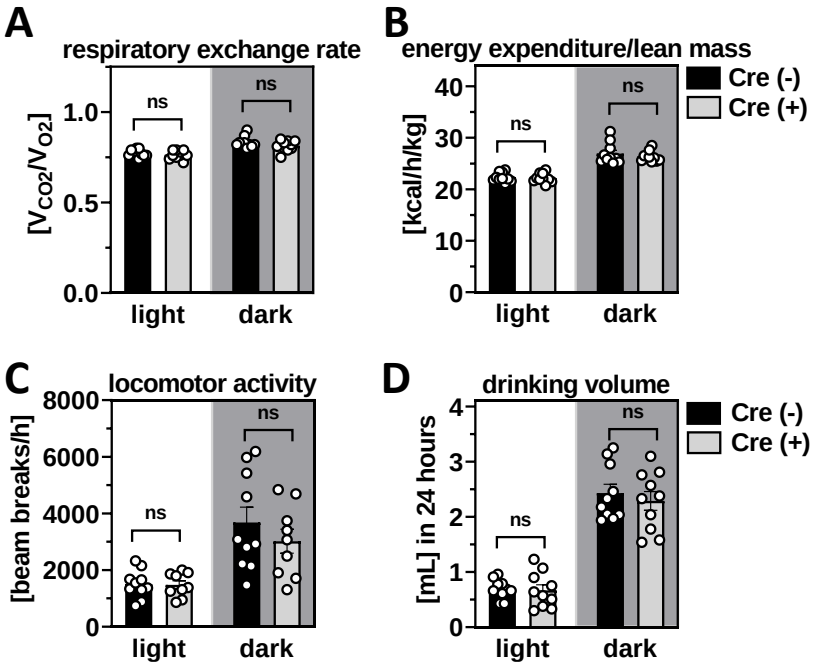

Figure 13: *RetSat* deletion in adult male mice did not affect energy homeostasis or drinking volume. (A) Respiratory exchange ratio (RER), **(B)** Energy expenditure relative to lean mass, **(C)** Locomotor activity, and **(D)** Drinking volume of 20 week-old male mice on NC in the light and dark phase over a period of 48 h, (n =10,10). Data are represented as individual data points and mean ± sem. ns = not significant.

The TSE LabMaster indirect calorimetry system was used to assess energy expenditure, locomotor activity, respiratory exchange rate and food and water intake in 20-week-old male mice. As shown in **Figure 13A**, RER, expressed as the ratio of carbon dioxide production (VCO2) to oxygen consumption (VO2), is not affected by the *RetSat* knockout. In addition, EE adjusted for lean body mass showed no changes in mice lacking *RetSat* in the kidney. Locomotor activity and drinking during the night and day followed natural habits with an increased level in the dark phase, but both parameters were similar between genotypes (**Figure 13B - D**).

4.10 Middle-aged *RetSat*-deficient mice showed an increase in body weight that was independent from food intake, but body composition has changed

In 13-week-old male mice, we did not observe any change in body weight or body composition. Given the later onset of body weight differences, we were interested in whether an increase in food intake contributed to the observed phenotype. Middle-aged mice (36 - 40 weeks) that differed in body weight (**Figure 14A**) were used to determine 24 h food intake. At this time point, we could not detect an increase in absolute food intake or relative to body weight over a 24 h period in Cre (+) animals compared to their Cre (-) littermates (**Figure 14B**). In another experiment, we assessed body composition. Interestingly, absolute lean mass and free water were significantly increased, whereas fat mass did not differ in middle-aged male mice with *RetSat* deletion (**Figure 14C**). Normalization to body weight negates the effect on lean mass but not on free fluid (**Figure 14C).**

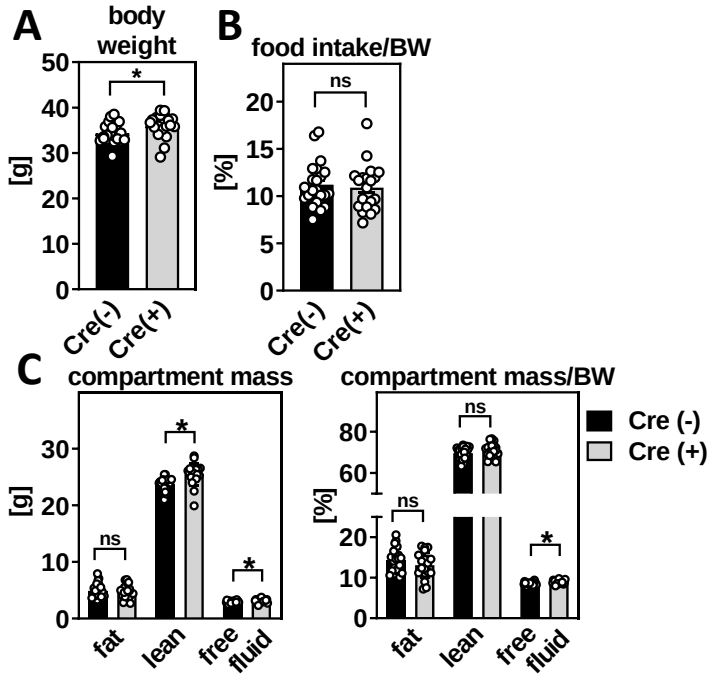

Figure 14: *RetSat* deletion resulted in an increase in body weight that was independent of food intake with changes in body composition in middle-aged male mice. (A) Body weights. **(B)** 24 h food intake relative to body weight. **(C)** Absolute compartment mass (left panel) and compartment mass relative to body weight (BW) (right panel) measured with NMR of 36 – 40 weeks old male mice on NC, (n = 22, 20). Data are represented as individual data points and mean ± sem. *P-value < 0.05 by two-tailed t-test, ns = not significant**.**

4.11 Middle-aged *RetSat*-deficient mice on NC showed comparable blood glucose and ketone levels in the fed and fasted state

RetSat is known to be differentially regulated in datasets associated with insulin resistance [86] and is upregulated in murine kidney in the fasting state [88] (**Figure 7D**). Therefore, we performed 16 h-fasting experiments to investigate the effects of *RetSat* deletion on blood glucose and ketone levels in middle-aged male mice displaying the body weight phenotype. As expected, blood glucose levels were lower in the fasting state compared to the fed state (**Figure 15A**). In contrast, β-hydroxybutyrate levels were elevated (**Figure 15B**). There were no significant changes in blood glucose and β-hydroxybutyrate levels between the two genotypes.

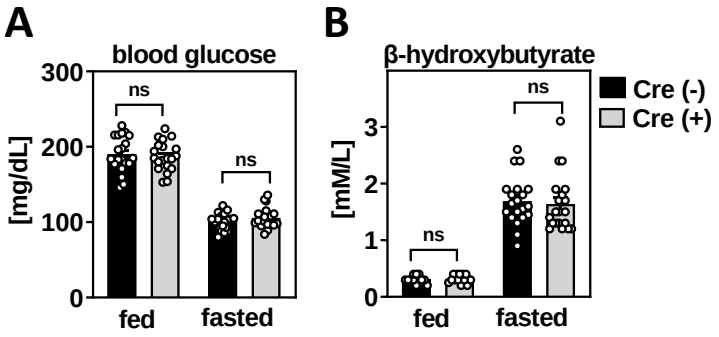

Figure 15: *RetSat* deletion showed comparable blood glucose and ketone levels in the fed and fasted state in middle-aged mice on NC. (A) Blood glucose levels, **(B)** β-hydroxybutyrate levels of 40-week-old mice on NC in the fed and 16 h fasted state, (n = 20, 20). Data are represented as individual data points and mean ± sem., ns = not significant.

4.12 *RetSat* knockout induced hypercalciuria and hypophosphaturia in middle-aged male mice

Age-related changes can lead to a functional decline in a variety of organs, such as the kidney in humans [135] and mice [136]. These changes can consist of alterations in renal structure and function [137]. To assess renal morphology and function H&E sections were examined under the light microscope in a genotype-blinded manner in 42-week-old middle-aged mice. The H&E staining images shown in **Figure 16A** are representative of kidney sections examined from at least three different animals per genotype. Cortical and medullary structures and the collecting duct were intact, and we could not detect any evidence of morphological changes or alterations in Cre (+) mice compared to their Cre (-) littermates. BUN and creatinine clearance were slightly decreased in Cre (+) animals, whereas serum creatinine levels were slightly but not significantly increased (**Figure 16B**). The relative mRNA expression of the acute injury markers *Ngal* and *Kim-1* was not altered in middle-aged mice lacking *RetSat*.

To investigate possible effects on renal excretion or reabsorption in middle-aged male mice, we collected serum and 24 h urine. We analyzed the same parameters in serum and 24 h urine as described in **section 4.6**. with a total of ten mice per genotype (n = 10,10). We did not observe any changes in the serum parameters of middle-aged male mice (Table 20). Interestingly, we observed higher Ca^{2+} concentrations in Cre (+) mice (6.3 ± 0.2 mg/dL) compared to their Cre (-) littermates (5.4 ± 0.3 mg/dL) Furthermore, we observed a significant decrease in Pi concentrations in mice with *RetSat* deletion (119 ± 7 mg/dL) when compared to Cre (-) mice (156 ± 13 mg/dL). Normalization to

urinary volume was performed as described in **section 3.4.7.** to calculate the excreted amount of analyte in 24 h. The calculated values are presented in **Table 20**. As shown in **Table 21,** excreted amounts of Pi were significantly reduced while Ca^{2+} excretion was slightly, but not significantly increased in mice with *RetSat* deletion.

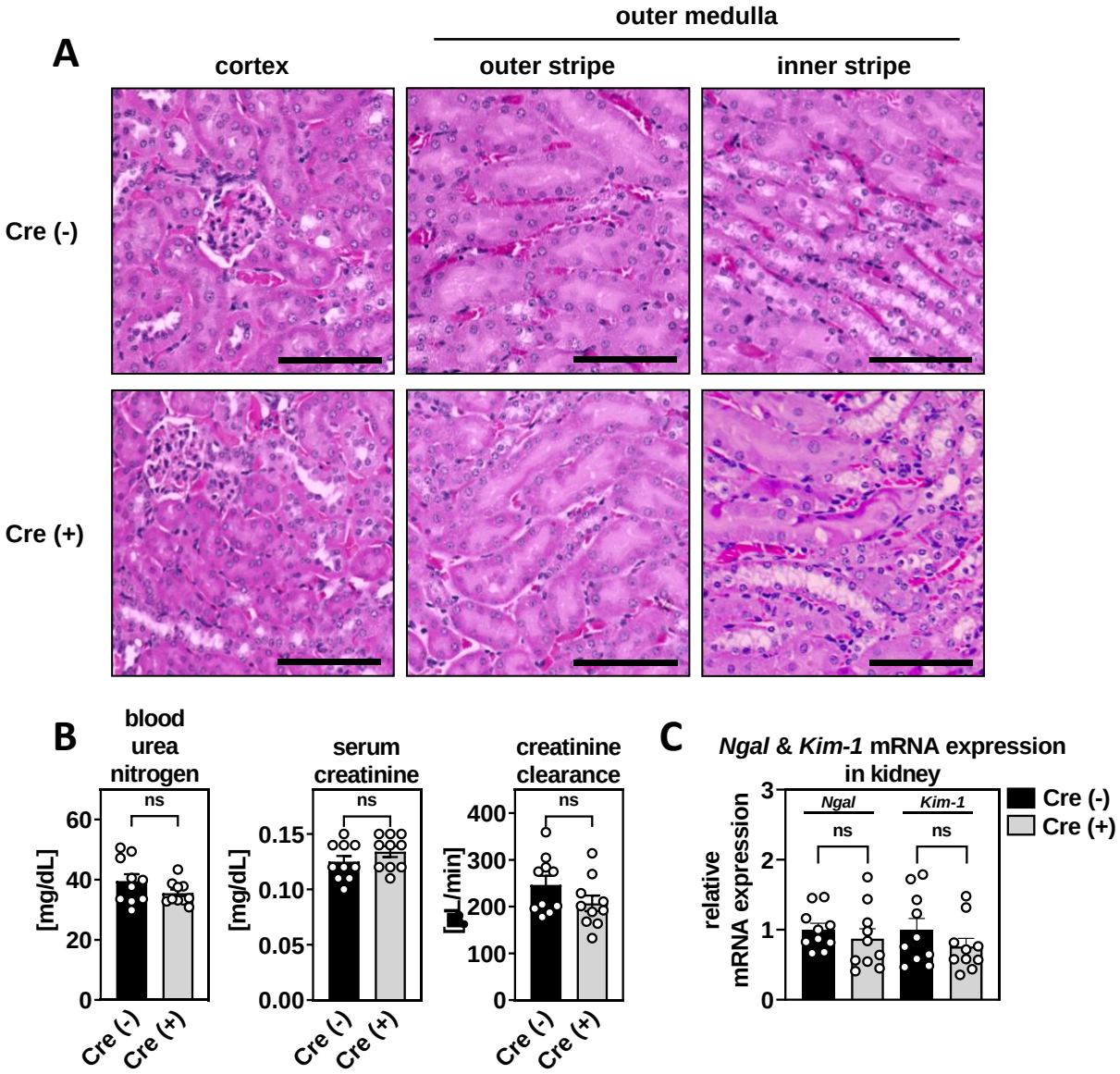

Figure 16: *RetSat* deletion does not affect renal morphology or function in middle-aged mice on NC. (A) Representative images of kidney sections stained with hematoxylin and eosin (H&E) of male mice showing renal cortex, the outer and inner stripe of the outer medulla, scale bar = 200 µM. **(B)** Blood urea nitrogen (BUN) levels, serum creatinine, and creatinine clearance of Cre (-) and Cre (+) male mice, (n = 10,10). **(C)** relative mRNA expression of *Ngal* & *Kim-1* in whole kidney tissue of Cre (-) and Cre (+) male mice, (n = 10,10). All male mice were 40 – 42 weeks old. Data are represented as individual data points and mean ± sem. *P-value < 0.05 by two-tailed t-test, ns = not significant.

In addition, the fractional excretion (FE) of the analytes was calculated as described in **section 3.4.7**. The FE of Ca^{2+} was significantly increased in Cre (+) animals (0.4 ± 0.0%) compared to their Cre (-) littermates (0.3 ± 0.0%) (**Table 22**). Although we could not detect any changes in the FE of Pi. Kidney-specific deletion of *RetSat* did not affect renal morphology or function but induced hypercalciuria and hypophosphaturia in middle-aged male mice.

Table 20: Serum and urinary parameter of middle-aged male mice

	Cre (-)	**Cre (+)**	***n***	**sex**
Serum parameter				
Na^+, mM/L	157.3 ± 0.7	156.0 ± 0.6	10/10	m
K^+, mM/L	9.2 ± 0.3	9.2 ± 0.4	10/10	m
Cl^-, mM/L	113.6 ± 0.9	113.2 ± 0.7	10/10	m
Ca^{2+}, mg/dL	10.0 ± 0.1	10.2 ± 0.1	10/10	m
Mg^{2+}, mg/dL	4.5 ± 0.1	4.2 ± 0.1	10/10	m
Pi, mg/dL	9.3 ± 0.2	9.0 ± 0.3	10/10	m
urea, mg/dL	84.6 ± 5.0	76.0 ± 2.5	10/10	m
creatinine, mg/dL	0.13 ± 0.0	0.13 ± 0.0	10/10	m
Urinary parameter				
Na^+, mM/L	85.2 ± 5.3	73.4 ± 3.0	10/10	m
K^+, mM/L	142.4 ± 10.2	124.9 ± 2.8	10/10	m
Cl^-, mM/L	89.9 ± 8.7	70.0 ± 5.7	10/10	m
Ca^{2+}, mg/dL	5.4 ± 0.3	**6.3 ± 0.2 ***	10/10	m
Mg^{2+}, mg/dL	40.8 ± 2.6	37.0 ± 1.7	10/10	m
Pi, mg/dL	156 ± 13	**119 ± 7 ***	10/10	m
urea, mg/dL	3398 ± 226	2957 ± 88	10/10	m
creatinine, mg/dL	24.4 ± 1.4	22.4 ± 1.2	10/10	m
urinary protein, mg/dL	895 ± 118	863 ± 52	10/10	m
urinary albumin, mg/dL	0.48 ± 0.0	0.4 ± 0.0	10/10	m
glucose, mg/dL	14.3 ± 0.1	12.5 ± 0.6	10/10	m
creatinine clearance, µL/min	246 ± 20	207 ± 17	10/10	m
pH	5.8 ± 0.1	5.9 ± 0.1	10/10	m
osmolality, mOsm/kg H_2O	996 ± 54	911 ± 19	10/10	m
urinary volume, mL	1.9 ± 0.2	1.8 ± 0.1	10/10	m
drinking volume, mL	1.8 ± 0.2	1.5 ± 0.2	10/10	m

Table 21: Excreted amounts of analytes in 24 h urine of middle-aged male mice

	Cre (-)	Cre (+)	*n*	sex
Amount excreted [mg in 24 h]				
Na^+	3.6 ± 0.3	3.0 ± 0.3	10/10	m
K^+	9.4 ± 1.0	7.4 ± 1.0	10/10	m
Cl^-	5.4 ± 0.6	3.8 ± 0.7	10/10	m
Ca^{2+}	5.4 ± 0.3	6.3 ± 0.2	10/10	m
Mg^{2+}	0.1 ± 0.0	0.1 ± 0.0	10/10	m
Pi	2.7 ± 0.1	**2.1 ± 0.1 ***	10/10	m
urea	60.2 ± 4.0	52.2 ± 3.0	10/10	m
creatinine	0.4 ± 0.0	0.4 ± 0.0	10/10	m
urinary protein	15.8 ± 1.8	15.0 ± 0.8	10/10	m
urinary albumin	0.008 ± 0.0	0.007 ± 0.0	10/10	m
glucose	0.3 ± 0.0	0.2 ± 0.0	10/10	m

Table 22: Fractional excretion of analytes in 24 h urine of middle-aged male mice

	Cre (-)	Cre (+)	*n*	sex
Fractional excretion (FE) [%]				
Na^+	0.3 ± 0.0	0.3 ± 0.0	10/10	m
K^+	8.0 ± 0.1	8.5 ± 0.1	10/10	m
Cl^-	0.4 ± 0.0	0.4 ± 0.0	10/10	m
Ca^{2+}	0.3 ± 0.0	**0.4 ± 0.0 ***	10/10	m
Mg^{2+}	4.7 ± 0.0	5.4 ± 0.0	10/10	m
Pi	8.6 ± 0.0	8.0 ± 0.0	10/10	m
urea	60.2 ± 4.0	52.2 ± 3.0	10/10	m
creatinine	0.4 ± 0.0	0.4 ± 0.0	10/10	m
urinary protein	15.8 ± 1.8	15.0 ± 0.8	10/10	m

4.13 *RetSat* knockout did not induce a nephrocalcinosis in middle-aged male mice

Hypercalciuria is known to be an important risk factor for kidney stone formation in humans [138-140] and rodents [141, 142]. In men, the majority of kidney stones are composed of calcium crystals, mainly calcium oxalate and calcium phosphate [143] [144].

Histological examination of kidney sections was performed, to investigate the possible formation of calcium deposits in middle-aged (42-weeks-old) male mice with hypercalciuria (**Table 20**). At least three animals per genotype were used for evaluation. Positive controls were provided by different working groups as described in **sections 3.3.3** and **3.3.4**.

Von Kossa and Alizarin Red S staining were used to visualize calcium deposits in Cre (+) mice and their respective Cre (-) littermates. **Figure 17A** shows von Kossa staining of a positive control with nephrocalcinosis (Cldn10-deficient mice [145]). Medullary calcium deposits are indicated by arrows. Compared to the positive control, representative images of kidney sections from Cre (-) (**Figure 17B**) and Cre (+) (**Figure 17C**) mice did not show any calcium deposits. Additionally, Alizarin Red S staining was performed and a positive control (mice fed a high oxalate diet) is shown in **Figure 17D**, where arrows indicate calcium deposits. Kidney sections examined from Cre (-) (**Figure 17E**) and Cre (+) (**Figure 17F)** did not show any calcium deposits.

Our histological examination of kidney sections showed that middle-aged male Cre (+) mice with hypercalciuria did not develop nephrocalcinosis.

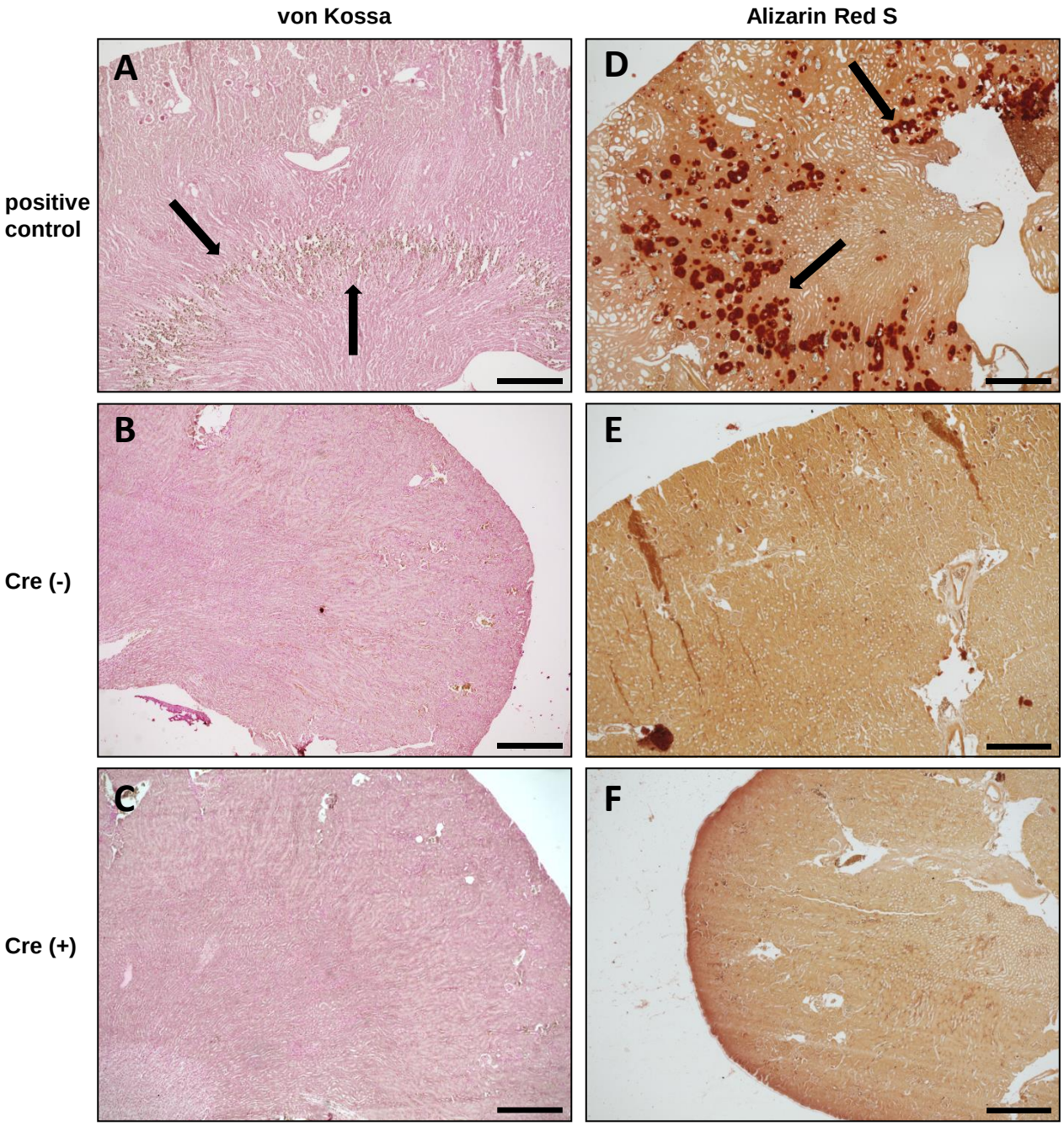

Figure 17: Middle-aged mice with *RetSat* deletion did not exhibit a nephrocalcinosis. Representative images of kidney sections stained with von Kossa **(A – C)**, Alizarin red S **(D – F)** of 42-week-old mice on NC with the positive control **(A & D)**, Cre (-) **(B & E)** and Cre (+) **(C & F)** genotype. Scale bars = 500 µm.

4.14 *RetSat* knockout induced the expression of vitamin D receptor and its target genes in middle-aged male mice

To gain further insight into the transcriptome of mice with kidney-specific *RetSat* deletion, we performed whole kidney tissue RNA sequencing of Cre (-) and Cre (+) animals (n = 5,5). A total of 17,385 transcripts were detected. Of these 17,385 transcripts, 1,725 (~10%) were differentially expressed genes (DEG) with a threshold of P-value < 0.05, of which 716 were upregulated and 1,009 were downregulated. Adjustment of the P-value uisng Benjamini-Hochberg procedure for P-adjusted (padj) < 0.1 resulted in 29 up- and 46 down-regulated genes. While 18 genes were upregulated and 23 genes were downregulated with padj < 0.05. **Figure 18** shows a volcano plot of all detected transcripts with padj < 0.05 (horizontal dashed grey line) and $\log_2$ fold change > 0.244 (vertical dashed grey line). As expected, we detected reduced transcript levels of *RetSat* in Cre (+) mice (**Figure 18**). Surprisingly, the vitamin D receptor (*Vdr*) was upregulated in mice with kidney-specific deletion of *RetSat*. Furthermore, known renal target genes of *Vdr* [146], such as *Pvalb, Dsc2, Ptgfr, Ptgds, Col8a1, Kcnj2, Ptger3, Cyp7b1* and *Sprr2a1* were differentially expressed in Cre (+) mice.

Figure 19 shows a heatmap of DEG with padj < 0.05, filtered for predicted genes and ordered by their $\log_2$ fold changes in up- and downregulated genes. A total of 11 genes were upregulated while 23 genes were significantly downregulated in whole kidney tissue from middle-aged male mice with *RetSat* deletion.

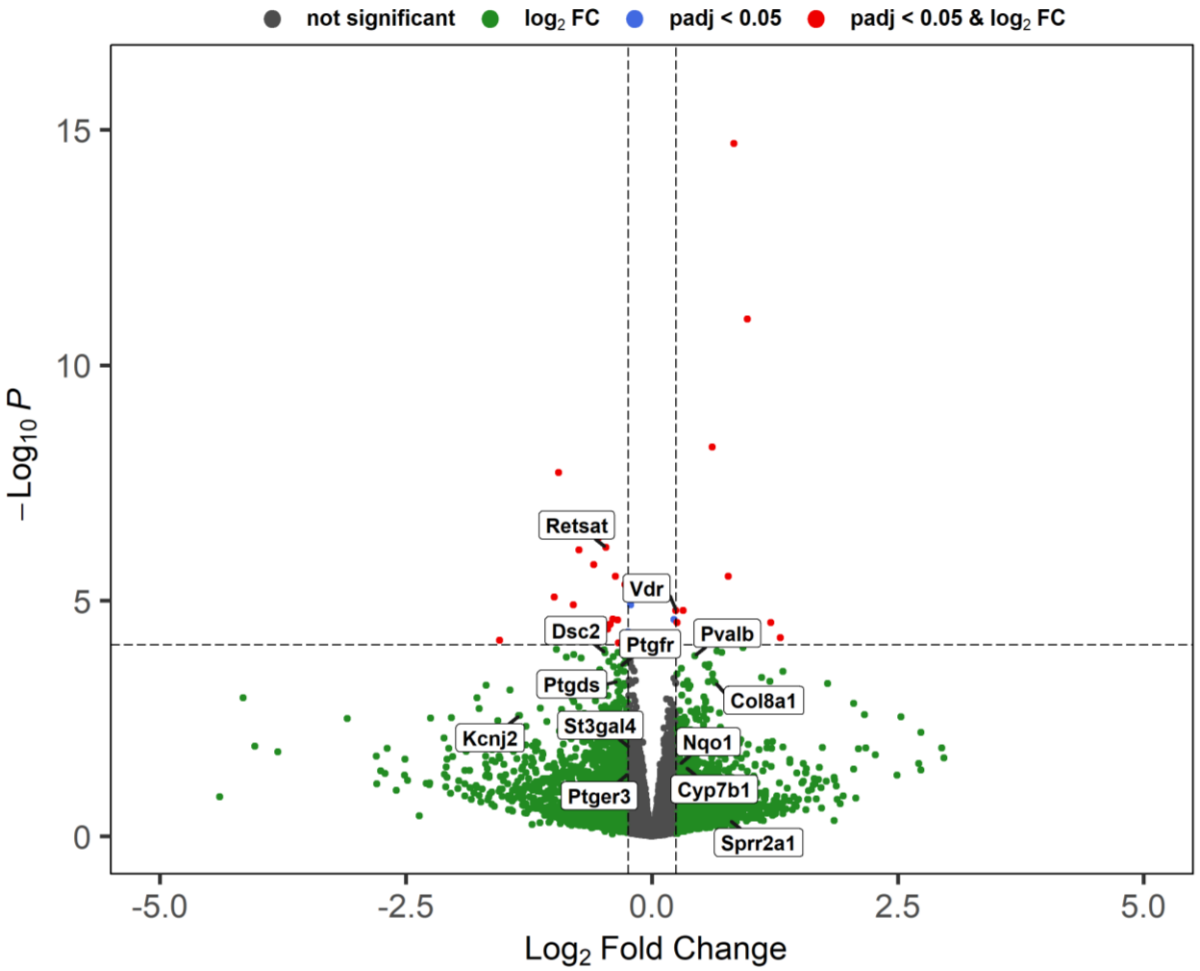

Figure 18: *RetSat* knockout induces mRNA expression of the vitamin D receptor (*Vdr*) and result in differential expression of its target genes. A volcano plot is illustrated with differentially expressed genes (DEG) in middle-aged male mice (n = 5,5). Genes are ranked according to their -$\log_{10}$ *P*-value and their relative fold change (Log_2 Fold Change) between Cre (+) and Cre (-) mice. A total of 17,385 transcripts were identified. Treshold for Log_2 Fold Change was set as 0.244 and padj < 0.05, corrected for Benjamini-Hochberg.

To confirm and validate that RNA-Seq. was adequately detecting gene expression, a selection of genes were analzed by RT-qPCR and are shown in **Figure 20A**. Whole kidney tissue from the same mice sent for RNA-Seq. were used for subsequent RT-qPCR. Indeed, genes measured in RNA-Seq. showed consistent results in RT-qPCR. Interestingly, a number of genes involved in cell adhesion & migration were significantly downregulated in mice lacking *RetSat* (*Aqp2, Kcnj10, Sphk2, Jup* and *Dsp*). In contrast, genes involved in Ca^{2+} transport were upregulated (*Vdr, Pvalb* and *Calcr*)

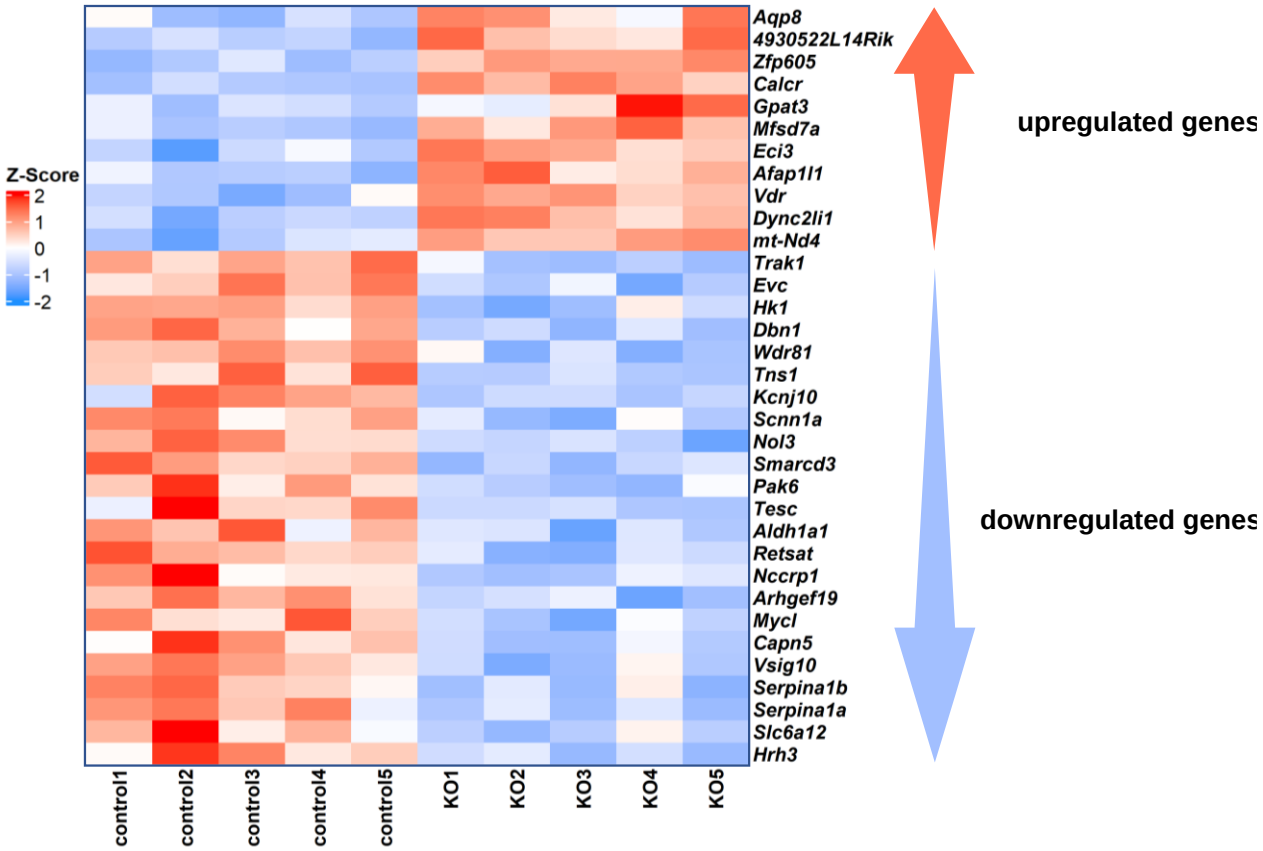

Figure 19: *RetSat* knockout induces the mRNA expression of the *Vdr* and other genes related to calcium homeostasis. Heatmap of DEG with padj < 0.05, 11 upregulated and 23 downregulated genes are shown, ranked after their log_2 FC. Whole kidney tissue was used for RNA-Seq analysis of middle-aged male Cre (-) and Cre (+) mice.

GO analysis for biological process (BP), molecular function (MF) and cellular component (CC) was performed for downregulated genes with P-value < 0.05 and is shown in **Figure 20B**. Top GO terms for BP included cell junction assembly (GO:0034329), positive regulation of cell adhesion (GO:0045785), and cell-substrate adhesion (GO:0031589). The top GO term for MF consisted of actin binding (GO:0003779) and for CC apical (GO:0045177) and basal (GO:0045178) parts of the cell. GO analysis of upregulated genes with P-value < 0.05 did not provide useful information and are therefore not shown.

Data obtained from RNA-Seq, RT-qPCR validation and gene ontology analysis suggests that kidney-specific deletion of *RetSat* impairs cell-cell interactions and affects the expression of vitamin D targe genes that are involved in Ca^{2+} homeostasis in middle-aged male mice.

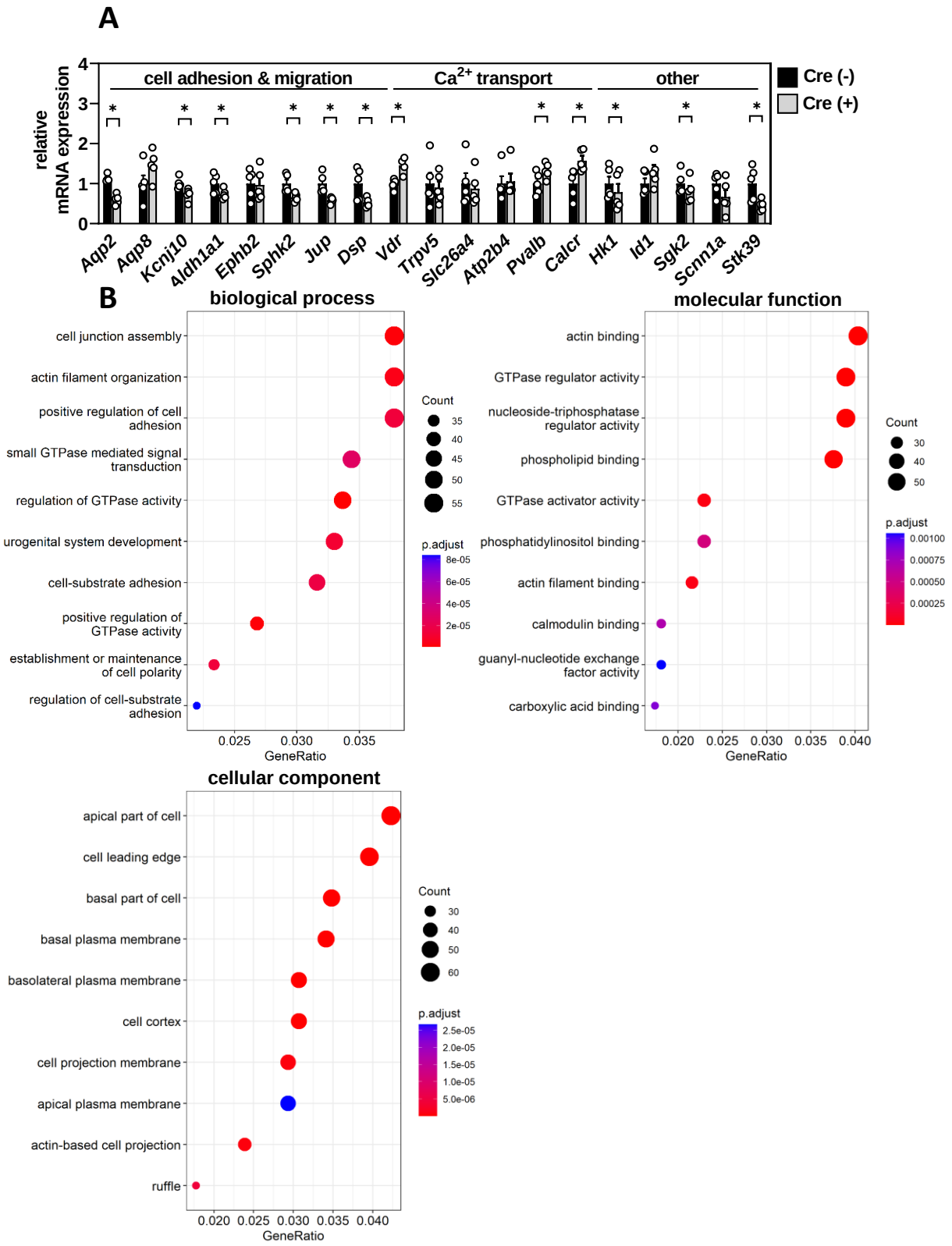

Figure 20: *RetSat* knockout reduces mRNA expression of genes involved in cell adhesion & migration and increased genes responsible for Ca^{2}+ transport. (A) RT-qPCR analysis of different genes on mRNA level to validate RNA-Seq. data (n = 5,5). All male mice were 40 – 42 weeks old. Data are represented as individual data points and mean ± sem. *P-value < 0.05 by two-tailed t-test, ns = not significant. **(B)** GO analysis of downregulated genes with P-value < 0.05 (1,009 transcripts).

4.15 *RetSat*-deficient mice on HFD showed an increased body weight and changes in body composition

A HFD is known to induce metabolic changes such as obesity, hyperglycaemia and an abnormal lipid profile in mice that are similar to those observed in humans with metabolic syndrome [105, 147]. It is widely accepted that obesity is a major and independent risk factor for the development of chronic kidney disease and end-stage renal disease [148], [149]. Previous results from the whole body *RetSat* knockout mice showed an increase in body weight gain when these mice were fed HFD [94]. Therefore, we characterized the metabolic phenotype of mice with kidney-specific *RetSat* deletion on HFD.

Cre (-) and Cre (+) adult male mice were fed HFD for 10 weeks (n = 15,15), body weight was measured weekly and the metabolic profile was then examined. Notably, Cre (+) mice showed an increase in body weight that was statistically significant when tested by ANOVA (P-value = 0.008) (**Figure 21A**). After 10 weeks of HFD, Cre (+) mice had an increased body weight of ~10% compared to Cre (-) mice. In line with the increased body weight, Cre (+) mice showed an increase in body weight gain (P-value = 0.003) (**Figure 21B**). After 10 weeks on HFD, mice with *RetSat deletion* showed an increase in absolute fat mass, while no changes in absolute lean mass or free fluid were observed (**Figure 21C**). Normalization to body weight resulted in increased relative fat mass and decreased relative lean mass, but no changes in relative free fluid in Cre (+) mice (**Figure 21C**). To investigate the contribution of food intake to the observed body weight in mice with kidney-specific *RetSat* deletion, 24 h food intake experiments were performed in 22-week-old mice. **Figure 21E** shows 24 h food intake relative to body weight. There was no significant difference in absolute or relative 24 h food intake between genotypes.

Cre (+) mice on a HFD showed an increase in body weight with increased body weight gain over a course of 10 weeks that was independent of the food intake. Their body composition changed to a higher proportion of relative fat mass and a lower proportion of relative lean mass.

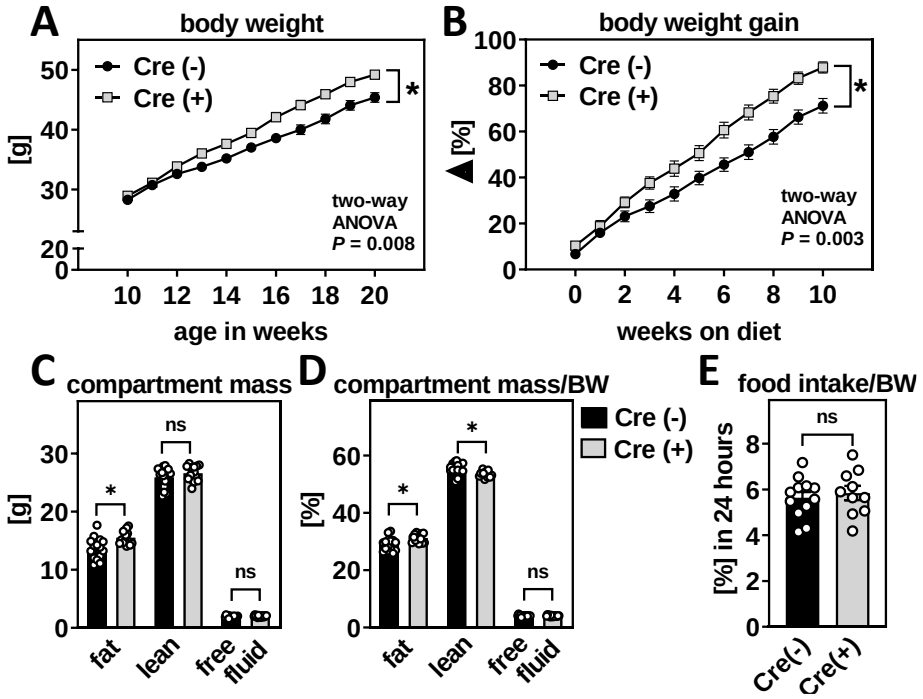

Figure 21: *RetSat* knockout did result in an increase in body weight that was independent of food intake and changed the body composition in adult male mice on HFD. (A) Body weights, **(B)** Relative body weight gain from initial weight after 10 weeks on HFD, (n = 15,15), the effect of genotype was analyzed by a two-way ANOVA, *P-value < 0.05 (C) absolute compartment mass, **(C)** Compartment mass relative to body weight (BW) measured with NMR of 20 – 21 weeks old mice on a HFD, (n = 15,15) **(D)** 24 h food intake relative to body weight of 22 – 24 weeks old mice, (n = 12,11). Data are represented as individual data points and mean ± sem. *P-value < 0.05 by two-tailed t-test, ns = not significant.

4.16 *RetSat*-deficient mice on HFD showed a decreased energy expenditure independent from food intake and locomotor activity

Energy homeostasis and drinking volume of 20-week-old male mice on HFD were assessed using a TSE LabMaster system. As shown in **Figure 22A**, the RER was not different in Cre (+) mice compared to their Cre (-) littermates. Interestingly, energy expenditure relative to body weight times the power of 0.75 was reduced in Cre (+) mice (**Figure 22B**). In contrast, normalization of energy expenditure to lean body mass did not result in a significant difference between genotypes (data not shown). As expected, we observed an increase in locomotor activity in the dark phase, but could not detect any significant changes in mice with kidney-specific *RetSat* deletion (**Figure 22C).** Cre (+) showed a decrease in drinking volume in the dark phase, which was borderline significant (P-value = 0.06), but no significant changes in the light phase (**Figure 22D**).

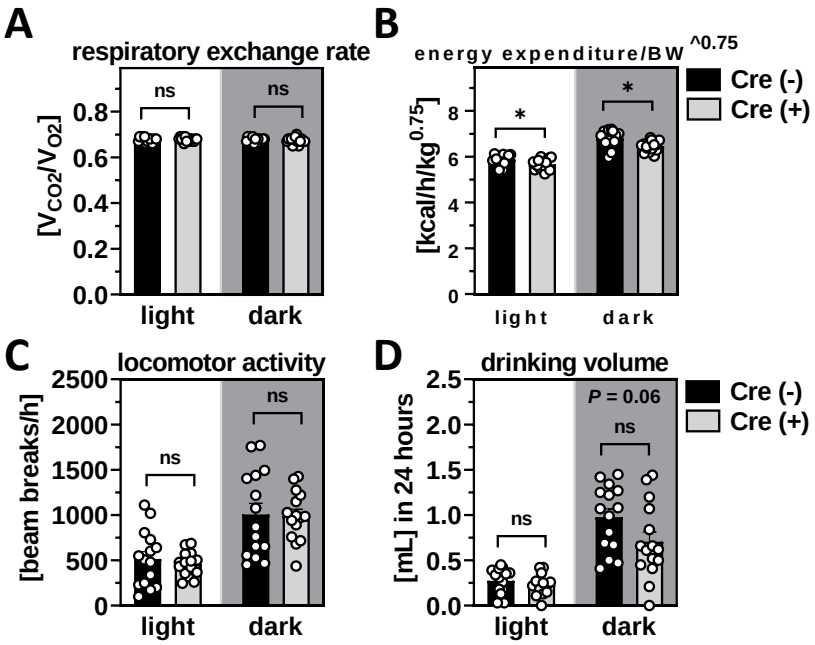

Figure 22: *RetSat* deletion resulted in a decrease in energy expenditure and a reduced water intake at night in adult male mice on HFD. (A) Respiratory exchange ratio (RER), **(B)** Energy expenditure relative to body weight$^{0.75}$, **(C)** Locomotor activity, and **(D)** drinking volume of 20-week-old male mice on a HFD in the light and dark phase over a period of 48h, (n =15,15). Data are represented as individual data points and mean ± sem. *P-value < 0.05 by two-tailed t-test, ns = not significant**.**

4.17 *RetSat*-deficient mice on HFD showed an impaired glucose clearance without the development of an insulin resistance

To test the hypothesis that deletion of *RetSat* in the kidney impairs glucose homeostasis in 23-week-old male mice on HFD, we performed an ipGTT after 16 h of fasting. Surprisingly, Cre (+) mice on HFD showed an impairment in glucose clearance compared to their Cre (-) littermates (**Figure 23A, left panel**), tested by two-way ANOVA (P-value = 0.013). This was confirmed by calculating the area under the curve (AUC) (**Figure 23A, right panel**). Blood glucose levels in the fed state did not change, whereas blood glucose levels in the fasted state increased in Cre (+) (**Figure 23B, left panel**). On the other hand, β-hydroxybutyrate concentrations were significantly reduced in the fasted state (**Figure 23B, right panel**).

Insulin sensitivity was assessed in 24-week-old male mice on HFD. The intraperitoneal insulin tolerance test (ipITT) was performed after 4 h of fasting. Cre (+) mice showed no difference in blood glucose levels after insulin injection compared to their Cre (-) littermates (**Figure 23D, left panel**). In addition, the calculated AUC did not differ (**Figure 23D, right panel**).

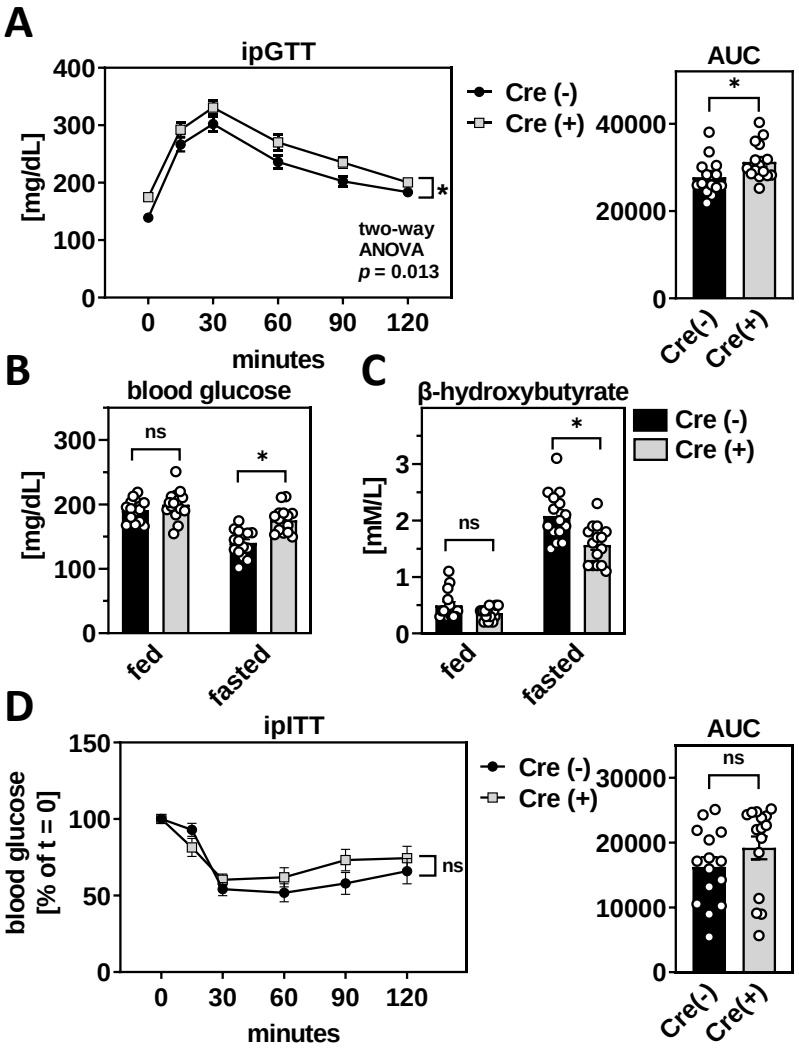

Figure 23: *RetSat* deletion does impair glucose clearance, but not insulin sensitivity, while blood glucose was increased and ketone bodies decreased after 16 h of fasting in mice on HFD. (A) Intraperitoneal glucose tolerance test (ipGTT) (left panel) and calculated area under the curve (AUC) (right panel), **(B)** Blood glucose, **(C)** And β-hydroxybutyrate levels of 22 – 23 weeks old mice fasted for 16 h, (n = 15,15). **(D)** iIntraperitoneal insulin tolerance test (ipITT) represented as blood glucose as % of t= 0 (left panel) and AUC (right panel) of 24-week-old mice fasted for 4 h, (n = 15,15). Data are represented as individual data points and mean ± sem. *P-value < 0.05 by two-tailed t-test, ns = not significant. The effect of genotype was analyzed by a two-way ANOVA, *P-value < 0.05, ns = not significant.

4.18 *RetSat*-deficient mice on HFD exhibited a decrease in kidney weight and a decreased accumulation of lipids in the renal cortex

We performed a baseline characterization with organ weight determination, histological examination of kidney sections and assessment of kidney function in 27-week-old male mice on HFD. Mice were divided into two groups, one fed and one fasted for 24 h.

In fed mice, absolute and relative kidney weights and relative heart weights were significantly reduced in Cre (+) animals (**Table 23**). Significantly higher absolute and relative liver weights and higher absolute spleen weights were observed in the 24 h fasted mice (**Table 24**). A decrease in relative eWAT weight was also observed.

Table 23: Body and organ weights of male animals on HFD in the fed state

	Cre (-)	**Cre (+)**	***n***	**sex**	**fed/fasted**
body weight (BW), g	47.1 ± 0.6	**50.0 ± 0.7 ***	8/7	m	
organ weight (OW), mg					
kidneys	194.8 ± 5.3	**174.9 ± 3.4 ***	8/7	m	fed
liver	1759 ± 104	1974 ± 162	8/7	m	fed
spleen	89.0 ± 6.0	83.4 ± 4.3	8/7	m	fed
heart	171.1 ± 4.9	159.4 ± 5.0	8/7	m	fed
eWAT	2203 ± 126	1963 ± 82	8/7	m	fed
relative organ weight (OW/BW)					
kidneys, %	0.43 ± 0.0	**0.37 ± 0.0 ***	8/7	m	fed
liver, %	3.9 ± 0.2	4.2 ± 0.3	8/7	m	fed
spleen, %	0.2 ± 0.0	0.2 ± 0.0	8/7	m	fed
heart, %	0.4 ± 0.0	**0.3 ± 0.0 ***	8/7	m	fed
eWAT, %	4.9 ± 0.3	4.2 ± 0.2	8/7	m	fed

Table 24: Body and organ weights of male animals on HFD in the fasted state

	Cre (-)	Cre (+)	*n*	sex	fed/fasted
body weight (BW), g	43.4 ± 0.8	**46.0 ± 0.5 ***	7/8	m	
organ weight (OW), mg					
kidneys	177.9 ± 8.8	177.3 ± 2.3	7/8	m	fasted
liver	1445 ± 98	**1876 ± 94 ***	7/8	m	fasted
spleen	73.6 ± 4.1	**84.1 ± 2.5 ***	7/8	m	fasted
heart	142.0 ± 4.3	147.0 ± 3.4	7/8	m	fasted
eWAT	2162 ± 206	1754 ± 117	7/8	m	fasted
relative organ weight (OW/BW)					
kidneys, %	0.41 ± 0.0	0.39 ± 0.0	7/8	m	fasted
liver, %	3.3 ± 0.2	**4.1 ± 0.2 ***	7/8	m	fasted
spleen, %	0.2 ± 0.0	0.2 ± 0.0	7/8	m	fasted
heart, %	0.3 ± 0.0	0.3 ± 0.0	7/8	m	fasted
eWAT, %	5.0 ± 0.5	**3.8 ± 0.3 ***	7/8	m	fasted

Some studies have shown that HFD induces severe nephropathy and morphological changes in rodents [150, 151]. Renal morphology was examined by H&E staining of kidney sections from fed mice. Representative images of kidney sections are shown in **Figure 24A**. Cortical and medullary structures as well as the collecting duct were intact, but we observed a reduced accumulation of lipid droplets in the renal cortex of Cre (+) mice compared to their Cre (-) littermates.

BUN levels, serum creatinine, and creatinine clearance were comparable in both genotypes (**Figure 24B**). The acute injury markers *Ngal* and *Kim-1* were not elevated in the kidneys of male mice on HFD (**Figure 24C**).

Figure 25 A-C shows H&E stained kidney sections from three different Cre (-) mice. Surprisingly, Cre (-) animals show an increased accumulation of droplets in number and size (arrows) compared to their Cre (+) littermates lacking *RetSat* in the kidney (**Figure 24 D-F**). These droplets appear to be confined to the renal cortex and may represent an accumulation of triglycerides.

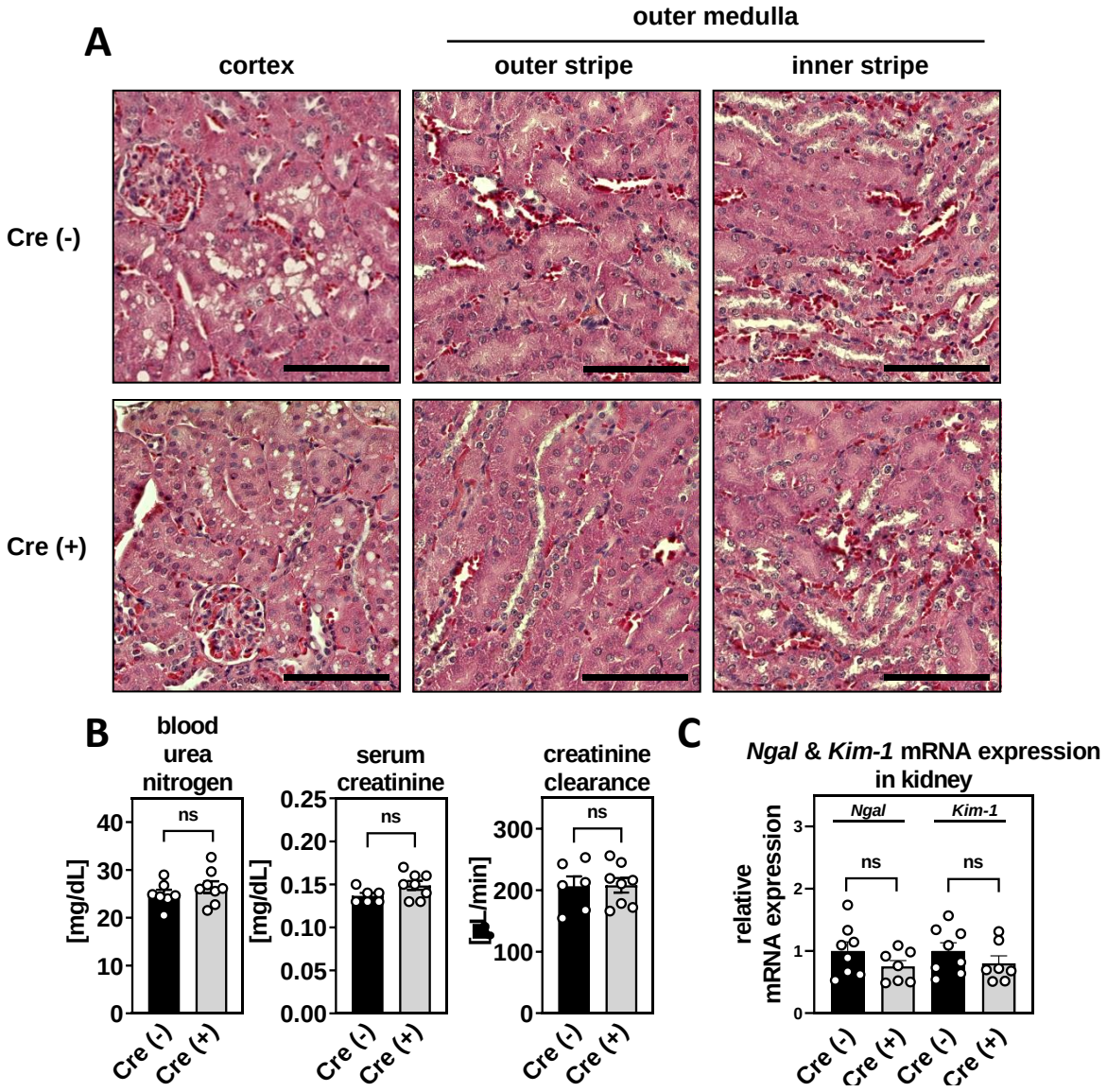

Figure 24: *RetSat* knockout mice on HFD exhibited a decreased cortical lipid accumulation but did not show an impairment of renal function. **(A)** Representative images of kidney sections stained with hematoxylin and eosin (H&E) of male mice showing renal cortex, the outer and inner stripe of the outer medulla, scale bar = 200 µM. **(B)** Blood urea nitrogen (BUN) levels, serum creatinine, and creatinine clearance of Cre (-) and Cre (+) male mice, (n = 7,8). **(C)** Relative mRNA expression of *Ngal* & *Kim-1* in whole kidney tissue of Cre (-) and Cre (+) male mice, (n = 10,10). All male mice were 25 – 27 weeks old. Data are represented as individual data points and mean ± sem. *P-value < 0.05 by two-tailed t-test, ns = not significant.

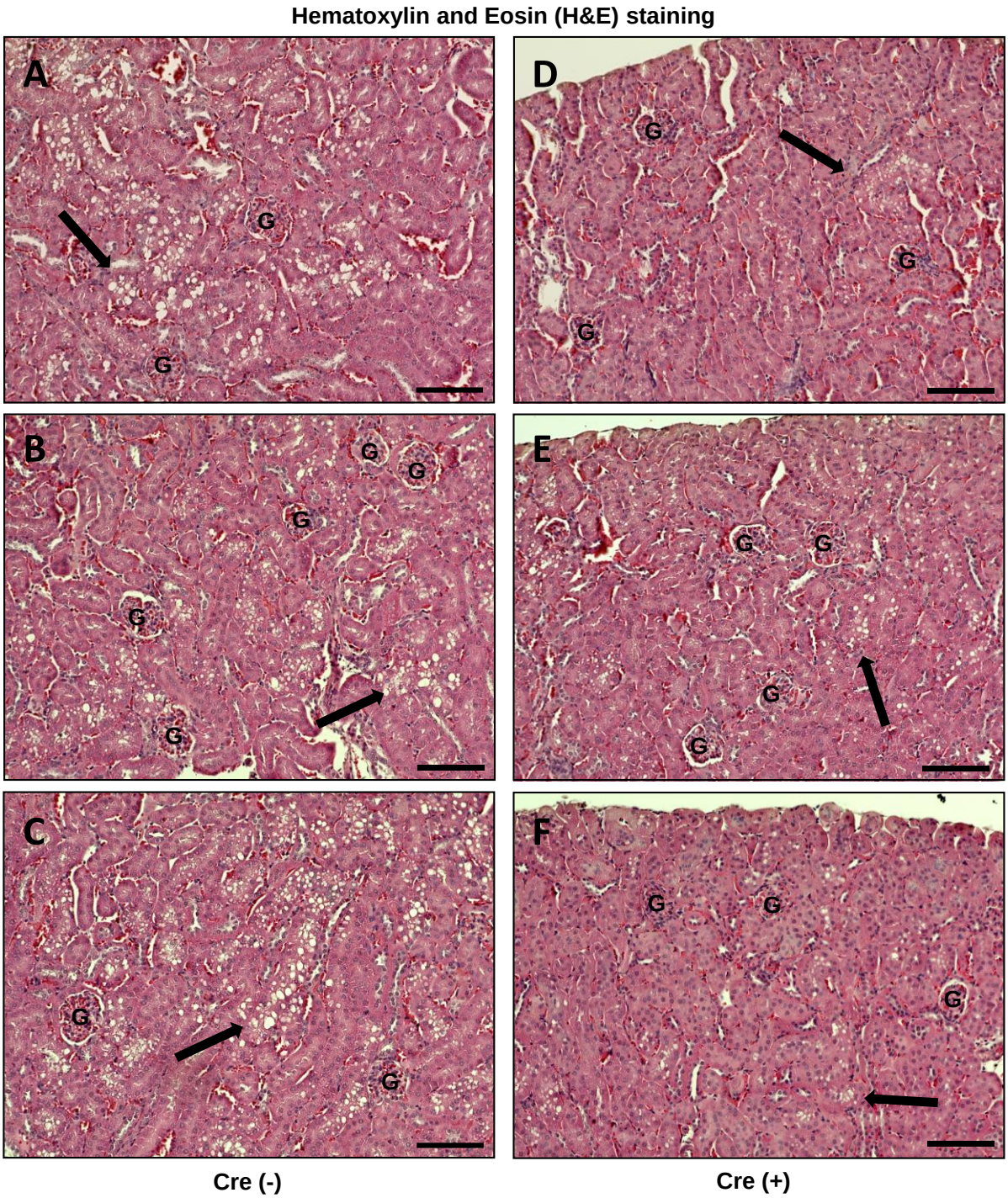

Figure 25: Adult *RetSat* knockout mice on a HFD exhibit less lipid accumulation in the renal cortex. Representative images of kidney sections stained with hematoxylin and eosin (H&E) of three different male mice per genotype showing the renal cortex and lipid accumulation (arrow) of Cre (-) mice (**A – C**) and Cre (+) mice (**D – F**), scale bar = 200 µM, G = glomerulus.

5. Discussion

5.1 Generation and validation of a novel mouse model with kidney-specific knockout of *RetSat*

To investigate the function of RetSat in the kidney, we successfully generated a novel mouse model with kidney-specific deletion of *RetSat* in tubular epithelial cells. In whole kidney tissue from C57BL/6J mice lacking *RetSat*, we observed a consistent reduction of RetSat at both mRNA and protein levels of approximately 35% (**Figure 8 A-C**). *RetSat* is heterogeneously expressed along the nephron with strongest expression in PT, TAL and in the DCT [5, 111], whereas Cdh16-Cre expression is high in the TAL, DCT, CD and low in PT [103, 104]. Therefore, we expect a significant knockout efficiency of *RetSat* in the TAL, DCT and CD of the mouse nephron. In addition, whole kidney tissue consists of a mixture of different cell types such as renal epithelial cells, endothelial cells, immune cells and fibroblasts. In these cell types, RetSat expression has been reported previously [95, 152]. Significantly higher knockout efficiencies with the Cdh16-Cre transgene were achieved when targeting genes expressed exclusively in the TAL [145] or in the distal tubulus and CD [153]. Compared to other commercially available transgenic mouse lines targeting kidney cells [154, 155], we were able to address the off-target deletion of *RetSat* in the thyorid in our mouse model. Furthermore, Cdh16-Cre affects not only a segment of the nephron, such as AQP2-CreTag or PEPCK-Cre [154], but a wide variety of renal tubular epithelial cells [104]. It was not necessary to implement a tamoxifen-inducible Cre in our mouse model, as *RetSat* has been shown to be non-essential for the development and viability in a whole-body knockout model [97].

We were able to show that Cdh16-Cre expression is present in thyroid but does not induce *RetSat* deletion in our mouse model (**Figure 8E**). In contrast, TPO-Cre showed a significant decrease in *RetSat* at the mRNA level in the thyroids of the TPO-Cre x $RetSat^{flox/flox}$ mouse model. These data strongly suggest that the phenotypes observed in our mouse model are related to the deletion of *RetSat* in the kidney, but not other organs. To our knowledge, this study is the first to directly compare the expression of Cdh16-Cre and TPO-Cre in the thyroid of male mice.

In conclusion, our novel mouse model with kidney-specific deletion of *RetSat* is a reliable model to study its function in a subset of renal tubular epithelial cells.

5.2 *RetSat* deletion induces proteinuria and alters urinary protein composition in adult mice

We observed a consistent increase of approximately 30% in protein concentration in the 24 h urine of male and female mice lacking *RetSat* (**Tables 17 & 18**). In addition, male mice showed a significant increase in urinary albumin concentration without changes in the circulation, and when the sexes were pooled, hyperphosphaturia was observed. To investigate the protein composition and to identify protein species of high abundance, we performed a proteomic approach using 24 h urine. In our study, we used two different normalization methods to account for changes in protein composition. We performed a commonly used pre-acquisition method and loaded equal amounts of protein [156]. As we were looking for unknown high abundance protein species that directly influence the total protein concentration, this approach could lead to biased data. Therefore, we performed a post-acquisition method and introduced a manual scaling factor for each sample based on the measured total protein concentration.

As expected, we observed major urinary proteins (MUPs) to be the most abundant proteins excreted (data not shown), which is consistent with reports in the literature [157]. MUPs are a class of the lipocalin superfamily that regulate chemical communication and nutrient metabolism [158, 159]. Their contribution to proteinuria in healthy mice is a species-specific characteristic and occurs under physiological conditions [160]. This is in contrast to humans, where proteinuria is associated with acute or chronic kidney disease [161, 162]. Surprisingly, we did not identify any particular MUP with higher abundance, but two species with lower abundance (*Mup17* & *Mup19*) in the 24 h urine of Cre (+) mice (**Figure 10**).

Interestingly, we observed an increased abundance of RBP4 in 24 h urine of Cre (+) mice. Retinol-bound RBP4 forms a complex with tetrameric TTR, which prevents its renal filtration due to its high molecular weight [56, 57, 163]. Only non-complexed and non-retinol bound apo-RBP4, as a single ~21 kDa protein, is freely filtered and reabsorbed in the glomerulus [158, 164]. In healthy kidneys, >99% of filtered RBP4 is reabsorbed by the megalin-tubulin system in the proximal tubule [165, 166]. In addition, urinary RBP4 is indicative of tubular injury and reflects the severity of proximal tubule

dysfunction [167], is highly elevated (> 10^4 fold) and associated with human diseases such as diabetes, glomerulopathies, chronic kidney disease and Dent's disease [166, 168-170]. In general, *Rbp4* is highly expressed in liver and adipose tissue [171], but very low in kidney [5, 111]. Renal expression of *Rbp4* in adult male mice was examined by qRT-PCR, but we did not detect any differences between the two genotypes (data not shown).

There are several explanations for the increased levels of urinary RBP4 levels observed in our Cre (+) mice. One possibility is that renal epithelial cells lacking *RetSat* have higher retinol levels. To counteract this imbalance, systemic RBP4 is increased to transport excess retinol to extrarenal tissues for storage. These effects could lead to increased renal filtration of apo-RBP4 and increased urinary RBP4 levels. To test this hypothesis, serum levels of RBP4 and retinol could be measured. Furthermore, hepatic and renal retinol, retinaldehyde and retinyl ester could be analyzed to understand retinoid homeostasis in mice lacking *RetSat*. Another possible explanation could be an impairment of mechanisms that directly influence renal function, such as impairment of glomerular barrier function or inhibition of the megalin-cubulin system. An impairment of renal function is unlikely as there were no changes in the parameters that determine renal function (**Figure 9B & C**). The moderate albuminuria we observed in males (**Table 17**) correlates with elevated urinary RPBP4 levels and has been reported in patients with diabetes and diabetic nephropathy [172-174]. In addition, there was a slight increase in renal Pi excretion without hypophosphatemia in male mice lacking *RetSat* (**Table 17**). Renal Pi reabsorption can be regulated by a number of factors, including dietary Pi intake, atRA, 1α,25$(OH)_2D_3$, parathyroid hormone (PTH) and fibroblast growth factor 23 (FGF23), which need to be evaluated to complete the understanding of the phenotypes occurring in adult male Cre (+) mice. The moderately elevated urinary excretion of RBP4, albuminuria and mild hyperphosphaturia suggest a possible onset of metabolic disease related to insulin resistance and type 2 diabetes, but do not reflect the >10^4 levels reported in diabetic nephropathy [172].

Hypothetically, increased cellular levels of retinol could lead to increased levels of atRA, which would induce the RAR and its target genes. We examined known target genes of *RAR*, such as *RARβ*, *Stra6* and *Pck1* [175, 176] in adult male mice, but found no difference between the two genotypes (data not shown). Interestingly, RNA-Seq. analysis of middle-aged male mice revealed a strong downregulation of *Aldh1a1* (**Figure 19**), the main enzyme that catalyzes the synthesis of atRA from retinaldehyde [177]. Unexpectedly, *Cyp26b1* an enzyme known to be responsible for the hydroxylation and clearance of atRA, was also downregulated in the RNA-Seq. data (data not shown). The expression of these two genes is contrasting and needs further evaluation. Notably, *Cyp26b1* has been shown to not only be regulated by RAR, but was also strongly upregulated in the presence of a PPARγ agonist [178]. The downregulation of *Cyp26b1* could therefore be an atRA-independent effect. To add another layer of complexity, we observed different phenotypes in adult male mice compared to middle-aged mice, with the latter lacking proteinuria, hypercalciuria and hypophosphaturia in the latter one (**Table 20**). Age-related effects or compensatory mechanisms could be responsible for the differentially expressed RAR target genes.

Another interesting finding of a protein with comparatively high abundance and significant differential expression was FXYD5 (**Figure 10**). FXYD5 is known to interact with and functionally and structurally modulate Na^+/K^+-ATPase. Co-expression of FXYD5 with Na^+/K^+-ATPase resulted in a 2-fold increase in V_{max} of the pump [179]. The FXYD5 protein exists as a ~24 kDa protein under physiological conditions, but has been reported to downregulate E-cadherin and is highly O-glycosylated in metastatic cells [180, 181]. Expression of FXYD5 in M1 collecting duct cells decreased paracellular electrical resistance and increased permeability to macromolecules [182]. Interestingly, a functional link between RETSAT and cancer was reported in another study [183]. Furthermore, the previously described bioinformatic approach linking RetSat to insulin resistance and diabetic state may contribute to higher glycosylation rates of FXYD5 [86]. The loss of *RetSat* in renal tubular epithelial cells could possibly increase FXYD5 expression by an as yet unknown mechanism and directly regulate cell-cell adhesion via structural modification of the Na^+/K^+-ATPase. This hypothesis is less likely, but cannot be excluded, since we only measured blood glucose concentrations in middle-aged male mice (**Figure 15A**) and not in adult male mice.

Post-acquisition normalization of urinary protein abundances using a manual scaling factor resulted in higher excretion of > 75% of the identified proteins in Cre (+) adult male mice (**Figure 11A**). These data are not consistent with the approximately 30% increase in protein concentration observed in **Table 17**. Nevertheless, we performed a pathway analysis of these more abundant proteins and found that these proteins are involved in wound healing, blood coagulation and homeostasis (**Figure 11B**). In principle, these pathways would be expected to restore cell integrity after injury. Genes indicative of acute kidney injury, such as *Ngal* and *Kim-1*, were not induced in adult Cre (+) animals (**Figure 9C**).

It is not clear from this study what are the underlying mechanistic effects of the proteinuria that occurs in adult Cre (+) mice. In addition, we could not explain why this phenotype disappeared in middle-aged mice. As discussed above, *RetSat* knockout could lead to higher intracellular atRA levels by providing more retinol as a substrate. Higher atRA levels are most likely not the cause of proteinuria, since atRA has been shown to have protective and preventive effects in rodent kidney diseases where glomerular barrier function is impaired [184-186]. Furthermore, atRA significantly reduced proteinuria and had anti-inflammatory effects in diabetic rats [76]. The underlying mechanisms and the role of *Vdr* remain to be elucidated and may provide targets for further studies.

5.3 *RetSat* deletion leads to the upregulation of *Vdr* in male mice

In our study, we showed that *RetSat* deletion increased *Vdr* expression in renal tubular epithelial cells of middle-aged male mice. RNA-Seq. revealed an upregulation of *Vdr* by approximately 20%. In addition, known *Vdr* target genes were differentially expressed in Cre (+) male mice (**Figure 18**). Surprisingly, in the same middle-aged mice we observed renal phenotypes such as significant hypercalciuria, hypophosphaturia without the occurrence of the proteinuria previously observed in adult mice (**Table 20**). The hypophosphaturia is in contrast to the hyperphosphaturia observed in adult male and female mice (**Tables 17 & 18**).

This study showed an increase in *Vdr* mRNA levels and differential expression of known *Vdr* target genes (**Figure 18**). Interestingly, *Vdr* expression along the nephron appears to have a similar expression pattern to *RetSat*, especially in nephron segments that are targeted by the Cdh16-Cre [5, 104]. Several of these differentially expressed target genes showed an induction in Cre (+) mice (*Pvalb, Col8a1, Nqo1, Cyp7b1* & *Sprr2a1*), whereas these genes were downregulated in mice with renal *Vdr* deletion [146]. Our findings regarding the downregulation of *Vdr* target genes (*Dsc2, Ptgfr, Ptgds, St3gal4, Kcnj2* & *Ptger3*) are consistent with increased *Vdr* expression and activity in Cre (+) mice, as these genes are upregulated in *Vdr* knockout mice [146]. Gene ontology pathway analysis revealed the involvement of downregulated genes with cell adhesion & migration and calcium transport, consistent with the pathways affected in *Vdr* knockout mice [146]. In particular, *Pvalb* has been shown to be involved in renal calcium handling [187]. *Pvalb* knockout mice did not show altered calcium handling at baseline, but when challenged with NaCl or furosemide. In contrast to our study, they developed a diuresis and hyperkaliuria phenotype [187], which we did not observe in our mouse model (**Table 20**). Independently of *Vdr*, a gene involved in renal calcium transport (Kcnj10) was differentially expressed in male Cre (+) mice (**Figures 19 & 20**). *Kcnj10* is highly expressed in the distal convoluted tubule of the mouse kidney [5] and encodes a specific potassium channel at the basolateral membrane responsible for generating the cell membrane potential [188]. Changes in cell membrane potential can affect the paracellular transport of calcium, resulting in increased renal excretion. In addition, cell membrane potential and subsequent K^+ recycling may affect Na^+/K^+-ATPase activity [189, 190]. In the previous chapter we

discussed the role of Na^+/K^+-ATPase and its modification by FXYD5 in the adult mouse. A possible relationship between the urinary phenotypes in our mouse model and direct or indirect effects on Na^+/K^+-ATPase cannot be excluded and needs to be further investigated. Another interesting finding of our study was the upregulation of the calcitonin receptor (Calcr). Its ligand calcitonin is a thyroid hormone that is released when the organism is hypercalcemic and induces renal excretion to counteract systemic calcium overload [191, 192]. In a global *Calcr* knockout mouse model, mice had elevated serum calcium levels [193]. The opposite effect, a strong upregulation of *Calcr* in Cre (+) mice, may contribute to the increased renal excretion of calcium. Furthermore, excessive urinary calcium excretion with normal serum calcium levels is a common risk factor for the development of nephrocalcinosis [142]. We did not observe nephrocalcinosis in our Cre (+) mice (**Figure 17**), but evidence for a relationship between polymorphisms in the human *VDR* gene and stone formation has been discussed [194]. In mice that developed nephrocalcinosis, urinary Ca^{2+} excretion was 50% higher than in controls [195], whereas Cre (+) mice excreted only about 20% more Ca^{2+} than their littermates (**Table 20**).

Vdr can be modulated, both positively and negatively, by a variety of steroids and peptide hormones, growth factors and cytokines [196]. In particular, atRA has been shown to induce *Vdr* in bone cells [197]. Deletion of *RetSat* in renal tubular epithelial cells could prevent the metabolism of all-*trans* retinol and therefore increase intracellular levels of this molecule [61]. Subsequent oxidation would increase retinoic acid levels and potentially induce *Vdr* expression. Interestingly, *Aldh1a1*, which is required for the synthesis of retinoic acid from retinal is a RARα target gene [198], was significantly downregulated in Cre (+) mice (**Figure 19**). This finding suggests that higher intracellular atRA levels are not responsible for the upregulation of *Vdr* in Cre (+) animals.

The proteinuria reported in adult males and females (**Tables 17 & 18**) was absent in middle-aged male mice (**Table 20**). In middle-aged male mice, genes involved in cell adhesion and migration were downregulated, and GO pathway analysis of downregulated genes suggests that *RetSat* deletion alters cell-cell assemblies (**Figure 20**). A study of mice overexpressing retinol dehydrogenase 9, the rate-limiting enzyme that converts retinol to retinal, showed a reduction in proteinuria was shown following

disease and toxin-induced nephropathy [73]. Topical application of retinoids has also been shown to cause retinoid dermatitis in humans with scaling, burning and itching [199]. In a study using hairless mice and cultured human keratinocytes, retinoids were shown to significantly increase corneocyte desquamation and corneodesmosome degeneration [200]. In particular, two calcium-dependent desmosomal cadherins, desmoglein (DSG 1) and desmocollin 1 (DSC1), were downregulated upon retinoid exposure. DSC1 is a paralog of desmocollin 2 (DSC2), which is a *Vdr* target gene and was significantly downregulated in our RNA-Seq. analysis (data not shown). The upregulation of *Vdr* in Cre (+) mice could also be a renoprotective effect that is induced by proteinuria. In a study conducted in mice with type 2 diabetes, Wang *et al*. were able to show that *Vdr* is expressed in podocytes and is highly inducible by $1\alpha,25(OH)_2D_3$ [201]. In follow-up studies, the authors we able to show that *Vdr* null mice develop robust albuminuria in the diabetic state and that nephrin, a key slit diaphragm protein, is transcriptionally induced by $1\alpha,25(OH)_2D_3$ [202, 203]. *Vdr* inhibits podocyte apoptosis by inhibiting p38 MAPK/ERK signalling and upregulating nephrin mRNA levels to contribute to the renoprotective effects [204]. The upregulation of *Vdr* and its proposed renoprotective effects may explain the disappearance proteinuria in middle-aged Cre (+) mice.

In our study, we observed an increase in body weight of male Cre (+) mice on NC (**Figure 12D**) with an onset after ~20 weeks of age. NMR experiments performed before this onset showed no differences in absolute and relative body composition (**Figure 12B & C**), but body composition changed in middle-aged male Cre (+) animals. Unexpectedly, absolute lean mass and absolute, as well as relative free water increased (**Figure 14C**). An increase in body weight has been reported in mice on a mixed 129Sv/C57BL6 background with a whole-body knockout of *RetSat* [94]. In contrast to our results, these mice showed an increase in body weight of more than 10% and an early onset of the weight difference from the first week of feeding NC. Interestingly, a study conducted with mice on a C57BL/6N background showed an increase in body weight compared to C57BL/6J mice on NC or HFD [205]. Furthermore, other studies have reported an increased caloric intake in C57BL/6N mice compared to their C57BL/6J counterparts fed a HFD [206] and have demonstrated distinct responsiveness of C57BL/6J sub-strains to a HFD [207]. Thus, the genetic background has a critical influence on the development of phenotypes. An

unevenly distributed genetic background could result in mice with more traits towards one genotype and could explain the observed differences. In addition, whole-body deletion of *RetSat* could drastically alter energy homeostasis and lead to an increased storage of excess energy in adipose tissue. On the other hand, a kidney-specific deletion only partially contributes to the lower increased body weight gain observed in Cre (+) mice. The later onset of obesity in our mouse model may indicate a compensatory mechanism involving a direct or indirect increase in body weight. In particular, the influence of circulating vitamin D levels and *Vdr* expression in metabolic diseases such as obesity and type 2 diabetes and its role in energy metabolism have been widely discussed [208-211]. In *Vdr* null mice on a 129/sv background, the authors observed reduced body weight including hypocalcaemia [212]. These results are consistent with another *Vdr* knockout study in C57BL/6 mice, which showed a significantly lower body weight, independent of food intake [213]. In the latter study, authors the authors showed an increase in basal EE in *Vdr* knockout mice, which was mediated by increased levels of uncoupling protein 1 & 3 (UCP1 & UCP3) in BAT. On the other side, addition of 1α,25$(OH)_2D_3$ directly downregulates UCP1 & UCP3 in primary BAT cells [213]. Therefore, we hypothesize that increased circulating 1α,25$(OH)_2D_3$ levels may be responsible for the increased body weight in middle-aged mice. It is known that *Vdr* expression is induced by 1α,25$(OH)_2D_3$ through autoregulation [214] and that 1α,25$(OH)_2D_3$ can suppress UCP1 & UCP3 which would potentially result in lower basal energy expenditure. We did not measure energy expenditure in middle-aged mice, but in adult mice on NC at 20 weeks of age (**Figure 13A-D**) and could not detect any differences. However, the onset of increased body weight in Cre (+) mice was after week 21/22 (**Figure 12D**). This association may be of greater significance and needs to be evaluated. In another study investigating metabolic changes in *Vdr* null mice, male juvenile and adult mice showed a decrease in body weight [210], supporting our hypothesis. Taken together, these results suggest that the increase in body weight is most likely due to increased systemic 1α,25$(OH)_2D_3$ levels in Cre (+) mice.

Other phenotypes in *Vdr* null mice include hypocalcemia, hypophosphatemia, hyperparathyroidism, elevated PTH levels, rickets and alopecia [212, 215-217]. In addition, *Vdr* null mice lack the feedback mechanism to autoregulate 1α,25$(OH)_2D_3$ levels, resulting in a systemic increase in 1α,25$(OH)_2D_3$. Interestingly, high levels of

1α,25$(OH)_2D_3$ suppress systemic PTH concentrations [218]. High systemic PTH levels have been shown to inhibit nephron phosphate reabsorption and lead to hyperphosphaturia [219], an effect we observed in adult Cre (+) animals (**Tables 17 & 18**). In middle-aged mice we observed the opposite phenotype (**Table 20**). This may further support the theory that Cre (+) mice develop a compensatory mechanism that results in a shift from high PTH levels in adult mice to lower PTH levels in middle-aged mice. Since high circulating PTH induces systemic 1α,25$(OH)_2D_3$ levels and, by a feedback mechanism, high 1α,25$(OH)_2D_3$ levels suppress PTH, we hypothesise that our mice have elevated systemic levels of 1α,25$(OH)_2D_3$. Excess vitamin D levels have been shown to be associated with hypercalciuria [220], another prominent phenotype in our Cre (+) mice (**Table 20**). Furthermore, in the presence of Ca^{2+}, 1α,25$(OH)_2D_3$ can strongly induce renal *Vdr* expression in vivo [221].

Overall, we have demonstrated an interesting new link between retinoid and vitamin D metabolism. It is not clear whether higher intracellular levels of retinol are responsible for the upregulation of *Vdr* in the kidney or whether higher systemic levels of 1α,25$(OH)_2D_3$ induced renal *Vdr* expression. Based on the data, an alteration in renal vitamin D metabolism and systemic vitamin D levels is more likely and could explain the observed phenotypes.

5.4 Influence of *RetSat* Deletion on high-caloric food intake in mice

A high dietary intake of saturated fat has been shown to contribute to the development of obesity, hyperglycaemia, insulin resistance and vascular disease in humans and rodents [222-224]. All of these metabolic disorders have been linked to the development of renal disease. To investigate the possible influence of renal *RetSat* depletion under a high calorie diet, we fed male mice an HFD (60 kcal % fat) for 20 weeks. As shown in **Figure 21A**, we observed an increase in body weight & increased body weight gain after 10 weeks on HFD. This increase in body weight was accompanied by relative changes in body composition with an expected higher proportion of fat mass and lower proportion of lean mass in Cre (+) animals (**Figure 21B**), independent of food intake (**Figure 21C**). Surprisingly, *RetSat* whole body knockout animals did not show an increase in body weight after 10 weeks, but an increase in body weight gain [94]. The higher proportion of fat mass observed is consistent with the reported increased adiposity in whole body knockout mice fed an HFD with 45 kcal % fat [97], which is lower than the HFD used in our study.

In contrast to NC-fed mice, where the onset of increased body weight occurred after week 20 (**Figure 12D**), HFD-fed mice showed a trend towards increased body weight from the beginning (**Figure 21A**). This HFD-induced increase in body weight could be a primary effect of the high caloric intake and an imbalance in energy expenditure, whereas the later onset in mice on NC could be due to the previously discussed secondary effect of systemic $1\alpha,25(OH)_2D_3$ levels and the upregulation of *Vdr*. However, mice fed an HFD and supplemented with cholecalciferol showed less weight gain than their littermates fed an HFD [225]. This study would support the idea that the observed increase in body weight in HFD mice may be independent of vitamin D and *Vdr* activation.

To further investigate energy balance and energy expenditure in mice on HFD, we performed metabolic cage experiments. After 20 weeks of age and 12 weeks on HFD, the mice were analyzed. RER and locomotor activity did not change between the two genotypes (**Figure 22A & C**). This is in contrast to a previously reported increase in locomotor activity in whole body knockout mice [94]. The authors suggested that the increase in body weight despite the observed increase in locomotor activity was due

to reduced energy expenditure. In our study, we demonstrated that Cre (+) mice on HFD showed a significant decrease in energy expenditure when considering body weight (data not shown) and body weight$^{0.75}$ (**Figure 22B**). The latter approach is used to circumvent the problem that energy expenditure does not increase in direct linear proportion to body mass and was determined by comparing basal metabloc rate [226]. In a recently proposed approach, Müller and colleagues showed that a regression-based analysis could distinguish between spurious (mass-dependent) and true (mass-independent) group differences [226]. In a subsequent analysis of energy expenditure in HFD mice, we were unable to detect a mass-independent effect in Cre (+) mice (data not shown). It is highly likely that the effects we observed are mass-dependent and therefore do not represent a true difference between the two genotypes.

HFD is known to induce obesity and contribute to the development of kidney disease [227, 228]. In the early stages of obesity, HFD can cause structural and functional changes in the kidney, including glomerular hyperfiltration, thickening of the glomerular basement membrane and mesengial cell proliferation [229]. Severe obesity is associated with focal and segmental glomerulosclerosis [230] and contributes to the pathogenesis of a nephropathy [227, 231, 232]. Surprisingly, we did not observe any morphological or functional changes indicative of renal injury in HFD-fed mice (**Figure 24A**). Serum parameters such as BUN and creatinine were comparable to adult mice (**Figure 9B**) and even lower compared to middle-aged mice (**Figure 16B**). In addition, markers of acute kidney injury were not elevated in Cre (+) mice compared to their Cre (-) littermates (**Figure 24C**). These results were not expected but could be explained by a reported strain-specific resistance of C57BL/6 mice to kidney injury [233] and diabetic nephropathy [234]. In contrast to these studies, other studies have demonstrated the induction of kidney injury in this particular strain [150, 235]. The underlying mechanism behind the strain specificity remains to be elucidated, but this could be the potential reason for the lack of renal injury in our mouse model.

In this study, we observed a significant increase in blood glucose levels in Cre (+) mice (**Figure 23B**), which was accompanied by a concomitant decrease in β-hydroxybutyrate levels (**Figure 23C**) in Cre (+) mice fasted for 16 h. Subsequent ipGTT revealed impaired glucose clearance (**Figure 23A**) without the development of significant insulin resistance (**Figure 23D**). Interestingly, blood glucose levels in *ad*

libitum fed and 4 h fasted mice were not affected by *RetSat* deletion. However, we observed higher blood glucose concentrations in the fasted state, suggesting increased endogenous release of glucose either through an increased reabsorption, an increased renal gluconeogenesis or indirectly through renal signalling to induce hepatic gluconeogenesis [236]. A possible increase in gluconeogenesis could be explained by increased activation of the transcription factor Forkhead Box O1 (*FoxO1*), which has been shown to be induced in the liver during fasting [237]. In addition, *FoxO1* has been reported to induce *RetSat* expression in the liver and to colocalise with *RetSat* in proximal renal epithelial cells [5, 91]. In the kidney, gluconeogenesis is restricted to proximal tubule epithelial cells, where specific gluconeogenic enzymes, such as G6p and phosphoenolpyruvate carboxykinase 1 (Pck1) are expressed [238-240]. In another study in a porcine kidney cell line, FoxO1 regulated the expression of endogenous G6p in an insulin-dependent manner [241]. These data suggest that the comparatively low knockout efficiencies reported in proximal tubule epithelial cells [103, 104] still have a major impact on glucose homeostasis in the fasted state in HFD mice. It could be speculated that FoxO1 regulates renal gluconeogenesis via the induction of *RetSat* in the fasted state. *RetSat* itself, or its enzymatic products might have an inhibitory effect on G6p activity. Other possibilities such as hepatorenal glucose reciprocity [22, 242], hormonal changes directly affecting gluconeogenesis [243] or glucose reabsorption processes [16] cannot be excluded as they were not addressed in this study.

In the present study, we surprisingly found a significant difference in absolute and relative kidney weight in HFD-fed mice (**Table 23**), whereas we did not observe this effect in overnight fasted mice (**Table 24**). Cre (+) mice showed a reduction in kidney weight of more than 10% compared to their Cre (-) littermates. Subsequent histological analysis revealed an increased accumulation of lipid droplets in the renal cortex of Cre (-) mice (**Figure 25 A-C**). These droplets were not present in kidney sections from Cre (+) animals (**Figure 25 D-E**). In a previous study, our laboratory demonstrated that *RetSat* is an upstream regulator of ChREBP in mouse liver [87]. ChREBP is a key regulator of glycolysis and *de novo* lipogenesis [244]. Loss of *RetSat* in renal tubular epithelial cells may impair ChREBP dependent *de novo* lipogenesis and may explain the decreased number and size of lipid droplets particularly in the renal cortex, since as ChREBP is highly expressed in the proximal tubule [5, 111]. Several studies have

shown that HFD induces lipid accumulation, particularly triglycerides, phospholipids and cholesteryl esters, and that their increased presence is associated with an adverse outcome in the progression of renal disease in rodents [245-247]. Interestingly, AMP-activated protein kinase (AMPK) is an important energy sensor that may be critical in regulating renal lipid accumulation in C57BL/6J mice fed an HFD [245]. Chronic AMPK activation with AMPK activator attenuated the number of vacuolated tubules, an effect similar to that observed in Cre (+) animals (**Figure 25 D-F**). HFD-induced obesity inhibits the activation of AMPK in renal cells and leads to increased lipogenesis, induction of cholesterol synthesis via 3-hydroxy-3-methylglutaryl-CoA reductase and sterol regulatory element binding transcription factor 1 [248]. This leads to an increased accumulation of cholesteryl esters and phospholipids. In particular, acyclic retinoid, a synthetic retinoid, is known to activate AMPK, which was then effective in preventing hepatocellular carcinoma in diabetic mice and humans [249, 250]. In addition, AMPK has previously been shown to be activated by retinoic acid in vitro [251, 252]. There appears to be a strong relationship between the activation of AMPK and retinoids in non-adipose tissues. As discussed above, loss of *RetSat* could increase intracellular retinoic acid concentrations and lead to increased AMPK activity, protecting renal tubular epithelial cells from lipid droplet accumulation. It should be emphasized that a deeper understanding of the biological functions of RetSat is still lacking and that other enzymatic products could be responsible for the observed phenotypes.

To summarise the results in our study, high calorie intake negatively affects metabolic balance but does not induce renal injury in C57BL/6J mice. Deletion of *RetSat* contributes to an increase in blood glucose concentration in the fasted state and changed absolute and relative body composition. In addition, kidney-specific *RetSat* deletion impaired lipid accumulation in the renal cortex.

6. Conclusion and Outlook

In this thesis we aimed to generate a novel mouse model with deletion of *RetSat* in a subset of renal tubular epithelial cells. We have successfully generated, validated and characterized this novel mouse model on NC and HFD. The expertise of our laboratory, collaboration and consultation with researchers at the Charité and affiliated institutes allowed us to gain new insights into renal vitamin and energy metabolism in mice on a C57BL/6J background. In particular, we were able to establish a link between the kidney-specific deletion of *RetSat* and an increased transcriptional expression of the *Vdr* in middle-aged mice. The renal upregulation of *Vdr* and its renoprotective effects could be the consequence of altered systemic vitamin D levels and may explain the disappearance of proteinuria in middle-aged mice, which was present in adult mice. Furthermore, this could be a potential underlying mechanism for the observed changes in urine composition in adult mice lacking *RetSat*, compared to their middle-aged mice littermates.

An increase in body weight was observed in mice on HFD lacking *RetSat* and could be reproduced in mice fed a NC. However, mice on NC developed the body weight phenotype later in life. In addition, our results show that a kidney-specific deletion of *RetSat* decreased systemic glucose clearance and increased fasting blood glucose concentrations in mice on HFD without inducing insulin resistance. Surprisingly, the same mice did not develop renal pathologies, which may be due to a strain-specific resistance against HFD induced renal injury. In contrast, *RetSat* deletion resulted in a reduced accumulation of lipid droplets in the renal cortex.

There are still many gaps in this study. The mechanism by which *RetSat* deletion increases *Vdr* expression remains to be elucidated. It is necessary to measure systemic concentrations of vitamin D and its metabolites, such as 1α,25$(OH)_2D_3$, its precursor 25$(OH)_2D_3$ and the metabolically inactivated form 24,25$(OH)_2D_3$ in all our cohorts. This is particularly important in adult and middle-aged mice, as it could explain the opposite urinary phenotypes observed. In addition, regulators of systemic vitamin D concentrations, such as PTH and FGF23 need to be measured to fully understand the interacting partners at the systemic level. We recognize that increased *Vdr* expression and observed metabolic changes are associations and could be completely

independent of the vitamin D status. In this study, we did not look at systemic, renal or hepatic levels of retinoid metabolites. This is one of our major limitations, as we cannot distinguish between direct or indirect effects of *RetSat* knockout on one or the other pathway.

Another remarkable finding is the occurrence of proteinuria in adult mice, but not in middle-aged mice. Comprehensive gene expression analysis, such as RNA-Seq., and a histological examination under an electron microscope could reveal possible structural changes in cell-cell adhesion or an impairment of cell integrity. Targeting other segments of the nephron would be another possibility to further elucidate the proteinuric effect in mice lacking *RetSat*. One option would be the iL1-sgtl2-Cre line, which induces a PT-specific knockout in mice [253]. This model could be used to study the influence of *RetSat* on the megalin system, the consequences on RBP4 reabsorption and its role in renal gluconeogenesis.

An impaired energy balance could be another possible explanation for the increase in body mass that we see in mice on NC and HFD. We studied energy expenditure in our mouse model but did not investigate the role of thermogenesis. As discussed, changes in circulating $25(OH)_2D_3$ levels influence UCP1 & UCP3 expression *in vivo* [213]. It would be very interesting to challenge mice with kidney-specific *RetSat* deletion in an acute cold tolerance test [254]. To investigate the decreased cortical accumulation of lipid droplets in mice lacking *RetSat*, renal triglyceride and cholesterol levels need to be measured and compared.

In addition, we did not address the role of *RetSat* on the cardiovascular system. In general, obesity is a major risk factor for the development of cardiovascular disease [255]. The observed increase in body weight could contribute to an altered blood pressure in mice lacking *RetSat*. An association between atRA and cardiovascular disease has already been shown before [256]. It would also be interesting to measure hormonal regulators of renal vasomotor activity, such as renin or aldosterone [257] in our mouse model.

This study highlights the complexity of vitamin metabolism in the kidney and its impact on whole body homeostasis. We may be able to establish new potential links between vitamin A and vitamin D metabolism and contribute to the understanding of the development of metabolic diseases, although the underlying mechanisms still need to be evaluated.

References

1. Fagerberg, L., et al., *Analysis of the human tissue-specific expression by genome-wide integration of transcriptomics and antibody-based proteomics.* Mol Cell Proteomics, 2014. **13**(2): p. 397-406.
2. Yue, F., et al., *A comparative encyclopedia of DNA elements in the mouse genome.* Nature, 2014. **515**(7527): p. 355-64.
3. Weber, P., et al., *Retinol Saturase: More than the Name Suggests.* Trends Pharmacol Sci, 2020. **41**(6): p. 418-427.
4. Skorecki, K., et al., *Brenner & Rector's the kidney*. 2016: Elsevier Philadelphia, PA.
5. Chen, L., C.L. Chou, and M.A. Knepper, *A Comprehensive Map of mRNAs and Their Isoforms across All 14 Renal Tubule Segments of Mouse.* J Am Soc Nephrol, 2021. **32**(4): p. 897-912.
6. Legouis, D., et al., *Renal gluconeogenesis: an underestimated role of the kidney in systemic glucose metabolism.* Nephrol Dial Transplant, 2022. **37**(8): p. 1417-1425.
7. Richart, T., Y. Li, and J.A. Staessen, *Renal versus extrarenal activation of vitamin D in relation to atherosclerosis, arterial stiffening, and hypertension.* Am J Hypertens, 2007. **20**(9): p. 1007-15.
8. Santoro, D., et al., *Interplay of vitamin D, erythropoiesis, and the renin-angiotensin system.* Biomed Res Int, 2015. **2015**: p. 145828.
9. Bertram, J.F., et al., *Human nephron number: implications for health and disease.* Pediatr Nephrol, 2011. **26**(9): p. 1529-33.
10. Short, K.M., et al., *Global quantification of tissue dynamics in the developing mouse kidney.* Dev Cell, 2014. **29**(2): p. 188-202.
11. Kanzaki, G., et al., *Factors associated with a vicious cycle involving a low nephron number, hypertension and chronic kidney disease.* Hypertens Res, 2015. **38**(10): p. 633-41.
12. McNamara, B.J., et al., *A comparison of nephron number, glomerular volume and kidney weight in Senegalese Africans and African Americans.* Nephrol Dial Transplant, 2010. **25**(5): p. 1514-20.
13. Puelles, V.G., et al., *Glomerular hypertrophy in subjects with low nephron number: contributions of sex, body size and race.* Nephrol Dial Transplant, 2014. **29**(9): p. 1686-95.
14. Ryan, G.B., *The glomerular sieve and the mechanisms of proteinuria.* Aust N Z J Med, 1981. **11**(2): p. 197-206.
15. Brenner, B.M., et al., *Determinants of glomerular permselectivity: Insights derived from observations in vivo.* Kidney Int, 1977. **12**(4): p. 229-37.
16. Vallon, V., *Molecular determinants of renal glucose reabsorption. Focus on "Glucose transport by human renal Na+/D-glucose cotransporters SGLT1 and SGLT2".* Am J Physiol Cell Physiol, 2011. **300**(1): p. C6-8.
17. Zelikovic, I. and R.W. Chesney, *Sodium-coupled amino acid transport in renal tubule.* Kidney Int, 1989. **36**(3): p. 351-9.
18. Christensen, E.I. and T.E. Willnow, *Essential role of megalin in renal proximal tubule for vitamin homeostasis.* J Am Soc Nephrol, 1999. **10**(10): p. 2224-36.
19. Schafer, J.A., *Renal water reabsorption: a physiologic retrospective in a molecular era.* Kidney Int Suppl, 2004(91): p. S20-7.
20. Ross, B.D., J. Espinal, and P. Silva, *Glucose metabolism in renal tubular function.* Kidney Int, 1986. **29**(1): p. 54-67.
21. Gerich, J.E., et al., *Renal gluconeogenesis: its importance in human glucose homeostasis.* Diabetes Care, 2001. **24**(2): p. 382-91.
22. Sharma, R. and S. Tiwari, *Renal gluconeogenesis in insulin resistance: A culprit for hyperglycemia in diabetes.* World J Diabetes, 2021. **12**(5): p. 556-568.
23. Alsahli, M. and J.E. Gerich, *Renal glucose metabolism in normal physiological conditions and in diabetes.* Diabetes Res Clin Pract, 2017. **133**: p. 1-9.

24. Iyer, M.S., et al., *Renal Denervation Reverses Hepatic Insulin Resistance Induced by High-Fat Diet.* Diabetes, 2016. **65**(11): p. 3453-3463.
25. Kazancioglu, R., *Risk factors for chronic kidney disease: an update.* Kidney Int Suppl (2011), 2013. **3**(4): p. 368-371.
26. Blomhoff, R., *Vitamin A in health and disease*. 1994: CRC Press.
27. Kawashima, H. and K. Kurokawa, *Metabolism and sites of action of vitamin D in the kidney.* Kidney Int, 1986. **29**(1): p. 98-107.
28. Leheste, J.R., et al., *Megalin knockout mice as an animal model of low molecular weight proteinuria.* Am J Pathol, 1999. **155**(4): p. 1361-70.
29. Raila, J., T.E. Willnow, and F.J. Schweigert, *Megalin-mediated reuptake of retinol in the kidneys of mice is essential for vitamin A homeostasis.* J Nutr, 2005. **135**(11): p. 2512-6.
30. Urena-Torres, P., et al., *Association of kidney function, vitamin D deficiency, and circulating markers of mineral and bone disorders in CKD.* Am J Kidney Dis, 2011. **58**(4): p. 544-53.
31. Mehrotra, R., et al., *Chronic kidney disease, hypovitaminosis D, and mortality in the United States.* Kidney Int, 2009. **76**(9): p. 977-83.
32. Pilz, S., et al., *Vitamin D status and mortality risk in CKD: a meta-analysis of prospective studies.* Am J Kidney Dis, 2011. **58**(3): p. 374-82.
33. Su, Y., et al., *The Association between Serum Retinol-Binding Protein 4 Levels and Cardiovascular Events in Patients with Chronic Kidney Disease.* Lab Med, 2020. **51**(5): p. 491-497.
34. Henze, A., et al., *Alterations of retinol-binding protein 4 species in patients with different stages of chronic kidney disease and their relation to lipid parameters.* Biochem Biophys Res Commun, 2010. **393**(1): p. 79-83.
35. McCollum, E.V. and M. Davis, *The Necessity of Certain Lipins in the Diet during Growth.* Journal of Biological Chemistry, 1913. **15**(1): p. 167-175.
36. Al Tanoury, Z., A. Piskunov, and C. Rochette-Egly, *Vitamin A and retinoid signaling: genomic and nongenomic effects.* J Lipid Res, 2013. **54**(7): p. 1761-75.
37. Blaner, W.S., *Retinol-binding protein: the serum transport protein for vitamin A.* Endocr Rev, 1989. **10**(3): p. 308-16.
38. Blaner, W.S., *STRA6, a cell-surface receptor for retinol-binding protein: the plot thickens.* Cell Metab, 2007. **5**(3): p. 164-6.
39. Morriss-Kay, G.M. and N. Sokolova, *Embryonic development and pattern formation.* FASEB J, 1996. **10**(9): p. 961-8.
40. Napoli, J.L., *Biochemical pathways of retinoid transport, metabolism, and signal transduction.* Clin Immunol Immunopathol, 1996. **80**(3 Pt 2): p. S52-62.
41. Nau, H. and W.S. Blaner, *Retinoids: the biochemical and molecular basis of vitamin A and retinoid action.* 2012.
42. Blegvad, O., *Xerophthalmia, keratomalacia and xerosis conjunctivae.* American Journal of Ophthalmology, 1924. **7**(2): p. 89-117.
43. Giguere, V., et al., *Identification of a receptor for the morphogen retinoic acid.* Nature, 1987. **330**(6149): p. 624-9.
44. Petkovich, M., et al., *A human retinoic acid receptor which belongs to the family of nuclear receptors.* Nature, 1987. **330**(6147): p. 444-50.
45. Dawson, M.I. and Z. Xia, *The retinoid X receptors and their ligands.* Biochim Biophys Acta, 2012. **1821**(1): p. 21-56.
46. Li, B., S.Y. Cai, and J.L. Boyer, *The role of the retinoid receptor, RAR/RXR heterodimer, in liver physiology.* Biochim Biophys Acta Mol Basis Dis, 2021. **1867**(5): p. 166085.
47. Heyman, R.A., et al., *9-cis retinoic acid is a high affinity ligand for the retinoid X receptor.* Cell, 1992. **68**(2): p. 397-406.
48. Levin, A.A., et al., *9-cis retinoic acid stereoisomer binds and activates the nuclear receptor RXR alpha.* Nature, 1992. **355**(6358): p. 359-61.
49. Ruhl, R., et al., *9-cis-13,14-Dihydroretinoic Acid Is an Endogenous Retinoid Acting as RXR Ligand in Mice.* PLoS Genet, 2015. **11**(6): p. e1005213.

50. Harrison, E.H., *Mechanisms involved in the intestinal absorption of dietary vitamin A and provitamin A carotenoids.* Biochim Biophys Acta, 2012. **1821**(1): p. 70-7.
51. Quadro, L., et al., *Transplacental delivery of retinoid: the role of retinol-binding protein and lipoprotein retinyl ester.* Am J Physiol Endocrinol Metab, 2004. **286**(5): p. E844-51.
52. O'Byrne, S.M. and W.S. Blaner, *Retinol and retinyl esters: biochemistry and physiology.* J Lipid Res, 2013. **54**(7): p. 1731-43.
53. Blomhoff, R., et al., *In vivo uptake of chylomicron [3H]retinyl ester by rat liver: evidence for retinol transfer from parenchymal to nonparenchymal cells.* Proc Natl Acad Sci U S A, 1982. **79**(23): p. 7326-30.
54. Sauvant, P., et al., *Retinol mobilization from cultured rat hepatic stellate cells does not require retinol binding protein synthesis and secretion.* Int J Biochem Cell Biol, 2001. **33**(10): p. 1000-12.
55. Shirakami, Y., et al., *Hepatic metabolism of retinoids and disease associations.* Biochim Biophys Acta, 2012. **1821**(1): p. 124-36.
56. Monaco, H.L., M. Rizzi, and A. Coda, *Structure of a complex of two plasma proteins: transthyretin and retinol-binding protein.* Science, 1995. **268**(5213): p. 1039-41.
57. Naylor, H.M. and M.E. Newcomer, *The structure of human retinol-binding protein (RBP) with its carrier protein transthyretin reveals an interaction with the carboxy terminus of RBP.* Biochemistry, 1999. **38**(9): p. 2647-53.
58. Kelly, M. and J. von Lintig, *STRA6: role in cellular retinol uptake and efflux.* Hepatobiliary Surg Nutr, 2015. **4**(4): p. 229-42.
59. Kawaguchi, R., et al., *STRA6-catalyzed vitamin A influx, efflux, and exchange.* J Membr Biol, 2012. **245**(11): p. 731-45.
60. Napoli, J.L., *Functions of Intracellular Retinoid Binding-Proteins.* Subcell Biochem, 2016. **81**: p. 21-76.
61. Moise, A.R., et al., *Activation of retinoic acid receptors by dihydroretinoids.* Mol Pharmacol, 2009. **76**(6): p. 1228-37.
62. Kedishvili, N.Y., *Enzymology of retinoic acid biosynthesis and degradation.* J Lipid Res, 2013. **54**(7): p. 1744-60.
63. Teletin, M., et al., *Roles of Retinoic Acid in Germ Cell Differentiation.* Curr Top Dev Biol, 2017. **125**: p. 191-225.
64. Topletz, A.R., et al., *Induction of CYP26A1 by metabolites of retinoic acid: evidence that CYP26A1 is an important enzyme in the elimination of active retinoids.* Mol Pharmacol, 2015. **87**(3): p. 430-41.
65. Rosselot, C., et al., *Non-cell-autonomous retinoid signaling is crucial for renal development.* Development, 2010. **137**(2): p. 283-92.
66. El Kares, R., et al., *A human ALDH1A2 gene variant is associated with increased newborn kidney size and serum retinoic acid.* Kidney Int, 2010. **78**(1): p. 96-102.
67. Chiba, T., et al., *Retinoic Acid Signaling Coordinates Macrophage-Dependent Injury and Repair after AKI.* J Am Soc Nephrol, 2016. **27**(2): p. 495-508.
68. Yago-Ibanez, J., et al., *Retinoic acid receptor-beta prevents cisplatin-induced proximal tubular cell death.* Biochim Biophys Acta Mol Basis Dis, 2020. **1866**(7): p. 165795.
69. Balasubramanian, S., et al., *Orphan nuclear receptor Nur77 promotes acute kidney injury and renal epithelial apoptosis.* J Am Soc Nephrol, 2012. **23**(4): p. 674-86.
70. Peired, A., et al., *Proteinuria impairs podocyte regeneration by sequestering retinoic acid.* J Am Soc Nephrol, 2013. **24**(11): p. 1756-68.
71. Dai, Y., et al., *Retinoic acid improves nephrotoxic serum-induced glomerulonephritis through activation of podocyte retinoic acid receptor alpha.* Kidney Int, 2017. **92**(6): p. 1444-1457.
72. Nakamura, J., et al., *Myofibroblasts acquire retinoic acid-producing ability during fibroblast-to-myofibroblast transition following kidney injury.* Kidney Int, 2019. **95**(3): p. 526-539.
73. Li, X., et al., *Induction of retinol dehydrogenase 9 expression in podocytes attenuates kidney injury.* J Am Soc Nephrol, 2014. **25**(9): p. 1933-41.

74. Datta, P.K. and E.A. Lianos, *Retinoic acids inhibit inducible nitric oxide synthase expression in mesangial cells.* Kidney Int, 1999. **56**(2): p. 486-93.
75. Rafael Rodriguez, E.M., *Protective Effects of Retinoic Acid on Streptozotocin-Induced Type I Diabetes.* Pancreatic Disorders & Therapy, 2014. **04**(03).
76. Han, S.Y., et al., *Effect of retinoic acid in experimental diabetic nephropathy.* Immunol Cell Biol, 2004. **82**(6): p. 568-76.
77. Moise, A.R., et al., *Identification of all-trans-retinol:all-trans-13,14-dihydroretinol saturase.* J Biol Chem, 2004. **279**(48): p. 50230-42.
78. Park, H., et al., *Identification of the carotenoid isomerase provides insight into carotenoid biosynthesis, prolamellar body formation, and photomorphogenesis.* Plant Cell, 2002. **14**(2): p. 321-32.
79. Breitenbach, J., A. Vioque, and G. Sandmann, *Gene sll0033 from Synechocystis 6803 encodes a carotene isomerase involved in the biosynthesis of all-E lycopene.* Z Naturforsch C J Biosci, 2001. **56**(9-10): p. 915-7.
80. Dailey, T.A. and H.A. Dailey, *Identification of an FAD superfamily containing protoporphyrinogen oxidases, monoamine oxidases, and phytoene desaturase. Expression and characterization of phytoene desaturase of Myxococcus xanthus.* J Biol Chem, 1998. **273**(22): p. 13658-62.
81. Schupp, M., et al., *Retinol saturase promotes adipogenesis and is downregulated in obesity.* Proc Natl Acad Sci U S A, 2009. **106**(4): p. 1105-10.
82. Moise, A.R., et al., *Stereospecificity of retinol saturase: absolute configuration, synthesis, and biological evaluation of dihydroretinoids.* J Am Chem Soc, 2008. **130**(4): p. 1154-5.
83. Moise, A.R., et al., *Metabolism and transactivation activity of 13,14-dihydroretinoic acid.* J Biol Chem, 2005. **280**(30): p. 27815-25.
84. Moise, A.R., et al., *Specificity of zebrafish retinol saturase: formation of all-trans-13,14-dihydroretinol and all-trans-7,8- dihydroretinol.* Biochemistry, 2007. **46**(7): p. 1811-20.
85. Toomey, M.B., et al., *Complementary shifts in photoreceptor spectral tuning unlock the full adaptive potential of ultraviolet vision in birds.* Elife, 2016. **5**.
86. Park, P.J., et al., *Integration of heterogeneous expression data sets extends the role of the retinol pathway in diabetes and insulin resistance.* Bioinformatics, 2009. **25**(23): p. 3121-7.
87. Heidenreich, S., et al., *Retinol saturase coordinates liver metabolism by regulating ChREBP activity.* Nat Commun, 2017. **8**(1): p. 384.
88. Sun, Y., et al., *Identification and characterization of a novel mouse peroxisome proliferator-activated receptor alpha-regulated and starvation-induced gene, Ppsig.* Int J Biochem Cell Biol, 2008. **40**(9): p. 1775-91.
89. Gu, J., et al., *Identification of functional peroxisome proliferator-activated receptor alpha response element in the human Ppsig gene.* Biochemistry (Mosc), 2011. **76**(2): p. 253-9.
90. Hall, R.K., et al., *Regulation of Phosphoenolpyruvate Carboxykinase and Insulin-like Growth Factor-binding Protein-1 Gene Expression by Insulin.* Journal of Biological Chemistry, 2000. **275**(39): p. 30169-30175.
91. Shin, D.J., et al., *Genome-wide analysis of FoxO1 binding in hepatic chromatin: potential involvement of FoxO1 in linking retinoid signaling to hepatic gluconeogenesis.* Nucleic Acids Res, 2012. **40**(22): p. 11499-509.
92. Galan-Caridad, J.M., et al., *Zfx controls the self-renewal of embryonic and hematopoietic stem cells.* Cell, 2007. **129**(2): p. 345-57.
93. Nagaoka-Yasuda, R., et al., *An RNAi-based genetic screen for oxidative stress resistance reveals retinol saturase as a mediator of stress resistance.* Free Radic Biol Med, 2007. **43**(5): p. 781-8.
94. Pang, X.Y., et al., *Retinol saturase modulates lipid metabolism and the production of reactive oxygen species.* Arch Biochem Biophys, 2017. **633**: p. 93-102.
95. Sarang, Z., et al., *Macrophages engulfing apoptotic cells produce nonclassical retinoids to enhance their phagocytic capacity.* J Immunol, 2014. **192**(12): p. 5730-8.
96. Sarang, Z., et al., *Retinol Saturase Knock-Out Mice are Characterized by Impaired Clearance of Apoptotic Cells and Develop Mild Autoimmunity.* Biomolecules, 2019. **9**(11).

97. Moise, A.R., et al., *Increased adiposity in the retinol saturase-knockout mouse.* FASEB J, 2010. **24**(4): p. 1261-70.
98. Tontonoz, P. and B.M. Spiegelman, *Fat and beyond: the diverse biology of PPARgamma.* Annu Rev Biochem, 2008. **77**: p. 289-312.
99. Witte, N., et al., *The Glucose Sensor ChREBP Links De Novo Lipogenesis to PPARgamma Activity and Adipocyte Differentiation.* Endocrinology, 2015. **156**(11): p. 4008-19.
100. Yamashita, H., et al., *A glucose-responsive transcription factor that regulates carbohydrate metabolism in the liver.* Proc Natl Acad Sci U S A, 2001. **98**(16): p. 9116-21.
101. Ye, J., et al., *Primer-BLAST: a tool to design target-specific primers for polymerase chain reaction.* BMC Bioinformatics, 2012. **13**: p. 134.
102. Heidenreich, S., *Neue Regulatoren des zellulären Glukosestoffwechsels*. 2019.
103. Shao, X., et al., *A minimal Ksp-cadherin promoter linked to a green fluorescent protein reporter gene exhibits tissue-specific expression in the developing kidney and genitourinary tract.* J Am Soc Nephrol, 2002. **13**(7): p. 1824-36.
104. Shao, X., S. Somlo, and P. Igarashi, *Epithelial-specific Cre/lox recombination in the developing kidney and genitourinary tract.* J Am Soc Nephrol, 2002. **13**(7): p. 1837-46.
105. Surwit, *Diet-Induced Type II Diabetes in C57BL/6J Mice.* 1988.
106. Surwit, *Control of Expression of Insulin Resistance and Hyperglycemia by Different Genetic Factors in Diabetic C57BL/6J Mice.* 1991.
107. Huang, T.T., et al., *Genetic modifiers of the phenotype of mice deficient in mitochondrial superoxide dismutase.* Hum Mol Genet, 2006. **15**(7): p. 1187-94.
108. Taicher, G.Z., et al., *Quantitative magnetic resonance (QMR) method for bone and whole-body-composition analysis.* Anal Bioanal Chem, 2003. **377**(6): p. 990-1002.
109. Tschop, M.H., et al., *A guide to analysis of mouse energy metabolism.* Nat Methods, 2011. **9**(1): p. 57-63.
110. Tuck, E., et al., *A gene expression resource generated by genome-wide lacZ profiling in the mouse.* Dis Model Mech, 2015. **8**(11): p. 1467-78.
111. Ransick, A., et al., *Single-Cell Profiling Reveals Sex, Lineage, and Regional Diversity in the Mouse Kidney.* Dev Cell, 2019. **51**(3): p. 399-413 e7.
112. Hinze, C., et al., *Kidney Single-cell Transcriptomes Predict Spatial Corticomedullary Gene Expression and Tissue Osmolality Gradients.* J Am Soc Nephrol, 2021. **32**(2): p. 291-306.
113. Lee, J.W., C.L. Chou, and M.A. Knepper, *Deep Sequencing in Microdissected Renal Tubules Identifies Nephron Segment-Specific Transcriptomes.* J Am Soc Nephrol, 2015. **26**(11): p. 2669-77.
114. Pillot, B., et al., *Protein feeding promotes redistribution of endogenous glucose production to the kidney and potentiates its suppression by insulin.* Endocrinology, 2009. **150**(2): p. 616-24.
115. van Schaftingen, E. and I. Gerin, *The glucose-6-phosphatase system.* Biochem J, 2002. **362**(Pt 3): p. 513-32.
116. Mutel, E., et al., *Control of blood glucose in the absence of hepatic glucose production during prolonged fasting in mice: induction of renal and intestinal gluconeogenesis by glucagon.* Diabetes, 2011. **60**(12): p. 3121-31.
117. Owen, O.E., et al., *Liver and kidney metabolism during prolonged starvation.* J Clin Invest, 1969. **48**(3): p. 574-83.
118. Ekberg, K., et al., *Contributions by kidney and liver to glucose production in the postabsorptive state and after 60 h of fasting.* Diabetes, 1999. **48**(2): p. 292-8.
119. Rajas, F., et al., *Immunocytochemical localization of glucose 6-phosphatase and cytosolic phosphoenolpyruvate carboxykinase in gluconeogenic tissues reveals unsuspected metabolic zonation.* Histochem Cell Biol, 2007. **127**(5): p. 555-65.
120. Arion, W.J., et al., *On the involvement of a glucose 6-phosphate transport system in the function of microsomal glucose 6-phosphatase.* Mol Cell Biochem, 1975. **6**(2): p. 75-83.
121. Austin, S., M. Ziese, and N. Sternberg, *A novel role for site-specific recombination in maintenance of bacterial replicons.* Cell, 1981. **25**(3): p. 729-36.

122. Thomson, R.B., et al., *Isolation and cDNA cloning of Ksp-cadherin, a novel kidney-specific member of the cadherin multigene family.* J Biol Chem, 1995. **270**(29): p. 17594-601.
123. Thomson, R.B., et al., *cDNA cloning and chromosomal localization of the human and mouse isoforms of Ksp-cadherin.* Genomics, 1998. **51**(3): p. 445-51.
124. Cali, G., et al., *Conditional inactivation of the E-cadherin gene in thyroid follicular cells affects gland development but does not impair junction formation.* Endocrinology, 2007. **148**(6): p. 2737-46.
125. Cali, G., et al., *CDH16/Ksp-cadherin is expressed in the developing thyroid gland and is strongly down-regulated in thyroid carcinomas.* Endocrinology, 2012. **153**(1): p. 522-34.
126. Kusakabe, T., et al., *Thyrocyte-specific expression of Cre recombinase in transgenic mice.* Genesis, 2004. **39**(3): p. 212-6.
127. Dunn, S.R., et al., *Utility of endogenous creatinine clearance as a measure of renal function in mice.* Kidney Int, 2004. **65**(5): p. 1959-67.
128. Dossetor, J.B., *Creatininemia versus uremia. The relative significance of blood urea nitrogen and serum creatinine concentrations in azotemia.* Ann Intern Med, 1966. **65**(6): p. 1287-99.
129. Duarte, C.G. and H.G. Preuss, *Assessment of Renal Function—Glomerular and Tubular.* Clinics in Laboratory Medicine, 1993. **13**(1): p. 33-52.
130. Nankivell, B.J., *Abnormal Laboratory Results: Creatinine clearance and the assessment of renal function.* Australian Prescriber, 2001. **24**(1): p. 15-17.
131. Han, W.K., et al., *Kidney Injury Molecule-1 (KIM-1): a novel biomarker for human renal proximal tubule injury.* Kidney Int, 2002. **62**(1): p. 237-44.
132. Mishra, J., et al., *Identification of neutrophil gelatinase-associated lipocalin as a novel early urinary biomarker for ischemic renal injury.* J Am Soc Nephrol, 2003. **14**(10): p. 2534-43.
133. Spiegelman, B.M. and J.S. Flier, *Obesity and the regulation of energy balance.* Cell, 2001. **104**(4): p. 531-43.
134. Hill, J.O., H.R. Wyatt, and J.C. Peters, *Energy balance and obesity.* Circulation, 2012. **126**(1): p. 126-32.
135. Campbell, K.H. and A.M. O'Hare, *Kidney disease in the elderly: update on recent literature.* Curr Opin Nephrol Hypertens, 2008. **17**(3): p. 298-303.
136. Davies, I., A.P. Fotheringham, and B.E. Faragher, *Age-associated changes in the kidney of the laboratory mouse.* Age Ageing, 1989. **18**(2): p. 127-33.
137. Baylis, C. and B. Corman, *The aging kidney: insights from experimental studies.* J Am Soc Nephrol, 1998. **9**(4): p. 699-709.
138. Scheinman, S.J., *New insights into causes and treatments of kidney stones.* Hosp Pract (1995), 2000. **35**(3): p. 49-50, 53-6, 62-3 passim.
139. Prie, D., et al., *Frequency of renal phosphate leak among patients with calcium nephrolithiasis.* Kidney Int, 2001. **60**(1): p. 272-6.
140. Worcester, E.M. and F.L. Coe, *Clinical practice. Calcium kidney stones.* N Engl J Med, 2010. **363**(10): p. 954-63.
141. Bushinsky, D.A., *Genetic hypercalciuric stone-forming rats.* Current Opinion in Nephrology and Hypertension, 1999. **8**(4): p. 479-488.
142. Khan, S.R., *Nephrocalcinosis in animal models with and without stones.* Urol Res, 2010. **38**(6): p. 429-38.
143. Walker, V., E.M. Stansbridge, and D.G. Griffin, *Demography and biochemistry of 2800 patients from a renal stones clinic.* Ann Clin Biochem, 2013. **50**(Pt 2): p. 127-39.
144. Evan, A.P., et al., *Contrasting histopathology and crystal deposits in kidneys of idiopathic stone formers who produce hydroxy apatite, brushite, or calcium oxalate stones.* Anat Rec (Hoboken), 2014. **297**(4): p. 731-48.
145. Breiderhoff, T., et al., *Deletion of claudin-10 (Cldn10) in the thick ascending limb impairs paracellular sodium permeability and leads to hypermagnesemia and nephrocalcinosis.* Proc Natl Acad Sci U S A, 2012. **109**(35): p. 14241-6.
146. Li, X., W. Zheng, and Y.C. Li, *Altered gene expression profile in the kidney of vitamin D receptor knockout mice.* J Cell Biochem, 2003. **89**(4): p. 709-19.

147. West, D.B., et al., *Dietary obesity in nine inbred mouse strains.* Am J Physiol, 1992. **262**(6 Pt 2): p. R1025-32.
148. Camara, N.O., et al., *Kidney disease and obesity: epidemiology, mechanisms and treatment.* Nat Rev Nephrol, 2017. **13**(3): p. 181-190.
149. Hsu, C.Y., et al., *Body mass index and risk for end-stage renal disease.* Ann Intern Med, 2006. **144**(1): p. 21-8.
150. Sun, Y., et al., *High-fat diet promotes renal injury by inducing oxidative stress and mitochondrial dysfunction.* Cell Death Dis, 2020. **11**(10): p. 914.
151. Altunkaynak, M.E., et al., *The effects of high-fat diet on the renal structure and morphometric parametric of kidneys in rats.* J Anat, 2008. **212**(6): p. 845-52.
152. Karlsson, M., et al., *A single-cell type transcriptomics map of human tissues.* Sci Adv, 2021. **7**(31).
153. Wang, W., et al., *Quantitative proteomics reveals TMOD1-related proteins associated with water balance regulation.* PLoS One, 2019. **14**(7): p. e0219932.
154. Wu, F., *Conditional targeting in the kidney.* Nephron Physiol, 2007. **107**(1): p. p10-6.
155. Kohan, D.E., *Progress in gene targeting: using mutant mice to study renal function and disease.* Kidney Int, 2008. **74**(4): p. 427-37.
156. O'Rourke, M.B., et al., *What is Normalization? The Strategies Employed in Top-Down and Bottom-Up Proteome Analysis Workflows.* Proteomes, 2019. **7**(3).
157. Charkoftaki, G., et al., *Update on the human and mouse lipocalin (LCN) gene family, including evidence the mouse Mup cluster is result of an "evolutionary bloom".* Hum Genomics, 2019. **13**(1): p. 11.
158. Flower, D.R., *The lipocalin protein family: structure and function.* Biochem J, 1996. **318 (Pt 1)**(Pt 1): p. 1-14.
159. Zhou, Y. and L. Rui, *Major urinary protein regulation of chemical communication and nutrient metabolism.* Vitam Horm, 2010. **83**: p. 151-63.
160. Beynon, R.J., et al., *Mice, MUPs and myths: structure-function relationships of the major urinary proteins.* Chemical Signals in Vertebrates 9, 2001: p. 149-156.
161. Parr, S.K., et al., *Acute kidney injury is a risk factor for subsequent proteinuria.* Kidney Int, 2018. **93**(2): p. 460-469.
162. Gorriz, J.L. and A. Martinez-Castelao, *Proteinuria: detection and role in native renal disease progression.* Transplant Rev (Orlando), 2012. **26**(1): p. 3-13.
163. Steinhoff, J.S., A. Lass, and M. Schupp, *Retinoid Homeostasis and Beyond: How Retinol Binding Protein 4 Contributes to Health and Disease.* Nutrients, 2022. **14**(6).
164. Fiseha, T. and Z. Tamir, *Urinary Markers of Tubular Injury in Early Diabetic Nephropathy.* Int J Nephrol, 2016. **2016**: p. 4647685.
165. Christensen, E.I., et al., *Endocytic receptors in the renal proximal tubule.* Physiology (Bethesda), 2012. **27**(4): p. 223-36.
166. Norden, A.G., M. Lapsley, and R.J. Unwin, *Urine retinol-binding protein 4: a functional biomarker of the proximal renal tubule.* Adv Clin Chem, 2014. **63**: p. 85-122.
167. Bernard, A.M., et al., *Assessment of urinary retinol-binding protein as an index of proximal tubular injury.* Clin Chem, 1987. **33**(6): p. 775-9.
168. Yaqoob, M., et al., *Relationship between markers of endothelial dysfunction, oxidant injury and tubular damage in patients with insulin-dependent diabetes mellitus.* Clin Sci (Lond), 1993. **85**(5): p. 557-62.
169. Li, A., et al., *Urinary NGAL and RBP Are Biomarkers of Normoalbuminuric Renal Insufficiency in Type 2 Diabetes Mellitus.* J Immunol Res, 2019. **2019**: p. 5063089.
170. Devuyst, O. and R.V. Thakker, *Dent's disease.* Orphanet Journal of Rare Diseases, 2010. **5**(1): p. 28.
171. Steinhoff, J.S., A. Lass, and M. Schupp, *Biological Functions of RBP4 and Its Relevance for Human Diseases.* Front Physiol, 2021. **12**: p. 659977.
172. Wu, J., et al., *Urinary RBP and NGAL Levels are Associated with Nephropathy in Patients with Type 2 Diabetes.* Cell Physiol Biochem, 2017. **42**(2): p. 594-602.

173. Mahfouz, M.H., A.M. Assiri, and M.H. Mukhtar, *Assessment of Neutrophil Gelatinase-Associated Lipocalin (NGAL) and Retinol-Binding Protein 4 (RBP4) in Type 2 Diabetic Patients with Nephropathy.* Biomark Insights, 2016. **11**: p. 31-40.
174. Park, S.E., et al., *Association of urinary RBP4 with insulin resistance, inflammation, and microalbuminuria.* Eur J Endocrinol, 2014. **171**(4): p. 443-9.
175. Savory, J.G., et al., *Identification of novel retinoic acid target genes.* Dev Biol, 2014. **395**(2): p. 199-208.
176. Obrochta, K.M., et al., *Insulin regulates retinol dehydrogenase expression and all-trans-retinoic acid biosynthesis through FoxO1.* J Biol Chem, 2015. **290**(11): p. 7259-68.
177. Molotkov, A. and G. Duester, *Genetic evidence that retinaldehyde dehydrogenase Raldh1 (Aldh1a1) functions downstream of alcohol dehydrogenase Adh1 in metabolism of retinol to retinoic acid.* J Biol Chem, 2003. **278**(38): p. 36085-90.
178. Tay, S., et al., *A comparison of the roles of peroxisome proliferator-activated receptor and retinoic acid receptor on CYP26 regulation.* Mol Pharmacol, 2010. **77**(2): p. 218-27.
179. Lubarski, I., et al., *Interaction with the Na,K-ATPase and tissue distribution of FXYD5 (related to ion channel).* J Biol Chem, 2005. **280**(45): p. 37717-24.
180. Ino, Y., et al., *Dysadherin, a cancer-associated cell membrane glycoprotein, down-regulates E-cadherin and promotes metastasis.* Proc Natl Acad Sci U S A, 2002. **99**(1): p. 365-70.
181. Tsuiji, H., et al., *Aberrant O-glycosylation inhibits stable expression of dysadherin, a carcinoma-associated antigen, and facilitates cell-cell adhesion.* Glycobiology, 2003. **13**(7): p. 521-7.
182. Lubarski, I., C. Asher, and H. Garty, *FXYD5 (dysadherin) regulates the paracellular permeability in cultured kidney collecting duct cells.* Am J Physiol Renal Physiol, 2011. **301**(6): p. F1270-80.
183. Jiang, X., et al., *RETSAT Mutation Selected for Hypoxia Adaptation Inhibits Tumor Growth.* Front Cell Dev Biol, 2021. **9**: p. 744992.
184. Ratnam, K.K., et al., *Role of the retinoic acid receptor-alpha in HIV-associated nephropathy.* Kidney Int, 2011. **79**(6): p. 624-634.
185. He, J.C., et al., *Retinoic acid inhibits HIV-1-induced podocyte proliferation through the cAMP pathway.* J Am Soc Nephrol, 2007. **18**(1): p. 93-102.
186. Wagner, J., et al., *Retinoic acid reduces glomerular injury in a rat model of glomerular damage.* J Am Soc Nephrol, 2000. **11**(8): p. 1479-1487.
187. Belge, H., et al., *Renal expression of parvalbumin is critical for NaCl handling and response to diuretics.* Proc Natl Acad Sci U S A, 2007. **104**(37): p. 14849-54.
188. Garcia, M.A., et al., *Effect of renal ischemia/reperfusion on gene expression of a pH-sensitive K+ channel.* Nephron Physiol, 2007. **106**(1): p. p1-7.
189. Hebert, S.C., et al., *Molecular diversity and regulation of renal potassium channels.* Physiol Rev, 2005. **85**(1): p. 319-71.
190. Wang, W., S.C. Hebert, and G. Giebisch, *Renal K+ channels: structure and function.* Annu Rev Physiol, 1997. **59**: p. 413-36.
191. Copp, D.H., et al., *Evidence for calcitonin--a new hormone from the parathyroid that lowers blood calcium.* Endocrinology, 1962. **70**: p. 638-49.
192. Quamme, G.A., *Effect of calcitonin on calcium and magnesium transport in rat nephron.* Am J Physiol, 1980. **238**(6): p. E573-8.
193. Davey, R.A., et al., *Calcitonin receptor plays a physiological role to protect against hypercalcemia in mice.* J Bone Miner Res, 2008. **23**(8): p. 1182-93.
194. Vezzoli, G., et al., *Genetics and calcium nephrolithiasis.* Kidney International, 2011. **80**(6): p. 587-593.
195. Curry, J.N., et al., *Claudin-2 deficiency associates with hypercalciuria in mice and human kidney stone disease.* J Clin Invest, 2020. **130**(4): p. 1948-1960.
196. Zella, L.A., et al., *Multifunctional enhancers regulate mouse and human vitamin D receptor gene transcription.* Mol Endocrinol, 2010. **24**(1): p. 128-47.
197. Chen, T.L. and D. Feldman, *Retinoic acid modulation of 1,25(OH)2 vitamin D3 receptors and bioresponse in bone cells: species differences between rat and mouse.* Biochem Biophys Res Commun, 1985. **132**(1): p. 74-80.

198. Elizondo, G., et al., *Feedback inhibition of the retinaldehyde dehydrogenase gene ALDH1 by retinoic acid through retinoic acid receptor alpha and CCAAT/enhancer-binding protein beta.* J Biol Chem, 2000. **275**(50): p. 39747-53.
199. MacGregor, J.L. and H.I. Maibach, *The Specificity of Retinoid-Induced Irritation and Its Role in Clinical Efficacy.* Exogenous Dermatology, 2002. **1**(2): p. 68-73.
200. Kim, M.Y., et al., *Retinoid Induces the Degradation of Corneodesmosomes and Downregulation of Corneodesmosomal Cadherins: Implications on the Mechanism of Retinoid-induced Desquamation.* Ann Dermatol, 2011. **23**(4): p. 439-47.
201. Wang, Y., et al., *Altered vitamin D metabolism in type II diabetic mouse glomeruli may provide protection from diabetic nephropathy.* Kidney International, 2006. **70**(5): p. 882-891.
202. Zhang, Z., et al., *Renoprotective role of the vitamin D receptor in diabetic nephropathy.* Kidney Int, 2008. **73**(2): p. 163-71.
203. Deb, D.K., et al., *Molecular mechanism underlying 1,25-dihydroxyvitamin D regulation of nephrin gene expression.* J Biol Chem, 2011. **286**(37): p. 32011-7.
204. Wang, Y., et al., *Vitamin D receptor signaling in podocytes protects against diabetic nephropathy.* J Am Soc Nephrol, 2012. **23**(12): p. 1977-86.
205. Nemoto, S. and T. Kubota, *Metabolic differences and differentially expressed genes between C57BL/6J and C57BL/6N mice substrains.* bioRxiv, 2022.
206. Rendina-Ruedy, E., et al., *A Comparative Study of the Metabolic and Skeletal Response of C57BL/6J and C57BL/6N Mice in a Diet-Induced Model of Type 2 Diabetes.* J Nutr Metab, 2015. **2015**: p. 758080.
207. Siersbaek, M.S., et al., *C57BL/6J substrain differences in response to high-fat diet intervention.* Sci Rep, 2020. **10**(1): p. 14052.
208. Strange, R.C., K.E. Shipman, and S. Ramachandran, *Metabolic syndrome: A review of the role of vitamin D in mediating susceptibility and outcome.* World J Diabetes, 2015. **6**(7): p. 896-911.
209. Park, J.E., P.B.T. Pichiah, and Y.S. Cha, *Vitamin D and Metabolic Diseases: Growing Roles of Vitamin D.* J Obes Metab Syndr, 2018. **27**(4): p. 223-232.
210. Lau, S.L., et al., *Metabolic changes in vitamin D receptor knockout mice.* PLoS One, 2022. **17**(6): p. e0267573.
211. Wallace, I.R., et al., *Vitamin D and insulin resistance.* Clin Endocrinol (Oxf), 2016. **84**(2): p. 159-171.
212. Li, Y.C., et al., *Targeted ablation of the vitamin D receptor: an animal model of vitamin D-dependent rickets type II with alopecia.* Proc Natl Acad Sci U S A, 1997. **94**(18): p. 9831-5.
213. Wong, K.E., et al., *Involvement of the vitamin D receptor in energy metabolism: regulation of uncoupling proteins.* Am J Physiol Endocrinol Metab, 2009. **296**(4): p. E820-8.
214. Zella, L.A., et al., *Enhancers located within two introns of the vitamin D receptor gene mediate transcriptional autoregulation by 1,25-dihydroxyvitamin D3.* Mol Endocrinol, 2006. **20**(6): p. 1231-47.
215. Feldman, D. and J.M. P, *Mutations in the vitamin D receptor and hereditary vitamin D-resistant rickets.* Bonekey Rep, 2014. **3**: p. 510.
216. Yoshizawa, T., et al., *Mice lacking the vitamin D receptor exhibit impaired bone formation, uterine hypoplasia and growth retardation after weaning.* Nat Genet, 1997. **16**(4): p. 391-6.
217. Kaufmann, M., et al., *A High-Calcium and Phosphate Rescue Diet and VDR-Expressing Transgenes Normalize Serum Vitamin D Metabolite Profiles and Renal Cyp27b1 and Cyp24a1 Expression in VDR Null Mice.* Endocrinology, 2015. **156**(12): p. 4388-97.
218. Ritter, C.S., et al., *25-Hydroxyvitamin D(3) suppresses PTH synthesis and secretion by bovine parathyroid cells.* Kidney Int, 2006. **70**(4): p. 654-9.
219. Brown, E.M., et al., *Cloning and characterization of an extracellular Ca(2+)-sensing receptor from bovine parathyroid.* Nature, 1993. **366**(6455): p. 575-80.
220. Nordin, B.E.C., A. Need, and H. Morris, *Metabolic bone and stone disease*. 1993: Churchill Livingstone.
221. Healy, K.D., et al., *Regulation of the murine renal vitamin D receptor by 1,25-dihydroxyvitamin D3 and calcium.* Proc Natl Acad Sci U S A, 2003. **100**(17): p. 9733-7.

222. Fried, L.F., T.J. Orchard, and B.L. Kasiske, *Effect of lipid reduction on the progression of renal disease: a meta-analysis.* Kidney Int, 2001. **59**(1): p. 260-9.
223. Parekh, P.I., et al., *Reversal of diet-induced obesity and diabetes in C57BL/6J mice.* Metabolism, 1998. **47**(9): p. 1089-96.
224. Molnar, J., et al., *Diabetes induces endothelial dysfunction but does not increase neointimal formation in high-fat diet fed C57BL/6J mice.* Circ Res, 2005. **96**(11): p. 1178-84.
225. Fan, Y., et al., *Vitamin D3/VDR resists diet-induced obesity by modulating UCP3 expression in muscles.* J Biomed Sci, 2016. **23**(1): p. 56.
226. Muller, T.D., M. Klingenspor, and M.H. Tschop, *Revisiting energy expenditure: how to correct mouse metabolic rate for body mass.* Nat Metab, 2021. **3**(9): p. 1134-1136.
227. Bagby, S.P., *Obesity-initiated metabolic syndrome and the kidney: a recipe for chronic kidney disease?* J Am Soc Nephrol, 2004. **15**(11): p. 2775-91.
228. Deji, N., et al., *Structural and functional changes in the kidneys of high-fat diet-induced obese mice.* Am J Physiol Renal Physiol, 2009. **296**(1): p. F118-26.
229. Henegar, J.R., et al., *Functional and structural changes in the kidney in the early stages of obesity.* J Am Soc Nephrol, 2001. **12**(6): p. 1211-1217.
230. Praga, M., *Obesity--a neglected culprit in renal disease.* Nephrol Dial Transplant, 2002. **17**(7): p. 1157-9.
231. Wisse, B.E., *The inflammatory syndrome: the role of adipose tissue cytokines in metabolic disorders linked to obesity.* J Am Soc Nephrol, 2004. **15**(11): p. 2792-800.
232. Guan, Y., *Peroxisome proliferator-activated receptor family and its relationship to renal complications of the metabolic syndrome.* J Am Soc Nephrol, 2004. **15**(11): p. 2801-15.
233. Wicks, S.E., et al., *Diet-induced obesity and kidney disease - In search of a susceptible mouse model.* Biochimie, 2016. **124**: p. 65-73.
234. Brosius, F.C., 3rd, et al., *Mouse models of diabetic nephropathy.* J Am Soc Nephrol, 2009. **20**(12): p. 2503-12.
235. Yu, Y., et al., *High Fat Diet Induces Kidney Injury via Stimulating Wnt/beta-Catenin Signaling.* Front Med (Lausanne), 2022. **9**: p. 851618.
236. Kaneko, K., et al., *The role of kidney in the inter-organ coordination of endogenous glucose production during fasting.* Mol Metab, 2018. **16**: p. 203-212.
237. Sato, T., et al., *Acute fructose intake suppresses fasting-induced hepatic gluconeogenesis through the AKT-FoxO1 pathway.* Biochem Biophys Rep, 2019. **18**: p. 100638.
238. Schmid, H., et al., *Carbohydrate metabolism in rat kidney: heterogeneous distribution of glycolytic and gluconeogenic key enzymes.* Curr Probl Clin Biochem, 1977. **8**: p. 282-9.
239. Guder, W.G. and U. Schmidt, *The Localization of Gluconeogenesis in Rat Nephron. Determination of Phosphoenolpyruvate Carboxykinase in Microdissected Tubules.* Biological Chemistry, 1974. **355**(1): p. 273-278.
240. Vandewalle, A., et al., *Distribution of hexokinase and phosphoenolpyruvate carboxykinase along the rabbit nephron.* Am J Physiol, 1981. **240**(6): p. F492-500.
241. Nakae, J., et al., *The forkhead transcription factor Foxo1 (Fkhr) confers insulin sensitivity onto glucose-6-phosphatase expression.* Journal of Clinical Investigation, 2001. **108**(9): p. 1359-1367.
242. Meyer, C., J.M. Dostou, and J.E. Gerich, *Role of the human kidney in glucose counterregulation.* Diabetes, 1999. **48**(5): p. 943-8.
243. Gerich, J.E., *Physiology of glucose homeostasis.* Diabetes Obes Metab, 2000. **2**(6): p. 345-50.
244. Iizuka, K., et al., *Deficiency of carbohydrate response element-binding protein (ChREBP) reduces lipogenesis as well as glycolysis.* Proc Natl Acad Sci U S A, 2004. **101**(19): p. 7281-6.
245. Decleves, A.E., et al., *Regulation of lipid accumulation by AMP-activated kinase [corrected] in high fat diet-induced kidney injury.* Kidney Int, 2014. **85**(3): p. 611-23.
246. Muller, C.R., et al., *Post-weaning Exposure to High-Fat Diet Induces Kidney Lipid Accumulation and Function Impairment in Adult Rats.* Front Nutr, 2019. **6**: p. 60.
247. de Vries, A.P., et al., *Fatty kidney: emerging role of ectopic lipid in obesity-related renal disease.* Lancet Diabetes Endocrinol, 2014. **2**(5): p. 417-26.

248. Juszczak, F., et al., *Critical Role for AMPK in Metabolic Disease-Induced Chronic Kidney Disease.* Int J Mol Sci, 2020. **21**(21).
249. Muto, Y., H. Moriwaki, and A. Saito, *Prevention of second primary tumors by an acyclic retinoid in patients with hepatocellular carcinoma.* N Engl J Med, 1999. **340**(13): p. 1046-7.
250. Shimizu, M., et al., *Acyclic retinoid inhibits diethylnitrosamine-induced liver tumorigenesis in obese and diabetic C57BLKS/J- +(db)/+Lepr(db) mice.* Cancer Prev Res (Phila), 2011. **4**(1): p. 128-36.
251. Lee, Y.M., et al., *Retinoic acid leads to cytoskeletal rearrangement through AMPK-Rac1 and stimulates glucose uptake through AMPK-p38 MAPK in skeletal muscle cells.* J Biol Chem, 2008. **283**(49): p. 33969-74.
252. Ishijima, N., et al., *Activation of AMP-activated protein kinase by retinoic acid sensitizes hepatocellular carcinoma cells to apoptosis induced by sorafenib.* Cancer Sci, 2015. **106**(5): p. 567-75.
253. Rubera, I., et al., *Specific Cre/Lox recombination in the mouse proximal tubule.* J Am Soc Nephrol, 2004. **15**(8): p. 2050-6.
254. Meyer, C.W., et al., *Adaptive thermogenesis and thermal conductance in wild-type and UCP1-KO mice.* Am J Physiol Regul Integr Comp Physiol, 2010. **299**(5): p. R1396-406.
255. Powell-Wiley, T.M., et al., *Obesity and Cardiovascular Disease: A Scientific Statement From the American Heart Association.* Circulation, 2021. **143**(21): p. e984-e1010.
256. Leigh, R.S. and B.L. Kaynak, *Vitamin A as a Transcriptional Regulator of Cardiovascular Disease.* Hearts, 2020. **1**(2): p. 126-145.
257. Brewster, U.C. and M.A. Perazella, *The renin-angiotensin-aldosterone system and the kidney: effects on kidney disease.* Am J Med, 2004. **116**(4): p. 263-72.